

THESIS ON NATURAL AND EXACT SCIENCES B219

Metal-Doped Aerogels Based on Resorcinol Derivatives

KRISTIINA KREEK

TUT
PRESS

TALLINN UNIVERSITY OF TECHNOLOGY
Faculty of Science
Department of Chemistry

This dissertation was accepted for the defence of the degree of Doctor of Philosophy in Natural and Exact Sciences on 29.09.2016.

Supervisor: Lead Research Scientist Dr. Mihkel Koel, Department of Chemistry, Tallinn University of Technology

Opponents: Prof. Dr. Maria-Magdalena Titirici, School of Engineering and Materials Science & Materials Research Institute, Queen Mary University of London, United Kingdom

Dr. Uno Mäeorg, Institute of Chemistry, University of Tartu, Estonia

Defence of the thesis: November 16, 2016

Declaration:

Hereby I declare that this doctoral thesis, my original investigation and achievement, submitted for the doctoral degree at Tallinn University of Technology has not been submitted for any academic degree.

Kristiina Kreek

Copyright: Kristiina Kreek, 2016

ISSN 1406-4723

ISBN 978-9949-83-027-5 (Publication)

ISBN 978-9949-83-028-2 (PDF)

LOODUS- JA TÄPPISTEADUSED B219

Resortsinooli derivaatidel põhinevad metalli sisaldavad aerogeelid

KRISTIINA KREEK

CONTENTS

LIST OF PUBLICATIONS	7
AUTHOR'S CONTRIBUTION TO THE PUBLICATIONS	8
INTRODUCTION	9
AIMS OF THE STUDY	11
ABBREVIATIONS	12
1. LITERATURE OVERVIEW	13
1.1. Preparation of organic and carbon aerogels.....	13
1.1.1. Gel preparation.....	14
1.1.2. Drying of gels.....	15
1.1.3. Pyrolysis and carbon aerogels.....	16
1.2. Aerogels prepared from 5-methylresorcinol, 2,6-dihydroxy-4-methylbenzoic acid and melamine.....	17
1.2.1. 5-methylresorcinol for aerogel preparation.....	17
1.2.2. 2,6-dihydroxy-4-methylbenzoic acid for aerogel preparation.....	18
1.2.3. Melamine for aerogel preparation.....	19
1.3. Metal-doped organic and carbon aerogels.....	20
1.3.1. Addition of the metal-precursor to aerogels before gelation.....	21
1.3.2. The ion-exchange method for doping with metals.....	22
1.3.3. Deposition of the metal precursor onto the organic or carbon aerogel.....	25
1.4. Metal-doped organic and carbon aerogels for various applications.....	25
1.4.1. Metal-doped aerogels as catalysts.....	25
1.4.2. Lanthanide-doped organic and carbon aerogels.....	27
1.4.3. Metal-doped carbon aerogels for electrical applications.....	28
2. EXPERIMENTAL	30
2.1. Reagents.....	30
2.2. Instrumentation and characterisation.....	30
2.3. Aerogel preparation.....	31
2.3.1. Metal doped aerogels prepared from 5-methylresorcinol and 2,6-dihydroxy-4-methylbenzoic acid.....	31
2.3.2. Preparation of metal-and nitrogen-doped aerogels.....	31
3. RESULTS	33
3.1. Co-, Cu- and Ni-doped aerogels.....	33
3.2. Lanthanide-doped aerogels.....	38
3.3. Lanthanide-doped aerogels as heterogeneous catalysts.....	40
3.4. Co-and N-doped carbon aerogels as electrocatalysts for ORR.....	41
3.5. Oxygen reduction reaction activity of Co-NCA catalysts.....	46
4. CONCLUSIONS	48
REFERENCES	49
ACKNOWLEDGEMENTS	57
ABSTRACT	58
KOKKUVÕTE	60

ORIGINAL PUBLICATIONS	63
Publication I.....	63
Publication II.....	77
Publication III.....	85
CURRICULUM VITAE	97
ELULOOKIRJELDUS	99

LIST OF PUBLICATIONS

This thesis is based on the following original publications:

- I. Kreek, K., Kulp, M., Uibu, M., Mere, A., Koel, M. Preparation of metal-doped carbon aerogels from oil shale processing by-products. - *Oil Shale*, 2014, 31, 185-194.
- II. Kreek, K., Kriis, K., Maaten, B., Uibu, M., Mere, A., Kanger, T., Koel, M. Organic and carbon aerogels containing rare-earth metals: Their properties and application as catalysts. – *Journal of Non-Crystalline Solids*, 2014, 404, 43-48.
- III. Kreek, K., Sarapuu, A., Samolberg, L., Joost, U., Mikli, V., Koel, M., Tammeveski, K. Cobalt-containing nitrogen-doped carbon aerogels as efficient electrocatalysts for the oxygen reduction reaction. – *Chemelectrochem*, 2015, 2, 2079-2088.

OTHER PUBLICATIONS IN RELATED FIELD

- IV. Sarapuu, A., Samolberg, L., Kreek, K., Koel, M., Matisen, L., Tammeveski, K. Cobalt- and iron-containing nitrogen-doped carbon aerogels as non-precious metal catalysts for electrochemical reduction of oxygen. - *Journal of Electroanalytical Chemistry*, 2015, 746, 9–17.

AUTHOR'S CONTRIBUTION TO THE PUBLICATIONS

Publication I

The autor designed the experiments and prepared all the materials. She interpreted the results of experiments and wrote the manuscript.

Publication II

The author designed and prepared all the materials. She interpreted the results of the materials characterisation experiments and wrote the major part of the publication. The author participated in the designing of the experiments for testing the materials as catalysts and also took part in the interpretation of the results.

Publication III

The author prepared all the materials, interpreted most of the results of the materials charcterisation experiments and wrote that part of the publication. The author also participated in discussing the results of the electrocatalytical tests.

INTRODUCTION

Carbon materials due to the different allotropes of carbon have very versatile properties and can be used for a variety of applications. Some examples of these diverse materials include activated carbon, carbon black, graphite, carbon foam, carbon nanotubes, carbon fiber, etc. These materials can be used as adsorbents, electrode materials, insulators, catalyst supports, etc.

The demand for carbon materials to fit specific applications calls for the need to fine-tune the properties of these materials. A promising class of such materials is carbon aerogels (CAs), which are known for the ability to adjust their porous structure. Carbon aerogels have high surface area, open porous structure with pores ranging from micro- to macropores and electrical conductivity. Doping these materials with metals enables one to further modify their structure, improve electrical conductivity or add the desired catalytic activity. The main applications for metal-doped carbon aerogels are as electrode materials and catalysts.

Different methods can be employed to introduce metals into the carbon aerogel structure. The ion-exchange method used in this work enables to evenly distribute metal species to the surface of the porous material. This method involves the use of an ion-exchange moiety containing monomer for aerogel preparation. Each repeat unit of the material will therefore be able to chemically bind metal species.

Different phenolic compounds together with formaldehyde are mostly used for carbon aerogel preparation. In this work 5-methylresorcinol (MR) and 2,6-dihydroxy-4-methylbenzoic acid (dHMBA), which has the ion-exchange moiety, are chosen for aerogel preparation. These compounds are suitable because 5-methylresorcinol is a by-product of the local oil shale processing industry and 2,6-dihydroxy-4-methylbenzoic acid can be easily synthesized from 5-methylresorcinol [1,2].

The goal of this work is to develop a method for doping metals into aerogels prepared from 5-methylresorcinol and 2,6-dihydroxy-4-methylbenzoic acid, to study the properties of the obtained materials and to test them for desired applications. The prepared materials are doped with various metals such as Co, Cu, Ni, La, Ce, Nd, Pr. The structure and morphology of metal-doped carbon aerogels are characterised by methods such as nitrogen adsorption analysis, scanning electron microscopy (SEM), transmission electron microscopy (TEM), X-ray diffraction (XRD) analysis and different elemental analysis techniques. The relationships between the conditions of preparation and properties of the obtained materials are discussed.

The metal-doped aerogels are tested for use as heterogeneous catalysts. At first, lanthanide-doped organic and carbon aerogels are tested as catalysts for the Michael addition reaction. This is relevant because the preparation and application of lanthanide-doped aerogels as catalyst materials has been poorly studied.

Secondly, the metal-doped carbon aerogels prepared in this work, are tested as electrocatalysts for the oxygen reduction reaction (ORR). This reaction occurs on the cathode in proton-exchange membrane (PEM) fuel cells, which are devices that use hydrogen as fuel to produce electricity. The need for less expensive and more durable catalysts is one of the main obstacles for a wider commercial use of these devices. In recent years the development of non-precious metal catalysts (NPMCs) has attracted a lot of attention due to them being good substitutes for expensive Pt-based catalysts which are currently used in fuel cell cathodes [3,4,5,6]. NPMCs can be prepared from different carbon nanomaterials. In this work cobalt- and nitrogen-doped carbon aerogels are developed for use as ORR catalysts. The nitrogen-doping, is achieved by using melamine (Mel) as one of the precursors for aerogel preparation. The physicochemical properties of carbon aerogels are characterised and the relationships between their properties and catalytic activity are discussed.

AIMS OF THE STUDY

The main goal of this work is to show that metal-doped organic and carbon aerogels can be successfully prepared from oil shale processing by-product 5-methylresorcinol and its derivative 2,6-dihydroxy-4-methylbenzoic acid and that these aerogels have potential for use as heterogeneous catalysts. More specific aims of individual studies are the following:

- developing a method for preparation of metal-doped organic and carbon aerogels from 5-methylresorcinol and 2,6-dihydroxy-4-methylbenzoic acid by using the ion-exchange method for metal doping;
- preparing aerogels doped with various metals and determining the relationships between the conditions for preparation and properties of materials;
- showing the potential of lanthanide-doped aerogels for use as heterogeneous catalysts;
- developing metal-doped carbon aerogels for use as catalysts in the oxygen reduction reaction and also characterising the materials;
- finding the relationships between the properties and catalytic activity of carbon aerogels in oxygen reduction reaction.

ABBREVIATIONS

CA	carbon aerogel
MR	5-methylresorcinol
dHMBA	2,6-dihydroxy-4-methylbenzoic acid
SEM	scanning electron microscopy
TEM	transmission electron microscopy
XRD	X-ray diffraction
ORR	oxygen reduction reaction
PEM	proton-exchange membrane
NPMC	non-precious metal catalyst
Mel	melamine
OA	organic aerogel
R	resorcinol
FA	formaldehyde
R-FA	resorcinol - formaldehyde
SOLV	solvent
Cat	catalyst
Mel-FA	melamine - formaldehyde
R-Mel	resorcinol - melamine
DHBA	2,4-dihydroxybenzoic acid
HRTEM	high-resolution transmission electron microscopy
XPS	X-ray photoelectron spectroscopy
DHBAF	2,4-dihydroxybenzoic acid - formaldehyde
MR-FA	5-methylresorcinol - formaldehyde
Ln	lanthanide
PEMFC	proton-exchange membrane fuel cell
M/N/C	metal-containing nitrogen-doped carbon
AAS	atom absorption spectroscopy
S _{BET}	Brunauer-Emmett-Teller surface area
V _{mic}	microporous volume
TGA	thermogravimetric analysis
AM	aromatic monomer
NaOAc	sodium acetate
Co-NCA	cobalt- and nitrogen-doped carbon aerogel
Co-CA	cobalt-doped carbon aerogel
NCA	nitrogen containing aerogel
S _{mic}	microporous surface area
V _{TOT}	total pore volume
PSD	pore size distribution
BSE	backscattered electron
ICP OES	inductively-coupled plasma optical emission spectrometry
CNT	carbon nanotube
RDE	rotating disk electrode

1. LITERATURE OVERVIEW

Aerogels are solid materials which are prepared by replacing the liquid component of gels with gas. They were first prepared by Kistler [7], who in 1931 published an article in which he dried silica aerogels by using a new supercritical drying method. The method involved increasing pressure and temperature over the critical parameters of the solvent, so that during drying the crossing of the boundary from liquid to gas, which causes capillary stress to emerge, could be avoided.

Aerogels are known for their low density, open porous structure and high surface area. The properties of aerogels depend on the nature of the precursor gel, which can be prepared from different compounds. Besides silica aerogels, different metal oxides and organic compounds can be used for aerogel preparation. Depending on precursors and the preparation method used, aerogels can have various favourable properties such as low thermal and sound conductivity, good electrical conductivity, high hydrophobicity and low refractive index. Some of the applications for aerogels include thermal insulators, adsorbents, electrode materials, drug delivery systems, platforms for chemical sensors, etc [8].

Carbon aerogels (CAs) are mainly composed of carbon as the name suggests. These aerogels are usually prepared by pyrolysing organic aerogels (OAs) which themselves are obtained by drying organic gels. The properties of CAs are largely dependent on the structure and morphology of the parent organic gel. Therefore the study of the properties of carbon aerogels starts with elucidating the relationship between the gel preparation conditions and properties of the gels obtained. The drying method and pyrolysis conditions used also affect the properties of resulting CAs.

The most studied procedure for preparation of organic aerogels was introduced in 1989 by Pekala [9], who used resorcinol (R) and formaldehyde (FA) for gel preparation, followed by the supercritical drying of the gel. Subsequently, the preparation of carbon aerogels by pyrolysing resorcinol-formaldehyde (R-FA) organic aerogels was described [10]. Over the years several other precursors have been used for carbon aerogel preparation, like melamine, phenol, cresol, polymeric isocyanate, polyvinyl chloride, phloroglucinol, ovalbumin/glucose, cellulose, tannins etc., but none of them have been nearly as popular and thoroughly studied as R-FA aerogels [8,11]. The effect of gel preparation conditions, different drying methods and pyrolysis conditions on the properties of the obtained aerogels will be reviewed based on the literature.

1.1. Preparation of organic and carbon aerogels

Since resorcinol and formaldehyde are the most studied precursors for organic aerogel preparation and 5-methylresorcinol and 2,6-dihydroxy-4-methylbenzoic acid are derivatives of resorcinol and form gels in a similar way

[1], the preparation and properties of carbon aerogels will be explained on the basis of resorcinol-formaldehyde aerogels which have been thoroughly studied in the literature. The structure and properties of carbon aerogels are affected by all the stages of the material preparation, so the overview of carbon aerogel preparation starts with explaining the gel formation.

1.1.1. Gel preparation

The preparation of carbon aerogels starts with obtaining an organic gel through sol-gel polymerisation. For R-FA aerogels the monomers resorcinol (R) and formaldehyde (FA) are mixed together into the solvent (SOLV) along with a catalyst (Cat) (acidic or basic). The formation of the gel is shown in Figure 1. Resorcinol is able to bind formaldehyde in positions 2-, 4- and 6- in its aromatic ring. When sodium carbonate is used as catalyst, the polymerisation reaction between R and FA consists of two main reactions: the addition reaction where hydroxymethyl derivatives are formed and the condensation reaction of the hydroxymethyl derivatives to form methylene (-CH₂-) and methylene ether (-CH₂OCH₂-) bridged compounds (Fig. 1) [12]. The polymerisation reaction results in the formation of clusters, which aggregate into colloidal particles and then form a three-dimensional interconnected structure (gel). The pores are filled with the solvent [12].

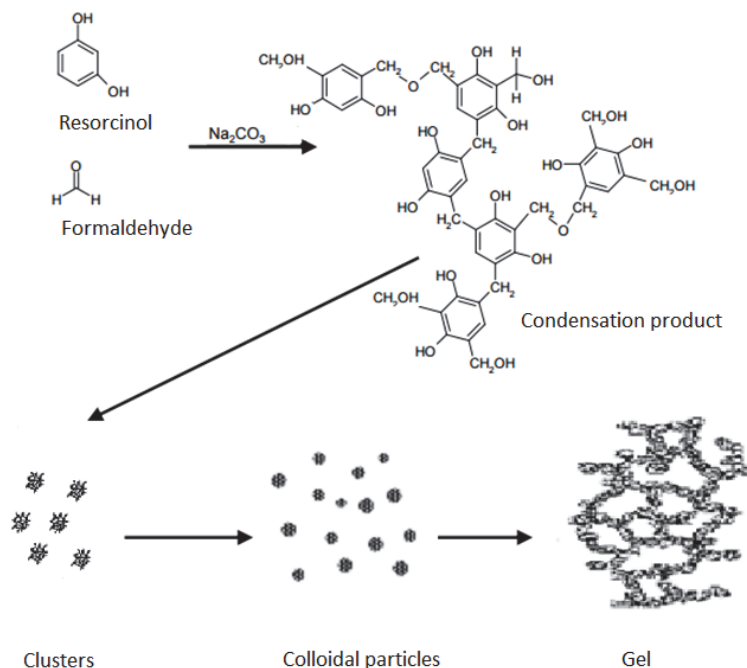


Figure 1. Diagram of the formation of the R-FA gel through sol-gel polymerisation (the figure is adapted and modified from [1]).

The molar ratios of substances can be varied during preparation, which greatly affects the properties of the obtained gel. The molar ratios of R to FA, SOLV to R and R to Cat can all be changed. According to the literature data, the molar ratio of R to FA is usually kept at 0.5 [12] and tuning of the aerogel structure and properties is carried out by changing SOLV to R and R to Cat ratios.

Increasing the amount of solvent (increasing the SOLV to R molar ratio) results in the dilution of the mixture and decreases the density of the obtained gel. Diluting the sol too much will hinder the gel formation though [13]. Decreasing the SOLV to R molar ratio leads to a more dense gel. The higher density of the gel can lead to a decrease in porosity and surface area of the subsequently obtained aerogel [12].

The amount of catalyst (R to Cat molar ratio) has the biggest effect on the properties of R-FA aerogels. Aerogels prepared using high catalyst amounts (the molar ratio of R/Cat is about 50) result in small particles (about 3-5 nm in diameter) that are joined together by large necks, which are referred to as “polymeric“ R-FA aerogels. This produces higher density gels that exhibit substantial shrinkage even during supercritical drying and have high surface areas [8,10,12,14]. Lower catalyst amounts (high R to Cat molar ratios (R/Cat = 200)) result in larger particles (ca 11-14 nm in diameter) that are connected by narrow necks and are referred to as “colloidal“ R-FA aerogels [8,10,12,14]. These gels exhibit little shrinkage during supercritical drying, have lower surface areas and weaker mechanical properties [8].

1.1.2. Drying of gels

To obtain an aerogel, the solvent in the pores of the gel needs to be removed in a way that does not involve crossing the boundary between liquid and gaseous phase, which results in the formation of capillary stresses inside the pores that lead to the destruction of the gel structure. Drying in the atmospheric conditions (the liquid is allowed to evaporate and that causes considerable shrinkage) would lead to the formation of a xerogel, which has higher density and lower surface area. Different drying methods can be used to avoid the collapse of the structure during drying. Among these methods the most popular is supercritical drying.

Supercritical drying involves bringing the solvent in the pores of the gel to the supercritical state. The phase diagram in Figure 2 shows that the idea of the drying is to remove the solvent by at first bringing it from the liquid state (A) to the supercritical state (B) by raising the pressure and temperature above the critical parameters (P_c and T_c). After that the pressure is lowered and the fluid is brought to the gaseous state (C). This avoids crossing the liquid-gas boundary and formation of capillary forces.

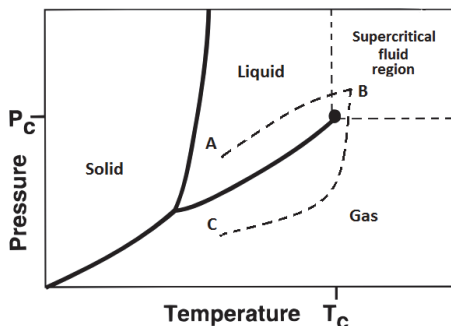


Figure 2. Phase diagram. (Reprinted and modified with permission from [15]. Copyright 1999 American Chemical Society).

For supercritical drying the use of CO_2 is preferred over the other solvents due to the relatively low critical parameters and safety [16]. The solvent inside the pores of the gel needs to be miscible with CO_2 for it to be extracted out of the pores. For example, if the gel has been prepared with water as the solvent, which is not miscible with CO_2 , then it needs to be replaced before drying with another solvent like acetone. This process is diffusion limited and thus time consuming. Later the acetone in the pores of the gel is replaced by liquid CO_2 and then supercritical drying follows.

1.1.3. Pyrolysis and carbon aerogels

Carbon aerogels are prepared by pyrolysing organic aerogels. Pyrolysis (also called carbonization) is a process during which the material is heated in inert (N_2 , Ar or He are most commonly used) atmosphere. This transforms the organic aerogel into a material which is mostly composed of carbon. The properties and structure of the carbon aerogel are affected by the pyrolysis temperature (temperatures from 600 - 2100 °C can be used) [12]. The initial structure of the organic aerogel is largely preserved during pyrolysis, but shrinkage and mass loss (about 20-50 wt%) occur [8,12].

Al-Muhtaseb and Ritter [12] have described the effect of pyrolysis temperature on the properties of the resulting CAs in a review article. Carbon aerogels have a greater density than R-FA organic aerogels. The density of CAs is decreased with increasing pyrolysis temperature, eventually reaching a limiting value at 800 °C [17].

During pyrolysis the burnout of the organic material leads to the formation of new small pores in the solid network of the aerogel. Due to these new micro- and mesopores the surface area of the aerogel increases. However, at higher pyrolysis temperatures (above 600 °C) the surface areas of R-FA aerogels tend to reduce. [10,12,17]. This is because of the shrinkage of the meso- and macropores that were present in the organic aerogel.

Pyrolysis changes the pore sizes of R-FA aerogels, but does not change the trend of pore size distribution [17]. It is possible to control the amount of micropores and mesopores independently, which is one of the advantages of

CAs as a porous carbon material [18]. Micropores can be related to the intra-particle structure, which form during pyrolysis inside the solid aerogel network due to the burn-off of the organic material, whereas mesopores and macropores are related to the inter-particle structure of the aerogel that is formed during gelation [18]. When R-FA aerogels were pyrolysed at 900 °C, micropores were formed due to the formation of new pores in the aerogel structure, but the mesopore volume of the carbon aerogel was smaller than that of the original R-FA OA (probably due to shrinkage of the initial pores in OA) [19].

For carbon aerogels [20] and xerogels [21] to be electrically conductive a pyrolysis temperature above 750 °C is recommended [12]. The formation of graphitic structures in R-FA carbon aerogels can be observed at around 1050 °C [12,22].

1.2. Aerogels prepared from 5-methylresorcinol, 2,6-dihydroxy-4-methylbenzoic acid and melamine

Since instead of resorcinol its derivatives MR and dHMBA and also melamine are used in this work for aerogel preparation, an overview of the previously published results significant for this thesis is given.

1.2.1. 5-methylresorcinol for aerogel preparation

The preparation of organic and carbon aerogels from 5-methylresorcinol and their properties have previously been studied in our laboratory. MR is a phenolic compound which is obtained from the local oil shale industry where it is available as a by-product of oil shale processing. MR is produced by extraction from oil shale retort liquor [23].

MR-FA aerogels were synthesized using a doubly catalysed polycondensation (after gelation the gel was immersed in an acetic acid solution), with Na₂CO₃ as catalyst and supercritically dried with CO₂. Pyrolysis was carried out at temperatures 700 and 1000 °C [24]. 5-methylresorcinol is a trifunctional monomer which is able to react with FA in the 2nd, 4th and 6th positions of the aromatic ring. The formation of the gel was proven to be faster for the MR-FA gel than for R-FA gels and at lower temperature. This was due to an additional directing group (-CH₃) in the 5th position of the aromatic ring. The gel was formed at 25 °C within 100 minutes and was ready for handling after 24 hours [25].

The obtained CAs had properties comparable to those of R-FA aerogels. CAs with a density of 0.13 g/cm³ and specific surface area of over 500 m²/g can be obtained [24]. Aerogels were prepared at different MR to catalyst molar ratios, MR to water molar ratios and pyrolysis temperatures. The highest surface areas for CAs were obtained at a pyrolysis temperature of 900 °C and at an MR to Cat molar ratio of 90 [24].

The morphology of MR-FA carbon aerogels was evaluated by SEM analysis and proved to be similar to that of R-FA CAs as demonstrated in Figure 3. Both

are composed of interconnected particles. The sizes of particles depend on the preparation conditions [1,12].

Overall, MR behaved in a similar way to R during aerogel preparation with similar properties being achieved for aerogels.

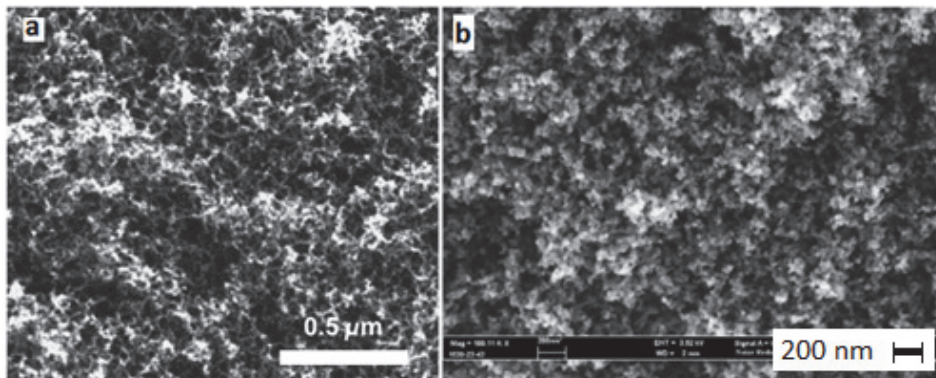


Figure 3. SEM pictures of carbon aerogels: a) a “conventional” R-FA carbon aerogel. Reproduced from [26], with permission from Elsevier; b) a typical MR-FA carbon aerogel. Reproduced from [24], with permission from Elsevier.

1.2.2. 2,6-dihydroxy-4-methylbenzoic acid for aerogel preparation

dHMBA is obtained by synthesizing it from MR [2]. dHMBA is a bifunctional monomer which is capable of forming bonds with FA in two positions of the aromatic ring. It can also act as an acidic catalyst to promote polymerisation [27].

dHMBA and FA without adding a trifunctional monomer like MR will not form a gel. Figure 4 shows that varying the amount of MR and dHMBA changes the aerogels morphology. At higher MR amounts (85/15), the structure of OAs is composed of uniform spherical particles (diameters 24-25 nm), which is similar to that of MR-FA aerogels [1,27]. Increasing the percentage of dHMBA leads to the formation of strings of particles and formation of large macropores (pore diameter > 50 nm) as is the case with aerogels 50/50 and 25/75 [1,27].

The specific surface area of OAs was shown to increase when dHMBA was added. The highest specific surface area and the largest total pore volume, 600 m²/g and 800 mm³/g, respectively, were achieved at a MR/dHMBA ratio of 75/25. Compared to MR-FA OAs, these values are higher [1,27].

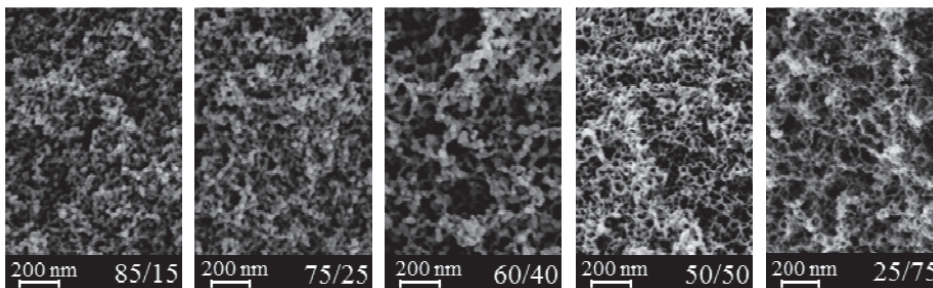


Figure 4. SEM pictures of organic aerogels prepared at different MR/dHMBA ratios. The molar ratio of MR to dHMBA was varied from 85/15 mol% (meaning 85% of moles out of aromatic monomers was MR and 15% of moles was dHMBA) to 25/75 mol%. Reproduced from [1,27].

1.2.3. Melamine for aerogel preparation

Its cheap price and high nitrogen content makes melamine a suitable substance for aerogel preparation. Melamine-formaldehyde (Mel-FA) organic aerogels with low densities, high surface areas, continuous porosity and optical clarity were first prepared by Pekala [10,28]. The Mel-FA OAs can also be pyrolyzed in an inert atmosphere to obtain carbon aerogels.

Figure 5 shows a schematic diagram of the formation of the cross-linked polymer network by the reaction of melamine and formaldehyde. Melamine is a hexafunctional monomer which is capable of reacting at each of the amine hydrogens [28]. During polymerisation diamino methylene (-NHCH₂NH-) and diamino methylene ether (-NHCH₂OCH₂NH-) bridges form [28]. The structure and properties of the aerogel are dependent on the polymerisation conditions. Factors such as pH, reactant ratio, and temperature influence the cross-linking chemistry and growth processes taking place prior to gelation [28].

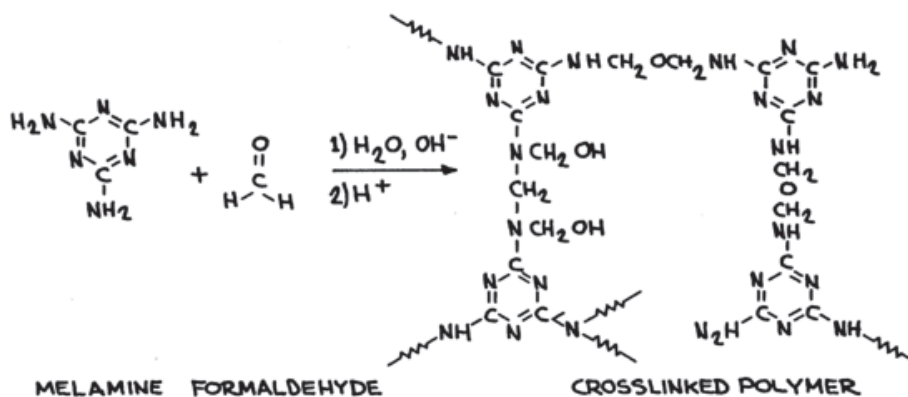


Figure 5. Schematic diagram of the melamine-formaldehyde reaction. Reproduced from [28].

Melamine-formaldehyde aerogels have been prepared by adding other monomers like phenol [29], cresol [30] and resorcinol [31,32,33,34,35] to the sol. The aim is usually to obtain nitrogen containing materials whose microstructure can be fine-tuned.

Carbon aerogels with various molar ratios of resorcinol to melamine have been prepared [33]. Changing the molar ratio of R to Mel allowed control of the nitrogen content in the materials. However, adding melamine reduced the surface areas and microporosity of materials [33]. The addition of melamine also lead to significant changes in the material morphology as seen from SEM pictures (Figure 6). Figure 6a shows the morphology of a typical R-FA CA [12,33], with a particle size ranging from 20-30 nm. A material to which melamine has also been added (Fig. 6b) shows the presence of “interconnected sphere-like nanoparticles“. It was also noted that particle size tended to increase with increasing melamine content [33]. In the case of 1:0.8 R-Mel CA, the decomposition of the spherical structure was observed (Fig. 6c) [33].

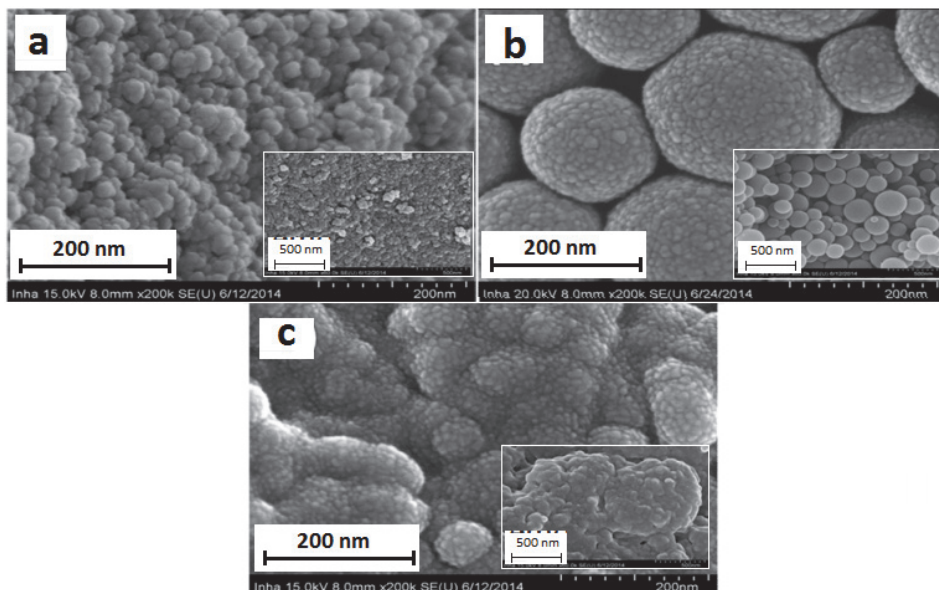


Figure 6. SEM images of CAs prepared at R to Mel molar ratios of a) 1:0, b) 1:0.3 and c) 1: 0. Adapted from [33].

1.3. Metal-doped organic and carbon aerogels

The preparation of metal-doped aerogels has earlier been reviewed once by Moreno-Castilla and Maldonado-Hódar [18]. The purpose of adding metals to the aerogels is to modify their structure, conductivity and catalytic activity. These aerogels can be used as catalysts and electrode materials.

The methods used for doping can be divided into three categories [18]. First method involves the addition of the metal precursor to the initial mixture before gelation. Secondly, the ion-exchange method can be used. In this approach the

gel, which has ion-exchange moieties, is immersed in the solution of metal ions. Lastly, the metal precursor can be deposited on the organic or carbon aerogels by using various deposition methods. Each doping method affects the structure and properties of the resulting materials differently.

An overview of the methods used for metal-doping will be given in the next sub-chapters, with emphasis on the ion-exchange method. The properties of OAs and CAs prepared by using this technique will be discussed in detail. A short description of the other doping methods will be given.

1.3.1. Addition of the metal-precursor to aerogels before gelation

When the metal precursor is dissolved in the sol before gelation, then after gelation the dopant will be trapped within the gel structure. It has been suggested that the metal ions can be chelated by the functional groups of the polymer matrix [8,18,36]. Several different metal ions have been doped into aerogels this way, including Cr-, Mo-, W-, Fe-, Co-, Ni-, Pd-, Pt-, Cu- and Ag-ions [37,38,39,40].

The metal precursors (salts) added to aerogels can also act as catalysts for the polymerisation reaction. An early work by Bekyarova and Kaneko [36] showed that the concentration of the metal dopant and the pH of the reaction mixture can have a profound effect on the structure, porosity and physical properties of aerogels. It was suggested that both the nature of the metal dopant and the change in pH due to adding metal salts affect the sol-gel chemistry. It was found that the Ce- and Zr-doped CAs had developed a larger micropore volume and surface area due to the metals added.

The preparation of metal-doped aerogels by adding metal precursor before gelation has been extensively studied by Moreno-Castilla, Maldonado-Hódar and co-workers. Pt-, Pd- and Ag-doped carbon aerogels were prepared by adding the metal salts to the sol instead of a “typical“ Na_2CO_3 catalyst and it was found that this changed the porous structure of the materials [39]. Furthermore, while studying Fe-, Co-, Ni- and Cu-doped organic aerogels, it was found that depending on the metal salt used, the surface areas, pore volumes and sizes either increased, did not change or decreased compared to the undoped aerogel [40]. This means that each metal affects the polymerisation reaction in a different way.

The fact that metal salts used for doping also influence the polymerisation reaction and therefore the structure of the materials has been confirmed in many subsequent papers [41,42,43]. Adding the metal salt before gelation changes the porous structure of the aerogel and can make its porosity more difficult to control.

Generally a good dispersion of metal particles has been observed in carbon aerogels prepared by this doping method. It has been suggested that it is due to dopant elements being anchored to the carbon structure and thus preventing their migration and growth [18,36]. On the other hand, it has also been claimed that some metal particles can be encapsulated by the carbon matrix and this can

reduce the accessibility of gases and reactants to the metal when they are required for use as catalysts [18,43].

1.3.2. The ion-exchange method for doping with metals

This approach has been pioneered by Baumann and co-workers [44]. The method involves using 2,4-dihydroxybenzoic acid (DHBA) instead of resorcinol. The strategy is to use a resorcinol derivative that contains an ion-exchange moiety which for DHBA is the carboxylic group. This means that each repeat unit of the organic gel is able to bind metal ions and thus ensures a uniform distribution and better control over the content of metal ions. Since the metal precursor is introduced after gelation, it will not interfere with the sol-gel process and the resulting structure of the aerogel.

In a typical experiment, the aerogels would be prepared adding DHBA to the solvent (mostly water) and then K_2CO_3 is added to form a potassium salt of DHBA. Formaldehyde is then added to crosslink the DHBA molecules together and finally the catalyst is added, which is usually K_2CO_3 . The sol is allowed to gel and cure. After that the K^+ doped hydrogels are immersed in an aqueous solution of a desired metal ion. This process is carried out for three days and the metal ion solution is changed every 24 h. Finally the solvent change and drying are carried out.

The copper content in the organic aerogel, which was prepared in the above mentioned procedure, was measured to be 4.4 wt% and in the carbon aerogel 9.2 wt%. For comparison an R-FA aerogel was immersed in the copper solution to determine the role that the ion-exchange moiety plays in the metal ion incorporation [44]. This approach proved ineffective for metal-doping, because most of the copper ions had been washed out during the acetone exchange.

The morphology of Cu-doped DHBA aerogels can be seen in TEM pictures (Fig. 7). The organic aerogel (Fig. 7a) consists of a network of spherical particles with diameters ranging from 15 to 30 nm. No copper particles can be seen, which indicates that the copper ions are distributed throughout the material and have not aggregated [44].

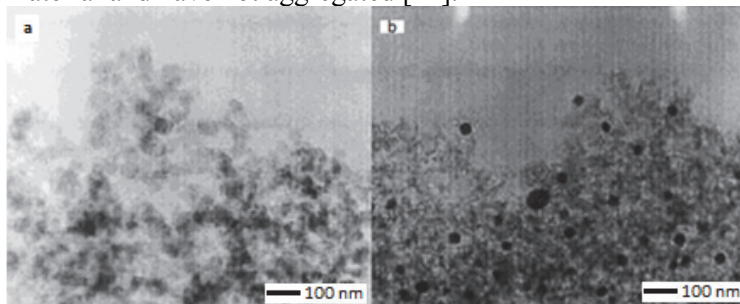


Figure 7. High-resolution transmission electron microscopy (HRTEM) pictures of Cu-doped aerogels: a) organic aerogel; b) carbon aerogel with 1% of Cu after carbonization at 1050 °C. Figure is reprinted with permission from [44]. Copyright 2005 American Chemical Society.

After carbonization at 1050 °C the general morphology of the material is retained (Fig 7b), although the particles forming the aerogel network appear to have slightly shrunk (particle diameter 10-15 nm). In Figure 7b, copper nanoparticles with a diameter from 10 to 50 nm can be seen. This happens due to the reduction of Cu^{2+} ions during pyrolysis. The size of copper nanoparticles depends on the copper content in aerogels, with larger particles forming with higher copper loading. As seen from Fig. 7b the distribution of copper nanoparticles is uniform.

The Cu-doped OAs and CAs exhibited a high surface area (ca 700 m^2/g) and pore diameters from 2 to 20 nm. The metal-doped materials retained the overall porous structure of the metal-free carbon aerogels [44].

The evolution of the morphology of metal-doped carbon aerogels during carbonization was more thoroughly studied for Co- and Ni-doped aerogels [45]. OAs were pyrolysed at temperatures from 300 to 1050 °C and characterised by X-ray diffraction (XRD) and transmission electron microscopy (TEM). The metal contents in the samples were from 9 to 10 wt%. The formation and size of metal nanoparticles were dependent on the carbonization temperature. At 450 °C small Co nanoparticles (ca 2 nm) started to form. With increasing carbonization temperature the size of Co nanoparticles also increased (up to 60 nm at 1050 °C). Based on X-ray photoelectron spectroscopy (XPS) and XRD analysis it was concluded that the Co^{2+} ions were not directly reduced to metal particles at lower pyrolysis temperatures. The XRD analysis results show that at pyrolysis temperatures below 400 °C the peaks corresponding to CoO are present and at 450 °C the peaks corresponding to Co start to emerge as well (Fig. 8a). At 1050 °C the peaks for CoO are not visible, indicating its full reduction (Fig. 8c) [45].

For Ni-doped CAs, small nanoparticles (ca 2-4 nm) started to form at 400 °C and at 1050 °C nanoparticles in the size range of 200-400 nm was observed from TEM pictures [45]. The formation of nickel oxide was not observed by XRD analysis (Fig. 8b,c).

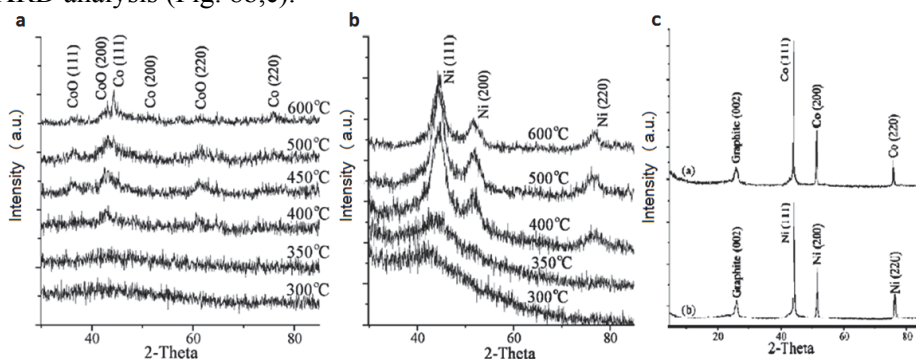


Figure 8. XRD patterns: a) Co-doped aerogels pyrolysed at temperatures 300-600 °C; b) Ni-doped aerogels pyrolysed at temperatures 300-600 °C; c) Co- and Ni-doped aerogels pyrolysed at 1050 °C. Figure is reprinted with permission from [45]. Copyright 2007 American Chemical Society.

The formation of highly ordered carbon structures in Co- and Ni-doped aerogels pyrolysed at 1050 °C was observed [45]. Figure 9a,b shows that carbon structures had formed around Co nanoparticles. Graphitic nanoribbons with width ranging from a few nanometers to 20 nm were observed throughout the CA structure (Fig. 9b). At lower temperatures (600 °C) the formation of graphitic structures in metal-doped aerogels did not occur. Despite the formation of graphitic structures, the surface areas, pore volumes and average pore diameters of the metal free sample, Co-and Ni-doped CA remained similar at 1050 °C [45]. The tendency for some metal-doped aerogels to catalyse the formation of carbon structures at relatively low temperatures has been used before to grow carbon nanotubes [46].

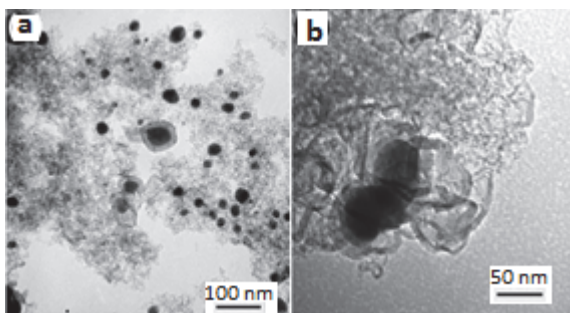


Figure 9. a,b) HRTEM pictures of Co-doped CAs pyrolysed at 1050 °C showing metal nanoparticles and graphitic structures. Figure is reprinted with permission from [45]. Copyright 2007 American Chemical Society.

The differences in the porosity and surface area for metal-doped organic aerogels and their non-metal containing counterparts is quite small when the ion-exchange doping method is used. This was noted for Fe-, Ni- and Cu-doped aerogels [47]. The changes that take place when metal precursors were added before gelation were far more significant [40].

2,4-dihydroxybenzoic acid-formaldehyde (DHBAF) organic aerogels have been prepared by also adding resorcinol to the materials [48]. The results showed that for DHBA and R containing organic aerogels (DHBARF) the surface area, pore volume, pore sizes and ion exchange capacity changed in a systematic fashion when the DHBARF ratio was varied. For DHBARF aerogels prepared with an equal amount of both R and DHBA in the mixture (the molar ratio of R to DHBA was 1:1), the mesopore volume and pore diameters were lower than in R-FA aerogels, but higher than in DHBAF aerogels. Compared to both RF and DHBAF aerogels the surface areas of DHBARF aerogels were the highest. It was also found that in all cases (R-FA, DHBAF and DHBARF aerogels) higher solids content in organic aerogels decreased pore volumes and surface areas [48].

The metal content was experimentally measured for OAs containing 40 to 100 molar percent of DHBA (explanation: 40 mol% of DHBA means there is 60 mol% of R). For both Ni-and Cu-doped OAs the ion-exchange capacity

stayed at its maximum value when at least 50 mol% of DHBA was in the material [48].

1.3.3. Deposition of the metal precursor onto the organic or carbon aerogel

When the metal precursor is deposited onto the already prepared organic or carbon aerogel, then the metal will not affect the formation of the aerogel structure. Different methods for deposition can be used, among them are incipient wetness, adsorption, sublimation and supercritical deposition [18,43,49,50,51,52].

After deposition of the metal precursor, heating of the doped aerogel in an inert atmosphere is usually necessary to reduce the metal precursor to metal particles. Since temperatures high enough for carbonization are not needed when ready-made CAs are doped with metal precursors, then materials with smaller metal nanoparticles can be obtained when lower temperatures (around 300 °C) are used for reduction of metal precursors [51]. The growth and aggregation of metal nanoparticles mainly occur at higher temperatures. For instance, it has been observed that Pt particles of size of a few nanometers were obtained when reduced at 500 °C, but at 1000 °C, the sizes and size distribution of metal nanoparticles had grown to 2-10 nm [52].

In several publications it has been noted that deposition of metal species onto carbon aerogels reduces their porosity [41,51,53]. In an early work Miller and Dunn showed that after doping a CA with a surface area of 700 m²/g with ruthenium precursor, the surface area had decreased to 280 m²/g [51]. Furthermore, the comparison of pore size distributions showed that all the pores with diameters under 2.5 nm had disappeared. The authors suggested that this could be due to the blocking of smaller pores by metal nanoparticles [51].

1.4. Metal-doped organic and carbon aerogels for various applications

As organic and carbon aerogels are materials with highly versatile properties, they show great promise in very different areas of technology. The main application areas for metal-doped aerogels are as catalysts or in various electrical applications. A short description of these application areas will be presented in the next chapter. Also, since in this thesis the lanthanide-doped aerogels have been characterised and tested as supported catalysts and Co-doped aerogels have been studied for use as electrocatalysts for ORR, then an introduction to these areas will also be given.

1.4.1. Metal-doped aerogels as catalysts

The use of carbon aerogels as catalysts has been reviewed before [18]. Their tunable surface area, porosity and pore size distributions make them promising materials for use as catalyst supports. Doping the materials with suitable metals

gives them desired catalytic activity. A few of the reactions where metal-doped CAs have been tested as catalysts are the isomerization reaction of 1-butene [38], synthesis of methyl-tert-butyl ether from methyl alcohol and tert-butyl alcohol [54], toluene combustion reaction [43] and photooxidation or ozonation of micropollutants [55,56]. In all these cases the metal-doped aerogels showed good catalytic activity and were proposed as new promising catalyst materials.

However, the tendency for carbon aerogels to burn-off at elevated temperatures in oxidizing conditions can be a drawback. This has been studied for Pt-doped CAs pyrolysed at 500 and 1000 °C [43]. Under air flow the burn-off of the materials started at temperatures between 300 to 400 °C, with the onset being at a bit higher temperature for the CAs pyrolysed at 1000 °C.

Organic and carbon aerogels have been compared to silica aerogels for use as catalyst supports. The catalytic activity of Pd-doped organic and carbon aerogels prepared from DHBA were compared to the Pd-doped silica aerogel in the Mizoroki-Heck coupling reaction [57]. It was found that the Pd-doped organic and carbon aerogel were more active catalysts than the Pd-doped silica aerogel. The authors suggested that since the use of DHBA enables each repeat unit of the organic polymer to bind metal ions, the uniform distribution of the metal dopant maximizes the contact of the catalyst with the reactants and can explain the difference in catalytic activity between doped organic/carbon and silica aerogels [57].

Different metal-doping methods affect the structure and properties of the resulting catalyst materials differently and thus the materials catalytic activity can be different. This has been studied before by preparing Pt-doped materials in two different ways. The Pt-doped carbon material was prepared by either impregnating of OA in an aqueous solution of the Pt-precursor or by adding the precursor to the initial sol during preparation [43]. The catalytic activity of the materials towards oxidation of toluene was studied and the results showed that both materials proved to be active catalysts and there was only a slight difference in the starting temperature of the combustion. The authors suggested it could have been due to different Pt-particle sizes.

However, when the ion-exchange method is used for metal-doping, the need for a temperature high enough for carbonization, may be a drawback. The catalytic activity of Pt-doped CAs for the oxygen reduction reaction was studied and it was found that at high carbonization temperatures (1050 °C) the platinum nanoparticles became blocked and thus the Pt-doped CA lost its catalytic activity [58]. At lower pyrolysis temperatures some activity of the Pt-doped CA remained. For comparison, when the Pt-doped material was prepared by immersing the CA with the Pt precursor, a chemical reduction instead of high temperatures could be used, so the Pt nanoparticles had small uniform sizes (2-5 nm) and the Pt particles were accessible [58].

Previously in our laboratory the preparation of the Pd-doped 5-methylresorcinol-formaldehyde (MR-FA) carbon aerogel has been studied. The material was prepared by impregnating the MR-FA carbon aerogel with Pd(C₄HF₆O)₂ in supercritical CO₂ and using H₂ for reducing the metal [25]. The

Pd-doped CA showed total conversion in the reduction of cyclooctene into cyclooctane and the material could be used several times.

1.4.2. Lanthanide-doped organic and carbon aerogels

Lanthanides are widely used in organic synthesis because lanthanide-mediated reactions display high chemo- and stereoselectivities [59,60]. Use in the Michael addition reaction is one example.

Lanthanides(III) supported on polymers or ion-exchange resins are developed and studied to take advantage of the catalytic activity of lanthanides on the one hand and the ability of the solid phase to simplify products isolation on the other. The potential use of lanthanide(III) catalysts supported on ion-exchange resins has been demonstrated in routine organic reactions [61]. The preparation of resin-supported catalysts is straightforward, and the resultant catalysts are stable and active under common conditions (acidic conditions and room temperature) in organic synthesis [61].

The support or entrapment of lanthanides or lanthanide species in aerogels or xerogels has been mostly performed with the goal of preparing luminescent materials [62]. The doping of aerogels with lanthanide species for use as supported catalysts has been poorly studied [63].

The europium-doped organic gels, and organic and carbon aerogels have previously been characterised and used as catalysts for the Michael addition reaction [63]. The gels were prepared from DHBA and the ion-exchange method was used for doping with $\text{Eu}(\text{OTf})_3$. The TEM pictures showed that the gel, OA and CA all had nanoparticles in their structure. The presence of various mixed europium oxides, sulphides and fluorides in CAs were confirmed by XRD analysis, as shown in Figure 10 [63]. The gel and OA were amorphous. The materials were tested as catalysts for the Michael addition reaction and the most active were the organic gels with over 90% yield after five cycles. The carbon aerogels did not catalyse the reaction.

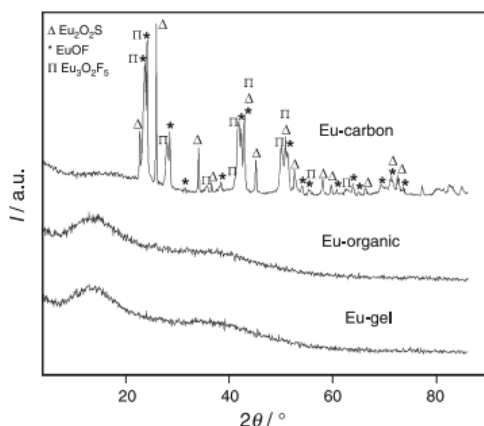


Figure 10. XRD pattern of Eu-doped materials. Reproduced from [63].

1.4.3. Metal-doped carbon aerogels for electrical applications

Carbon aerogels are appropriate materials for electrochemical storage of energy in supercapacitors. Adding metal species to the carbon structure can increase the capacitance values due to pseudocapacitance effects [8,64]. Carbon aerogels doped with the oxides of Ru, Co, Cu, Fe, Mn and Zn have been studied for use in supercapacitors [51,53,65].

For metal-doped carbon aerogels another promising application is as electrocatalysts in proton-exchange membrane fuel cells (PEMFC). The reaction that takes place on the cathode is the oxygen reduction reaction (ORR).

Currently platinum on porous carbon materials is used in almost all commercially available PEM fuel cells. Due to the high cost of Pt, the development of non-precious metal catalysts for PEM fuel cells is one of the most important goals [3,4,5,6,66].

A promising class of catalysts is transition metal-containing nitrogen-doped carbon materials (M/N/C catalysts) that can be prepared by pyrolysis of the carbon support in the presence of the nitrogen precursor and a transition metal (usually Co or Fe) salt [3,4,5]. Since the early studies of ORR on this type of pyrolysed materials by Yeager's group in 1989 [67] the electrocatalytic activity of M/N/C catalysts has been significantly improved and it currently approaches that of commercial Pt/C catalysts in acidic solution [5]. In some cases, their activity can even surpass that of Pt-based catalysts [68,69,70].

Various different carbon materials such as carbon nanotubes, carbon black, graphene and other porous carbon structures can be used for electrode preparation. Carbon aerogels show great promise for use as electrode materials in low-temperature fuel cells because of their high surface area, good electrical conductivity, chemical stability and it is possible to control the porous structure of the material. CAs for use as electrocatalysts in ORR have previously been prepared from various phenolic compounds like resorcinol and its derivatives [58,71,72,73,74,75], melamine [76,77,78], polyacrylonitrile [79], cellulose [80] and sustainable carbohydrate based derivatives like glucose, D-glucosamine aso [81,82].

The use of Pt-doped carbon aerogels for PEM fuel cell applications has been studied previously [58,71,72,73,80,83,84,85]. However, as nowadays most of the research is directed towards development of non-precious metal catalysts, there have also been attempts to prepare non-precious metal-containing carbon aerogels that would have high activity for ORR. This can be done by choosing the right precursors for aerogel preparation or through further modification of aerogels [70].

There are examples where carbon aerogels have previously been doped with nitrogen [81,82] or dual-doped with nitrogen and sulfur [86]. The metal free carbon aerogels showed increased activity towards ORR compared to non-doped materials, but this activity was still rather low [81,82,86]. Carbon aerogels or xerogels can be doped with nitrogen by either using different monomers which contain nitrogen in their structure, like melamine or

polyacrylonitrile [70,76,77,79,87,88] for aerogel preparation or by further modifying aerogels for instance by pyrolysis in a NH_3 atmosphere [74,75].

Doping CAs or xerogels with transition metals has been shown to increase their activity for ORR [74,75,76,77,78,79,89]. The transition metal was introduced either by adding the precursor to the sol before gelation [74,75,76,77] or was added later to the already existing aerogel [89].

For example, nitrogen-and cobalt-doped organic xerogels have been prepared from resorcinol and formaldehyde and tested as catalyts for ORR [74,75]. Cobalt nitrate was added to the materials before gelation. The content of cobalt in the carbonized xerogels was very low however (not higher than about 0.5 wt%). The materials were carbonized under NH_3 atmosphere at 800 °C. These materials showed similar activity to commercial Pt/C in alkaline solution [75], but somewhat lower activity in acidic media [74]. In both cases the catalysts showed good stability. The physical characterisation of the catalysts that were tested in alkaline solution showed that the amorphous carbon materials had metallic cobalt nanoparticles and the prevalent nitrogen species were pyridinic and pyrrolic, which have previously been observed in other active ORR catalysts [75,90,91].

Rather similar activities for ORR in acidic solution were observed for Co- or Fe-doped xerogels prepared from melamine instead of resorcinol [76,77]. Melamine is a good choice because of its affordable price and the high nitrogen content in the molecule.

It has also been shown that varying the melamine/resorcinol ratio in the synthesis of aerogels enables one to adjust the microstructure of the materials [70,78].

2. EXPERIMENTAL

2.1. Reagents

5-methylresorcinol with a reported a purity > 99% was provided by AS VKG, Estonia and 2,6-dihydroxy-4-methylbenzoic acid, with a purity > 99% was provided by AS Carboshale OÜ, Estonia. Sodium acetate ($\text{CH}_3\text{COONa}\cdot 3\text{H}_2\text{O}$), with a purity of 99.7 %, was obtained from Fisher Chemical, USA. The water used was purified employing a Milli-Q water system. Acetonitrile, HPLC purity, was obtained from Rathburn Chemical Ltd., Germany. Formaldehyde (37% w/w solution in water) was purchased from Sigma-Aldrich. CO_2 (99.8%) was obtained from AS Eesti AGA. Melamine, with a purity > 99%, was purchased from Aldrich Chemistry, USA. Anhydrous sodium carbonate with a purity of 99.8% was purchased from Riedel-de Haen, Germany.

Lanthanide (La, Ce, Pr, Nd) carbonates were obtained from AS Silmet (Molycorp), Estonia and were turned into nitrates by adding the carbonates to a stoichiometric amount of nitric acid and evaporating the excess solution.

Cobalt(II)nitrate hexahydrate with a purity > 98%, nickel(II) nitrate hexahydrate with a purity > 97% and copper(II)chloride with a purity > 97% were purchased from Sigma-Aldrich, USA.

2.2. Instrumentation and characterisation

The supercritical extraction system with a double clamp autoclave, 100 ml in volume, was constructed by NWA analytische Meßgeräte GmbH, Germany.

The MTF 12/38/400 pyrolysis oven with a maximum temperature of 1200°C was from Carbolite, England.

The bulk densities of carbon aerogels were calculated by measuring the dimensions and mass of each monolithic sample. Elemental analyses were performed by Spectra AA 220F flame (Agilent, USA) atomic absorption spectrometer (AAS), inductively coupled plasma optical emission spectrometry OPTIMA 7300 DV ICP OES (Perkin Elmer, USA) or using the Vario Micro Cube (Elementar, Germany).

Lanthanide contents were measured using an OPTIMA 7300DV ICP OES (Perkin Elmer). Nitrogen adsorption analyses were performed using a Sorptometer KELVIN 1042 built by Costech International. Helium was used as a carrier gas, nitrogen as an adsorptive gas. The specific surface area (S_{BET}) was calculated according to the Brunauer-Emmett-Teller theory. The specific micropore volume (V_{mic}) was determined *via* the t-plot and the pore size distributions were determined using the Barrett-Johner-Halendar method from the desorption branch. The XRD pattern was recorded with a Rigaku Ultima IV diffractometer (Japan) using a line detector DtexUltra. Cu-K_α radiation was used with a Ni filter for removing K_β radiation. The recorded diffractograms were analysed by Rigaku PDXL software. Energy-filtered transmission electron

microscopy (TEM) was carried out with the Leo 912 Omega microscope (Zeiss, Germany) at 120 kV, using a LaB₆ gun. Raman spectroscopy was carried out using a Raman spectrometer (Horiba Jobin Yvon LabRam HR800, Japan). SEM images were taken using ZEISS ULTRA 55 (Germany) microscope.

Thermogravimetric analysis (TGA) was conducted using a Labsys Evo TG-DTA 1600 °C (Setaram, France) and heating the samples in an Ar atmosphere at 10 °C/min to 800 °C.

2.3. Aerogel preparation

2.3.1. Metal doped aerogels prepared from 5-methylresorcinol and 2,6-dihydroxy-4-methylbenzoic acid

The gels were prepared by adding dHMBA and MR (the molar ratio of MR to dHMBA was either 1:1, 3:1 or 9:1) to the solvent (70 wt% acetonitrile and 30 wt% distilled water). The molar ratio of the solvent to aromatic monomers (MR and dHMBA) was 35:1. The moles of aromatic monomers (AMs) were calculated adding together the moles of MR and dHMBA and the moles for the solvent were calculated adding together the moles of acetonitrile and water. To the solution of aromatic monomers and the solvent a stoichiometric amount of sodium acetate (NaOAc) to dHMBA was added (the molar ratio of NaOAc to dHMBA was 1:1) to obtain the sodium salt of dHMBA. After that formaldehyde (FA) was added (the molar ratio of AM to FA was 1:2) and finally another amount of NaOAc was added as a catalyst (the molar ratio of AM to NaOAc was 50:1).

Glass molds containing the solutions were sealed and the mixture was allowed to gel and cure at 40 °C for seven days. The obtained Na⁺-doped gels were orange in colour and transparent. The gels were then soaked for three days in 0.1 M aqueous solutions of CuCl₂, Co(NO₃)₂ * 6H₂O, Ni(NO₃)₂ * 6H₂O or lanthanide nitrates, respectively. Each time the solution was renewed after every 24 hours. After that the gels were washed by soaking them in water for 24 hours, followed by acetone exchange, which lasted four to five days. Acetone was changed every 24 hours. The gels were dried with supercritical CO₂. A more detailed description of the drying method is published elsewhere [27]. Carbonization was performed in a N₂ atmosphere by raising the temperature to 700 °C (2.5°C/min), from then on to 900 °C (5 °C/min) and was kept at 900 °C for one hour.

2.3.2. Preparation of metal-and nitrogen-doped aerogels

The amounts of substances (in grams) to be used for gel preparation were calculated by the following equation (1):

$$\frac{\text{substances}}{\text{water}} = \frac{\text{monomers} + \text{FA} + \text{Na}_2\text{CO}_3}{\text{water added} + \text{water from FA solution}} = 0.25 \quad (1)$$

The ratio of substances to water was always kept at 0.25. During preparation the amounts of monomers (Mel, MR and dHMBA) were varied from 10 to 75 mol%:

$$\text{mol}\%_1(\text{Mel}) + \text{mol}\%_2(\text{MR}) + \text{mol}\%_3(\text{dHMBA}) = 100\%(\text{monomers}) \quad (2)$$

The amount of sodium carbonate used was calculated adding the amount needed for converting dHMBA into the sodium salt of dHMBA (the molar ratio of dHMBA to Na_2CO_3 was 2) and the catalytic amount (the molar ratio of monomers to Na_2CO_3 was 100). The molar ratio of FA to melamine was 3.7 and that of FA to resorcinol derivatives (MR and dHMBA) was 2. At first two separate solutions were prepared in two vials. In one vial a mixture of Mel, the FA solution and half of the water used was prepared. The mixture was kept at 70 °C for about 25 min to allow melamine to dissolve. In the second vial a mixture of MR, dHMBA, sodium carbonate and half of the water was prepared. Both homogeneous solutions were poured into one vial, mixed and poured into glass test tubes and allowed to gel and cure for four days at 85 °C.

To obtain Co^{2+} -doped gels, the hydrogels were soaked in 0.1 M solution of cobalt nitrate for three days (the solution was changed every 24 hours), after which the sodium ions bound to the ion-exchange moiety (the carboxylic group) were exchanged for cobalt ions.

In order to use the supercritical CO_2 drying for aerogel preparation, the exchange of the solvent for acetone was carried out changing the solution every 24 hours, starting with a 25:75 mixture of acetone and water and proceeding with 50:50 and 75:25 mixtures and finally with 100% acetone for two days. A more detailed description of the method used for supercritical drying has been published elsewhere [27].

Carbon aerogels were prepared by pyrolysis in a N_2 atmosphere by heating at 10 °C/min to 800 °C and keeping at this temperature for one hour. The Co-containing N-doped aerogels prepared using different amounts of monomers are denoted as Co-NCA1, Co-NCA2, etc. (Table 4). For comparison, the nitrogen-free Co-containing carbon aerogel (Co-CA) and the cobalt-free material (NCA) were also prepared. In the latter case, the ion-exchange procedure was not performed.

3. RESULTS

3.1. Co-, Cu- and Ni-doped aerogels

In a previously developed method for the preparation of aerogels from MR and dHMBA, it was suggested that dHMBA in addition to being a monomer also acted as an acidic catalyst [27]. This was not the case with the materials prepared in this work, because NaOAc was also added to the sol, first to exchange the hydrogen proton for sodium ion in the carboxylic moiety and secondly an extra amount of NaOAc was added to act as a catalyst.

In the method developed by Baumann et al [44], potassium carbonate was used to neutralize the solution and as a catalyst, but in our case a stronger gel was obtained using sodium acetate instead. The use of NaOAc in our case resulted in the sol being slightly acidic (pH 5.5) due to the formation of acetic acid and therefore incomplete neutralization of the solution.

The gels containing Na⁺ ions were immersed in the solution of copper ions, after which the Na content in the obtained organic aerogels was measured and was found to be about 0.005 %. For comparison, in the same aerogel that had not been immersed in the solution of copper ions, the Na content was 6.40 %. It confirms that the exchange of sodium ions for copper ions takes place.

The effect that dHMBA has on the metal content in aerogels was studied. Gels at MR to dHMBA molar ratios of 1:1, 3:1 and 9:1 were prepared and dried. The results are shown in Figure 11. It can be seen that by increasing the dHMBA content in aerogels the metal content also increases, which is due to the presence of more ion-exchange moieties. Therefore, changing the MR to dHMBA molar ratio is an easy way to control the metal content in aerogels. The metal content in CAs was mostly higher than in the organic aerogels due to the burn-off of the organic material. CAs prepared at a 1:1 molar ratio of MR to dHMBA had about twice as high metal content as OAs.

In a previous study the ratio of the two phenolic compounds used (R and DHBA) was varied, to evaluate the ion-exchange capacity. Though it was also observed that at lower relative mole fractions of the ion-exchange monomer the ion-exchange capacity decreased, a change in metal content to the same extent as ours was not shown [48].

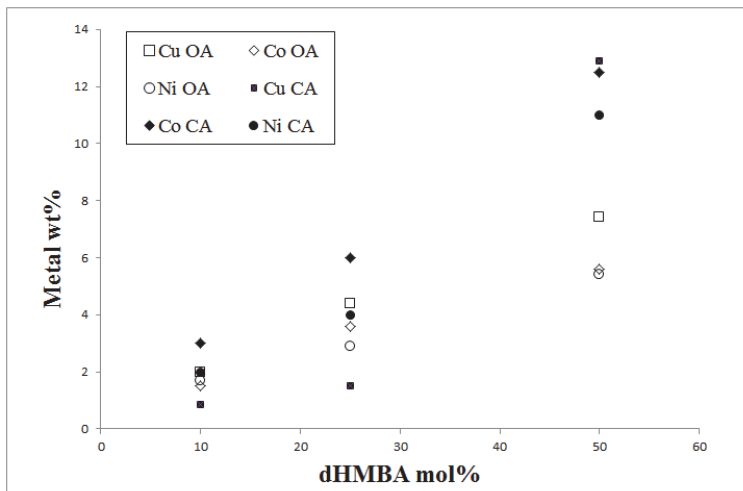


Figure 11. Metal contents in organic and carbon aerogels measured by AAS.

Table 1 presents the densities, specific surface areas and pore volumes of metal-doped carbon aerogels. The densities of organic and carbon aerogels were respectively in the range of 0.45-0.62 g/cm³ and 0.83-1.26 g/cm³. These values were higher than those of metal-doped carbon aerogels prepared from DHBA [92]. A possible explanation is that in our case we used higher solids content to prepare aerogels, which is known to cause higher densities [12].

Table 1 presents the specific surface areas and pore volumes of carbon aerogels doped with different metals. The surface areas and pore volumes of CAs doped with transition metals (Co, Cu, Ni) were larger than those of the corresponding blank sample (containing Na). Similar results have been obtained before for aerogels prepared from DHBA (the blank sample contained potassium) [92].

Table 1. Properties of Co-, Cu- and Ni-doped aerogels

Element	$\delta(\text{OA})$ (g/cm ³)	$\delta(\text{CA})$ (g/cm ³)	S_{BET} (m ² /g)	S_{mic} (m ² /g)	% S_{mic} (%)	V_{TOT} (mm ³ /g)	V_{mic} (mm ³ /g)	% V_{mic} (%)
Na	0.58	0.83	286	133	47	429	47	11
Cu	0.45	1.01	464	291	63	607	103	17
Co	0.62	1.03	519	353	68	610	124	21
Ni	0.59	1.26	379	273	72	446	96	22

Remark: All the samples were prepared at MR to dHMBA molar ratios of 1:1. All the properties measured correspond to those of carbon aerogels, unless otherwise indicated. ρ is the calculated density, S_{BET} is the Brunauer-Emmett-Teller surface area, S_{mic} is the microporous surface area, % S_{mic} is the percent of microporous surface area, V_{TOT} is the total pore volume, V_{mic} is the volume of micropores, % V_{mic} is the percent of microporous volume.

Transition metal-containing aerogels showed higher microporous surface area and microporous pore volume values compared to the Na-containing sample. The percent of microporous area and volume was almost twice as high for aerogels that contained transition metals. The increase in the micropore volume of transition metal-containing CAs could be attributed to the metals contributing to the formation of new microporosity during carbonization [36], or causing a more significant shrinkage of mesopores which due to that become micropores during carbon aerogel preparation [18,47]. The increase in the pore volume of transition metal-containing aerogels was due not only to the increase in microporosity, but also that the non-microporous volume of Cu and Co containing carbon aerogels was larger.

Pore size distributions (PSD) in Figure 12 show that for the Na-containing aerogel the peak in pore size distribution occurs around the pore diameters of 10-15 nm, whereas in the case of all the other doped aerogels the peak maximum is around 5-10 nm. Therefore, in this case, the addition of transition metals resulted in the reduction of pore diameters of carbon aerogels. This result is different from the finding of a previous study, which established that in the case of carbon aerogels made from DHBA, the incorporation of transition metals did not have a significant effect on pore size distributions [92].

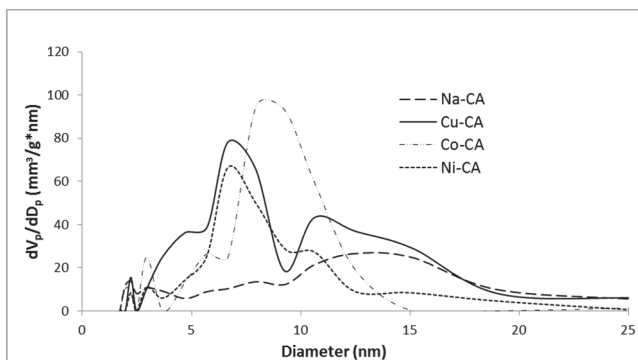


Figure 12. Pore size distributions of metal-doped carbon aerogels, molar ratio of MR to dHMBA was 1:1. The legend shows the metal the carbon aerogel contains.

The X-ray diffraction analysis results for carbon aerogels are shown in Figure 13. The diffractograms indicate the presence of peaks corresponding to metals (oxidation state 0) for all CAs. This implies that the metal ions were reduced during carbonization. For the copper-doped carbon aerogel there is also a peak corresponding to the copper(I)oxide present on the diffractogram. This could be caused by either incomplete reduction of copper during pyrolysis or oxidation afterwards.

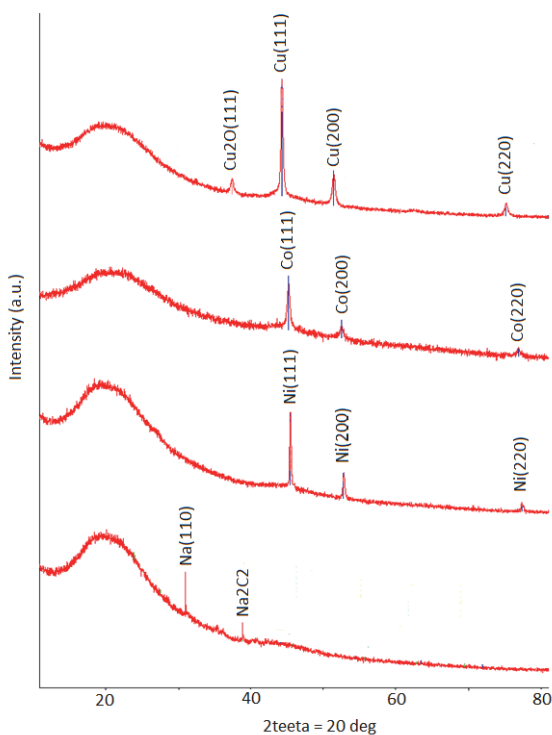


Figure 13. XRD results for metal-doped MR/dHMBA 1:1 aerogels.

TEM pictures of aerogels were taken to study the morphology of the materials. Figure 14a shows an organic aerogel, which before drying was soaked in the solution of cobalt nitrate. No metal nanoparticles were observed in this case, which is in agreement with previous studies where it was also concluded that metal ions were uniformly distributed throughout the organic aerogel [44]. When the same aerogel in presented in Figure 14a was pyrolysed (Figure 14b) the nanoparticles emerged. These were uniformly distributed in the carbon aerogel matrix and their size was in the range of 10-60 nm. Figure 14c and 14d show nickel- and copper-doped carbon aerogels prepared under the same conditions as the previously mentioned Co-doped carbon aerogel. The size of metal nanoparticles in the samples ranged of 20 to 150 nm for nickel-containing carbon aerogels and 3-100 nm for copper-containing carbon aerogels, showing that the metal nanoparticle diameters for different metals varied. In copper-containing carbon aerogels the nanoparticles had also clustered together. The pictures taken of metal-doped CAs from different locations showed that the metal nanoparticles were evenly distributed throughout the material.

Figure 14e shows a carbon aerogel prepared using a smaller amount of dHMBA (the molar ratio of MR to dHMBA was 9:1). It can be seen from the figure that the metal nanoparticles are smaller in size (about 2 to 40 nm) and are

not clustered together. This is due to the smaller amount of metal in the carbon aerogel. It has been observed before that higher metal content leads to larger metal nanoparticles in CAs [44].

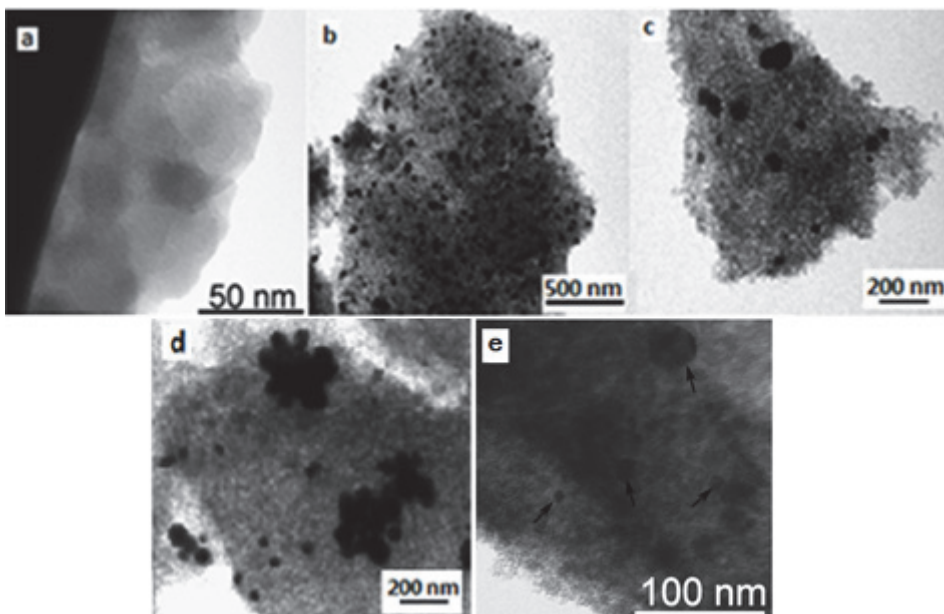


Figure 14. a-d) TEM pictures of MR/dHMBA 1:1 metal-doped aerogels. a) Co-doped organic aerogel; b) Co-doped carbon aerogel; c) Ni-doped carbon aerogel; d) Cu-doped carbon aerogel. e) copper-doped CA with a MR/dHMBA molar ratio of 9:1.

In the SEM picture (Fig 15a) of the Co-doped CA prepared at an MR to dHMBA molar ratio of 1:1, the cobalt nanoparticles are also distinguishable in the aerogel carbon network. A picture taken from the same location using backscattered electron (BSE) imaging shows the areas composed of heavier elements light up, confirming that these are cobalt nanoparticles. The morphology of the carbon aerogel matrix in Fig 15a and c indicates that the structure of the aerogel is similar to that of R-FA aerogels which are described as “polymeric”, meaning that they are composed of small particles that are conjoined by large necks [12].

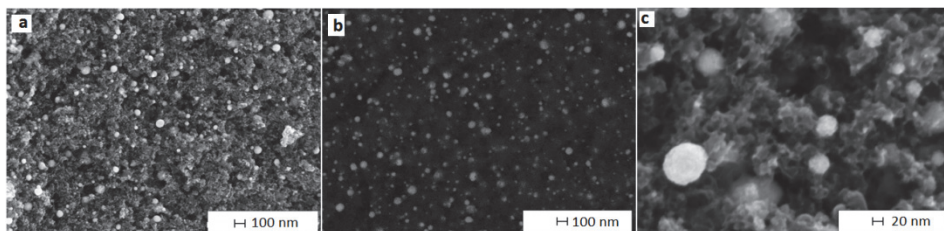


Figure 15. SEM pictures of Co-doped CAs prepared at a MR/dHMBA molar ratio of 1:1. Picture b was taken using backscattered electron imaging.

3.2. Lanthanide-doped aerogels

The same method that was used to prepare Cu-, Co-, and Ni-doped aerogels from MR and dHMBA was employed to make lanthanide-doped (Ln-doped) organic and carbon aerogels. The Ln-doped aerogels were prepared at MR to dHMBA molar ratio of 1:1.

The amount of lanthanides in aerogels was determined by inductively coupled plasma optical emission spectrometry (ICP OES) and the results are given in Table 2. The amount of lanthanides in OAs was about 11 wt% and in CAs 21 wt%, which was higher than in the corresponding Co-, Cu- and Ni-doped aerogels. This can be explained by the higher molecular mass of lanthanide compounds.

Table 2. Properties of La-, Ce-, Pr- and Nd-doped organic and carbon aerogels.

	OA				CA					OA	CA
	ρ (g/cm ³)	S _{BET} (m ² /g)	V _{TOT} (mm ³ /g)	V _{mic} (mm ³ /g)	ρ (g/cm ³)	S _{BET} (m ² /g)	V _{TOT} (mm ³ /g)	V _{mic} (mm ³ /g)	V _{mic} % (%)	Metal ¹ % (%)	Metal ² % (%)
La	0.54	429	889	2.0	1.16	321	477	58	12	11	22
Ce	0.52	393	734	2.5	1.03	368	533	78	15	11	21
Pr	0.53	371	721	3.1	1.14	255	302	55	18	12	21
Nd	0.53	378	659	2.0	1.08	257	301	52	17	11	22

Remark: ρ is the calculated density, S_{BET} is the Brunauer-Emmett-Teller surface area, V_{TOT} is the total pore volume, V_{mic} is the volume of micropores, V_{mic}% is the percent of microporous volume and metal% is the weight percent of metal in aerogels.

Nitrogen adsorption analysis results of organic and carbon aerogels (Table 2) show that the materials were mostly mesoporous. The total pore volume and specific surface area of organic aerogels were higher than those of the corresponding carbon aerogels. The decrease in porosity during pyrolysis can be explained by the shrinkage of pore diameters. Figure 16 shows the pore size distribution for La-doped organic and carbon aerogels. It can be seen that the overall shape of the PSD curve remains the same but it is shifted towards smaller diameters for La-doped CAs.

Organic aerogels have almost no microporous pore volume, while the V_{mic}% of carbon aerogels can be up to 18%. A certain portion of the microporosity was probably formed during pyrolysis by the burn-off of organic material, but some amount was likely generated additionally due to the shrinkage of mesopores [12].

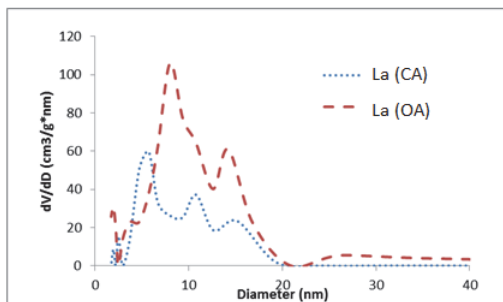


Figure 16. Pore size distribution of La-doped organic and carbon aerogels (MR/dHMBA molar ratio was 1:1).

The morphology of the prepared materials was determined from the TEM and SEM pictures of OAs and CAs, which were taken from different locations and are shown in Figure 17. Both the TEM and SEM pictures show that lanthanide nanoparticles are not distinguishable in the pictures. In previous studies, nanoparticles in metal-doped organic aerogels were also not observed [44,63]. During pyrolysis metal-ions in aerogels tend to reduce and form metal nanoparticles [18]. In this work it was not observed, showing that lanthanides require stronger reducing conditions to form nanoparticles. Except for the lack of metal nanoparticles, the morphology of La-doped CAs (Fig. 17e) is similar to that of the Co-doped CAs (Fig. 15a).

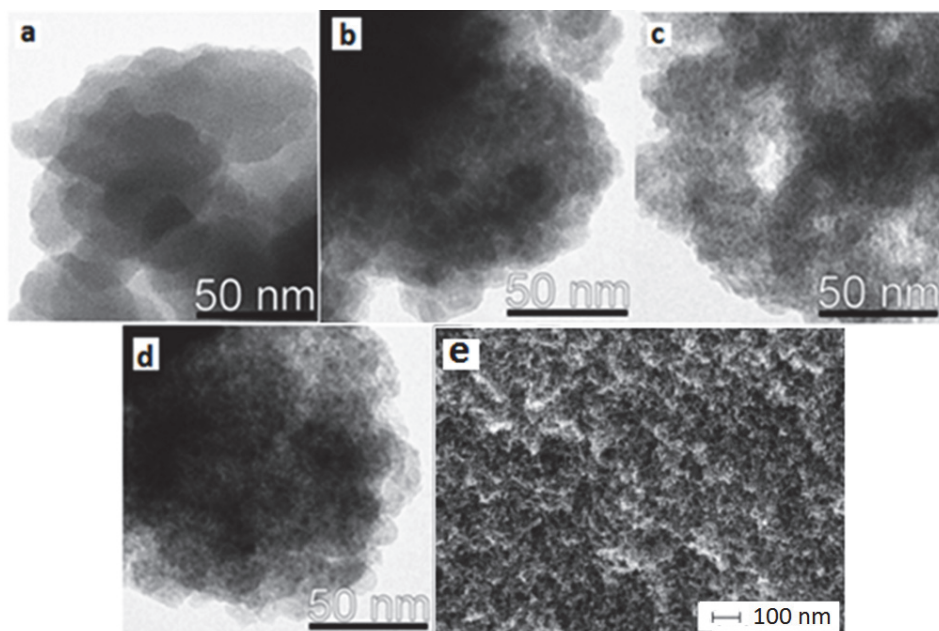


Figure 17. a,b) TEM pictures of a La-doped organic aerogels; c,d) TEM pictures of La-doped carbon aerogels; e) SEM picture of a La-doped carbon aerogel.

The amorphous nature of Ln-doped aerogels was also confirmed by XRD analysis results as shown in Figure 18a. Both La-doped OAs and CAs had no peaks in the diffractogram, which would have referred to the presence of crystal structures in aerogels. For metal-doped carbon aerogels it is common that various crystalline structures like oxides, metals (oxidation state 0) and graphitic structures are formed during pyrolysis [44,45,93], but in this case the material remained amorphous.

Raman spectroscopy on CAs was performed to evaluate the nature of carbon [94]. In Figure 18b the peak at 1590 cm^{-1} (G-band) can be attributed to the $2E_{2g}$ mode, which is present in both ordered and amorphous carbon materials. The peak at 1330 cm^{-1} (D-band) can be attributed to the A_{1g} mode, which is associated with defects in the G layers of the graphenic carbon.

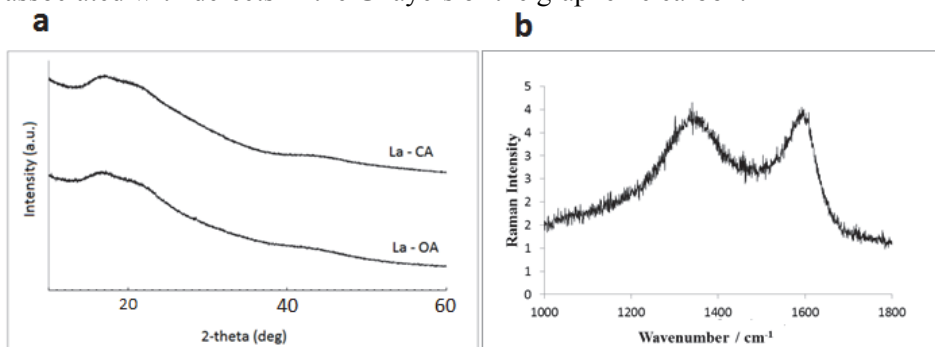
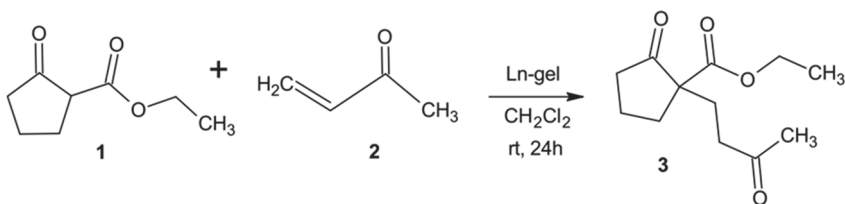


Figure 18. a) XRD analysis results for La-doped organic and carbon aerogels; b) Raman spectra for La-doped CA.

3.3. Lanthanide-doped aerogels as heterogeneous catalysts

The Ln-doped OAs and CAs were tested for use as heterogeneous catalysts in the Michael addition reaction of ethyl 2-oxocyclopentanecarboxylate 1 with 3-buten-2-one 2 (Scheme 1).



Scheme 1. Michael addition reaction of ethyl 2-oxocyclopentanecarboxylate (1) with 3-buten-2-one (2) in the presence of Ln-aerogels as catalysts. 0.006 mmol of the catalyst (3 mol% Ln with respect to the limiting reagent) was carried into the reaction vessel. 0.4 ml of CH_2Cl_2 , 0.6 mmol (excess of 3 times) of 3-buten-2-one and 0.2 mmol of ethyl 2-oxocyclopentanecarboxylate (the limiting reagent) were added and the mixture was stirred at room temperature for 24 hours. Conversion of the product was determined by gas chromatography. For OAs and CAs catalyst loadings of 7.5 mg and 4.0 mg were used, respectively [95].

The results in Table 3 demonstrate that Ln-doped OAs were active catalysts in the Michael addition reaction. The conversions within 24 hours ranged from 82 to 97 %.

La-, Pr- and Nd-doped carbon aerogels also exhibited some activity in the Michael addition reaction, however their activity was lower than that of OAs. In the case of Ce-doped CAs the formation of several by-products was observed. The decrease of catalytic activity of these CAs can be explained by the structural and chemical changes taking place during pyrolysis. After pyrolysis all lanthanide species might not be accessible to the reactants anymore and the lanthanide ions previously bound to the ion-exchange center may have formed new chemical bonds.

In a previous study, a mixture of Eu oxides, sulphides and fluorides had formed during pyrolysis (confirmed by XRD analysis) and the CA did not catalyse the reaction, but the Eu-doped OAs, which did not show crystalline structures in the XRD diffractogram (Figure 18a), was catalytically active [63]. In our case the presence of oxides or other crystalline structures was not detected in the XRD diffractogram of CAs. The TEM and SEM pictures did not show the presence of metal nanoparticles either. The absence of metal oxide nanoparticles could be the reason for our Ln-doped CAs being catalytically active, since it is known that rare-earth metal oxides are mostly inert as catalysts in the Michael addition reaction [63].

Table 3. Conversions for Michael addition reaction of ethyl 2-oxocyclopentanecarboxylate with 3-butene-2-one in the presence of Ln-doped aerogels as catalysts.

Element	Conversion (%)	
	OA	CA
La	84	49
Ce	82	-
Nd	97	92
Pr	91	32

3.4. Co-and N-doped carbon aerogels as electrocatalysts for ORR

To obtain active electrocatalysts for ORR, carbon aerogels were doped with nitrogen and cobalt or iron [70]. Besides MR, dHMBA and FA, melamine was also used as a monomer for gel preparation to introduce nitrogen into the materials. Melamine was chosen because of its affordable price and the presence of pyridinic nitrogen atoms in its molecule, which are expected to be active catalytic sites for ORR [90,91].

The first experiments in which the electrocatalytic activity of Co- or Fe- and N-doped CAs was measured, showed that the Co-doped CAs proved to be more active than the Fe-doped ones [70]. Materials pyrolysed at different

temperatures were also tested for electrocatalytic activity, the ones pyrolysed at 800 °C being the most active.

Subsequently, the composition of CAs was varied during the preparation process, using different amounts of melamine, MR and dHMBA, to study the effect this variation has on the properties of CAs and their activity towards ORR. Table 4 presents the molar percentages of monomers used during the preparation of different CAs and the experimentally measured elemental compositions of the samples. Co-containing N-doped CAs prepared using different amounts of monomers are denoted as Co-NCA1, Co-NCA2, etc. (Table 4). For comparison, nitrogen-free Co-containing CA (Co-CA) and a cobalt-free material (NCA) were also prepared. In the latter case, the ion-exchange procedure was not performed.

Table 4. Properties of Co- and N-doped carbon aerogels.

Sample	Monomers (mol%)			Elemental composition (wt%)				S_{BET} (m ² /g)	V_{TOT} (mm ³ /g)	V_{MIC} (mm ³ /g)	MA
	Mel	MR	dHMBA	Co	N	C	H				
Co-NCA1	30	60	10	2.0	1.6	87.0	1.3	370	330	85	2.8
Co-NCA2	30	45	25	4.3	2.5	82.2	1.0	314	230	70	3.2
Co-NCA3	40	40	20	4.1	2.9	80.2	1.4	461	399	95	3.4
Co-NCA4	60	15	25	5.3	2.6	81.0	0.7	316	228	54	14.4
Co-NCA5	75	0	25	5.6	8.4	68.9	1.2	118	93	1.5	12.5
Co-CA	0	75	25	2.6	0.03	n.d.	n.d.	n.d.	n.d.	n.d.	2.3
NCA	60	15	25	0	14.3	65.2	1.3	n.d.	n.d.	n.d.	0.23

Remark: S_{BET} is the Brunauer-Emmett-Teller surface area, V_{TOT} is the total pore volume, V_{mic} is the volume of micropores, MA is the mass activity (A/g) at -0.2 V.

The molar percentage (mol%) of dHMBA was varied from 10 to 25 mol%. With the increase in the amount of dHMBA in the composition of the aerogel, the Co content also increased (Table 4). This shows that changing the dHMBA amount in the aerogel enables to control the metal content, which is due to dHMBA having the ionexchange moiety (the carboxylic group) that binds Co^{2+} during immersion in the cobalt-nitrate solution. This result is in accordance with previous results of analysing Co-, Cu- and Ni-doped MR/dHMBA aerogels [93].

It was also possible to vary the nitrogen content in the aerogels by changing the melamine content. The nitrogen content in cobalt-containing samples was changed from 1.6 to 8.4 wt% by increasing the amount of melamine (Table 4). The increase in melamine content also decreased the carbon content of aerogels from 87 to 69 wt%.

N_2 -adsorption analysis was used to determine the specific surface areas and pore volumes of CAs (Table 4). Samples Co-NCA1 to Co-NCA4 had high surface areas ($S_{\text{BET}} = 314\text{--}461 \text{ m}^2/\text{g}$) and total pore volumes (V_{TOT}) of 228 to 399 mm³/g. Figure 19a shows the pore size distribution of sample Co-NCA2, indicating that in this material pores with a diameter (d_p) of 2 and 4 nm predominate.

Co-NCA5 had significantly lower S_{BET} and V_{TOT} values compared to samples Co-NCA1 to Co-NCA4. During preparation, Co-NCA5 had the highest

melamine content and no MR was added during preparation. The S_{BET} and V_{TOT} values of the organic aerogel precursor of Co-NCA5 were also measured, the respective figures being $868 \text{ m}^2/\text{g}$ and $1490 \text{ mm}^3/\text{g}$. This indicates that a drastic reduction in specific surface area and pore volume occurred during pyrolysis.

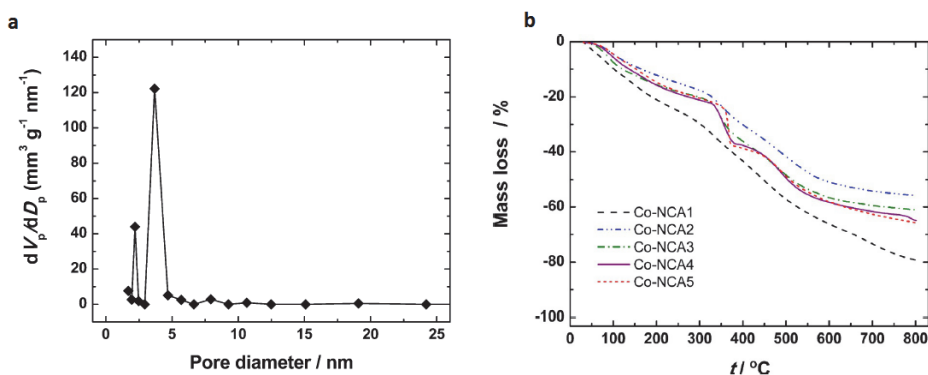


Figure 19. a) Pore size distribution analysis result for Co-NCA2; b) TGA results for materials Co-NCA 1 – Co-NCA 5. Samples analysed were pre-pyrolysed (organic aerogels).

Thermogravimetric analysis (TGA) results illustrated in Figure 19b show the mass-loss curves for organic aerogels (precursors of Co-NCA1–Co-NCA5) during heating in an Ar atmosphere using the same heating program that was used during pyrolysis for the Co-NCA materials. The mass loss of those OAs was between 56 and 80%. Samples that were prepared using higher melamine contents (Co-NCA3 to Co-NCA5) had similar mass losses (60–65 wt%). The mass-loss curves for Co-NCA1 and Co-NCA2 were smooth in shape, without abrupt changes. However, for Co-NCA4 and Co-NCA5, there was a steep change in mass at 340–370 °C. From literature it can be found that melamine resins also experienced significant mass loss, owing to the decomposition and evaporation of the products generated in the above temperature range [96]. The decomposition of melamine and, therefore, the structure of the material could explain the smaller surface area and porosity of CAs that were prepared using higher melamine contents.

The surface morphology of CAs was evaluated using scanning electron microscopy (Figure 20). The pictures were taken from different locations on the material. The morphology of the CA that was prepared using the highest MR content (Co-NCA1) was similar to that of resorcinol/formaldehyde CAs [12], with a grainy structure composed of linked spheres (Figure 20a and 20b). The Co-NCA2 aerogel was prepared using more dHMBA and less MR than for Co-NCA1. In the structure of Co-NCA2 (Figure 20d), separate particles forming the aerogel network were not visible and the morphology was different from that of resorcinol/formaldehyde CAs. This was also the case with samples prepared using higher melamine contents (Co-NCA4 and Co-NCA5), whose surfaces appear to be composed of particles that have merged together (Fig.

20h-k). This demonstrates that the addition of resorcinol derivatives is necessary to keep the bead-like structure that is associated with resorcinol/formaldehyde CAs. The structure of melamine-rich aerogels will be affected by the sudden mass loss and decomposition of melamine during pyrolysis [96].

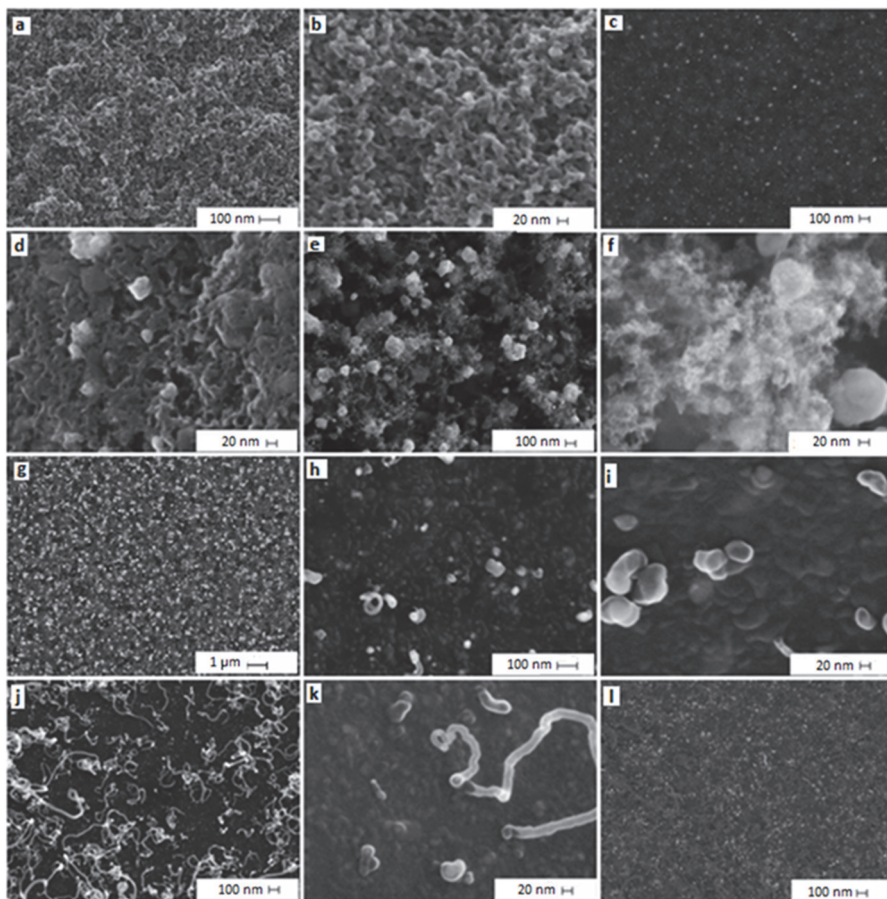


Figure 20. SEM images for a, b) Co-NCA1, c) Co-NCA1 (backscattered electron imaging), d) Co-NCA2, e–g) Co-NCA3, h, i) Co-NCA4, j, k) Co-NCA5 and l) Co-NCA5 (backscattered electron imaging taken at the same spot as in Figure 5j).

Figure 20c shows a SEM image of Co-NCA1 taken using backscattered electron (BSE) imaging, where brighter spots may be assigned to Co nanoparticles. These were evenly distributed in the sample and had sizes ranging from 5 to 40 nm (Figures 20a–c). The cobalt nanoparticles in Co-NCA3 were also evenly distributed (Figure 20g), but their sizes were larger (10–100 nm) than in Co-NCA1 (Figures 20e and 20f). This was caused by the increased amount of metal in the aerogel [44,93]. Samples Co-NCA4 and Co-NCA5 (Fig. 20h–l) had smaller nanoparticles (10–40 nm) than Co-NCA3, and their SEM images indicated the formation of long cylindrical structures with a diameter of

about 20 nm, which appeared to be carbon nanotubes (CNTs) or nanoribbons (Figures 20h,j,k). The BSE image (Figure 20j,l) shows brighter spots (Co nanoparticles) at the end of the long structures.

Cobalt nanoparticles are known to be used as catalysts for synthesis of CNTs [97]. The growth of nanoribbons has been observed before in cobalt-doped carbon aerogels [45]. From nitrogen-containing precursors, N-doped CNTs have been synthesised previously [98,99], so it is possible that the long carbon nanostructures in Co-NCA4 and Co-NCA5 are also nitrogen-doped CNTs [100].

Figure 21 shows X-ray diffraction (XRD) peaks for crystalline Co in all samples, which is an expected result under these pyrolysis conditions [45,93]. A small peak attributed to Co_3O_4 indicates to the oxidation of the surface of Co nanoparticles. The formation of graphitic structures is visible in samples Co-NCA1 and Co-NCA2. In Co-NCA5, a peak at the same location cannot be identified. This indicates that the increasing melamine content inhibits the formation of graphitic structures in this case. In the diffraction patterns shown in Figure 21, there are a few other small peaks visible at various degrees. The identification of these peaks is problematic, due to the limited amount of data. It is likely that various cobalt-carbon, cobalt-nitrogen or nitrogen-carbon structures have also formed in CAs.

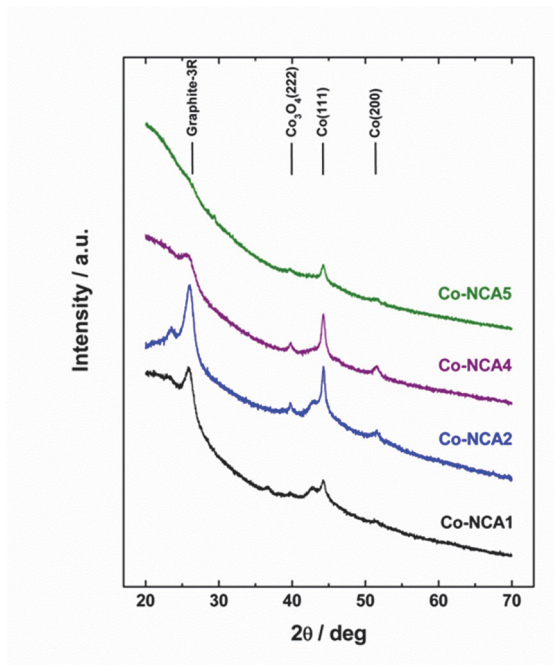


Figure 21. XRD analysis results for the Co-NCA materials.

3.5. Oxygen reduction reaction activity of Co-NCA catalysts

The electrocatalytic activity of the materials for ORR was studied using the rotating disk electrode (RDE) method in 0.1 M KOH solution [100]. RDE voltammetry curves of O₂ reduction for materials Co-NCA1 - Co-NCA5 are shown in Figure 22a. Co-NCA 4 and Co-NCA 5 were the most active. These materials had the highest cobalt content. The increased activity towards ORR has previously been observed for Co₃O₄-containing N-doped graphene [101]. The activity increased with higher Co content. Both the Co- and Co₃O₄ nanoparticles, which were observed in the XRD diffractogram for Co-NCAs (Fig. 21), could attribute to the ORR activity, according to the literature [101,102,103,104].

Compared to Co-NCA4, the nitrogen content of Co-NCA5 was significantly higher, although their activities were similar. This suggests that only a small fraction of nitrogen is composing the active centres for ORR and the remaining part is either in a passive form or inaccessible to O₂ molecules [100]. According to the literature, only certain types of nitrogen centres are considered to be involved in ORR electrocatalysis [5] and the activity of the catalysts does not directly depend on the total nitrogen content [105].

The surface area and pore volume of Co-NCAs do not seem to have a great effect on the ORR activity of the materials, because Co-NCA5, which has a low surface area and porosity, has a similar activity to Co-NCA4, whose S_{BET} and V_{TOT} values are much higher. However, the nanotubes or nanoribbons observed in Co-NCA4 and Co-NCA5 may contribute to their activity [100]. Both the metal-free and transition metal-containing N-doped CNTs have been shown to be very active catalysts for ORR in alkaline solutions [106,107,108].

The activity of the prepared Co-NCAs for ORR has been compared to that of Co- and N-free materials and also a commercial Pt/C catalyst (20 wt% Pt catalyst supported on Vulcan carbon XC-72(E-TEK)) [100]. Figure 22b shows that the activity of CA which contained nitrogen, but no cobalt (material marked NCA in Fig. 22b), had a much lower ORR activity than the Co-NCA materials. However, the ORR activity of the Co-CA material (contained cobalt, but no nitrogen), was higher than that of NCA, but still lower than for Co-NCA4. This suggests that the synergistic effect of cobalt or cobalt-oxide nanoparticles with nitrogen is what gives the Co-NCAs their high activity for ORR. This has also been proposed previously in literature [101,102,109].

Compared to the commercial Pt/C catalyst the Co-NCA4 was slightly less active (Fig. 22b). However in a short-term stability test the Co-NCA4 proved to be more stable [100].

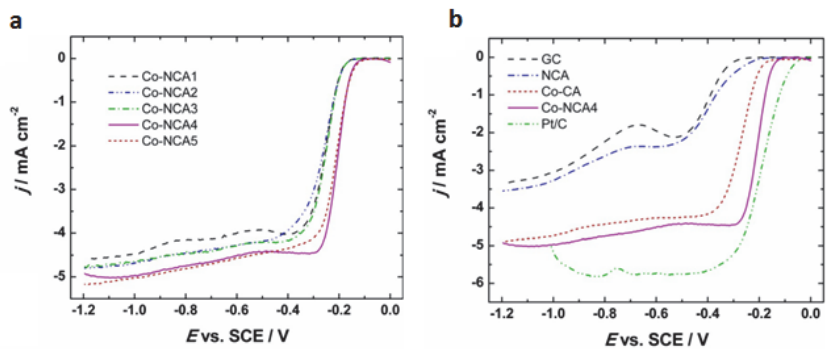


Figure 22. RDE voltammetry curves of oxygen reduction reaction for a) Co-containing N-doped CAs and b) for various CA-based catalysts, glassy carbon (GC) and Pt/C catalyst in O_2 -saturated 0.1 M KOH; $n=10 \text{ mVs}^{-1}$, $w=1900 \text{ rpm}$ [100].

4. CONCLUSIONS

In this work, a method for preparing metal-doped organic and carbon aerogels from 5-methylresorcinol and 2,6-dihydroxy-4-methylbenzoic acid was developed. The specific conclusions drawn are the following:

- The ion-exchange method was used to dope organic and carbon aerogels with Co, Cu, Ni, Ce, La, Nd and Pr.
- It was shown that this method allows one to easily control the metal content in aerogels. In Co-, Cu- and Ni-doped aerogels varying the MR to dHMBA molar ratio during preparation enabled changing the metal content in organic aerogels from around 1 to 8 wt% and in carbon aerogels from around 1 to 15 wt%. Ln-doped aerogels had metal contents of approximately 12 and 22 wt% for OAs and CAs, respectively. All the metal-doped organic and carbon aerogels had high specific surface areas (ca 250-520 m²/g) and pore volumes (ca 300-900 mm³/g). During pyrolysis Co-, Cu- and Ni-ions were reduced and metal nanoparticles formed in carbon aerogels. The size of nanoparticles ranged from 3 to 150 nm depending on the type and amount of the metal used for doping. However, the Ln-doped CAs remained amorphous and metal nanoparticles were not observed in their structure.
- Ce-, La-, Nd- and Pr-doped OAs and CAs were tested as catalysts for the Michael addition reaction. Organic aerogels containing different lanthanides catalysed the Michael addition reaction efficiently, with conversions ranging from 82 to 97 %. For carbon aerogels the conversion was modest, 32 % (Pr-doped) to high, 92 % (Nd-doped).
- To prepare active catalysts for the oxygen reduction reaction, the incorporation of nitrogen into the structure of CAs was necessary. A method for preparing Co- and N-doped carbon aerogels from MR and dHMBA was developed using melamine for nitrogen doping. The results showed that by varying the dHMBA or melamine content, the composition of CAs may be altered. Co-NCAs showed high surface area and had both meso- and microporosity. The increasing amount of melamine in the composition of aerogels decreased their surface area and pore volume. The morphology of the materials also changed drastically with increasing melamine amount. All the CAs had crystalline structures of cobalt and cobalt oxide as well as cobalt nanoparticles present in these materials. In CAs prepared using higher melamine and cobalt concentrations, carbon nanotube structures had also formed.
- The Co- and N-doped carbon aerogels were tested as electrocatalysts for the oxygen reduction reaction. The electrocatalytic activity of the materials for this reaction was rather high and depended on their composition. The materials with the highest Co content showed the highest activity for oxygen reduction reaction, which can be associated with the coexistence of cobalt nanoparticles and N-doped carbon structures in them.

REFERENCES

- ¹ Peikolainen, A. L. Organic aerogels based on 5-methylresorcinol: thesis on natural and exact sciences B115. Tallinn, Tallinn University of Technology, 2011.
- ² Crombie, L., Games, D. E., James, A. W. G. Reactions of fused and unfused α -pyrones with magnesium alkoxide, sodium alkoxide and water as the nucleophile: effects of chelation. - *Journal of the Chemical Society, Perkin Transactions 1*, 1996, 22, 2715-2724.
- ³ Jaouen, F., Proietti, E., Lefevre, M., Chenitz, R., Dodelet, J. P., Wu, G., Chung, H. T., Johnston, C. M., Zelenay, P. Recent advances in non-precious metal catalysis for oxygen-reduction reaction in polymer electrolyte fuel cells. - *Energy & Environmental Science*, 2011, 4(1), 114-130.
- ⁴ Chen, Z. W., Higgins, D., Yu, A. P., Zhang, L., Zhang, J. J. A review on non-precious metal electrocatalysts for PEM fuel cells. - *Energy & Environmental Science*, 2011, 4(9), 3167-3192.
- ⁵ Wu, G., Zelenay, P. Nanostructured nonprecious metal catalysts for oxygen reduction reaction. *Accounts of Chemical Research*, 2013, 46(8), 1878-1889.
- ⁶ Wood, K. N., O'Hayre, R., Pylypenko, S. Recent progress on nitrogen/carbon structures designed for use in energy and sustainability applications. - *Energy & Environmental Science*, 2014, 7(4), 1212-1249.
- ⁷ Kistler, S. S. Coherent expanded aerogels and jellies. - *Nature*, 1931, 127, 741-741.
- ⁸ a) Mulik, S., Sotiriou-Leventis, C. Resorcinol-formaldehyde aerogels. In Aegerter, M. A. (Ed.-in-Ch.), Leventis, N. (Ed.), Koebel, M. M. (Ed.), *Aerogels Handbook*, 2011, 215-234, Springer; b) Shen, J., Guan, D. Y. Preparation and application of carbon aerogels. In Aegerter, M. A. (Ed.-in-Ch.), Leventis, N. (Ed.), Koebel, M. M. (Ed.), *Aerogels Handbook*, 2011, 813-834, Springer.
- ⁹ Pekala, R. W. Low density, resorcinol-formaldehyde aerogels.- US Patent 4 873 218, 1989.
- ¹⁰ Pekala, R. W., Alviso, C. T., Kong, F. M., Hulsey, S. S. Aerogels derived from multifunctional organic monomers. - *Journal of Non-Crystalline Solids*, 1992, 145, 90-98.
- ¹¹ White, R. J., Brun, N., Budarin, V. L., Clark, J. H., Titirici, M. M. Always look on the "light" side of life: sustainable carbon aerogels. - *CHEMSUSCHEM*, 2014, 7(3), 670-689.
- ¹² Al-Muhtaseb, S. A., Ritter, J. A. Preparation and properties of resorcinol-formaldehyde organic and carbon gels. - *Advanced Materials*, 2003, 15, 101-114.
- ¹³ Zhang, R., Li, W., Li, K., Lu, C., Zhan, L., Ling, L. Effect of concentration of reactants on porosity of hydrogels, organic and carbon aerogels. - *Microporous and Mesoporous Materials*, 2004, 72, 167-173.
- ¹⁴ Gebert, M., Pekala, R. Fluorescence and light-scattering studies of sol-gel reactions. - *Chemistry of Materials*, 1994, 6(2), 220-226.
- ¹⁵ Darr, J. A., Poliakoff, M. New directions in inorganic and metal-organic coordination chemistry in supercritical fluids. - *Chemical Reviews*, 1999, 99, 495-542.
- ¹⁶ García-González, C. A., Camino-Rey, M. C., Alnaief, M., Zetzl, C., Smirnova, I. Supercritical drying of aerogels using CO₂: Effect of extraction time on the end material textural properties. - *Journal of Supercritical Fluids*, 2012, 66, 297-306.
- ¹⁷ Zhang, S. Q., Wang, J., Shen, J., Deng, S., Lai, Z. Q., Zhou, B., Attia, S. M., Chen, L. Y. The investigation of the adsorption character of carbon aerogels. - *Nanostructured Materials*, 1999, 11(3), 375-381.

-
- ¹⁸ Moreno-Castilla, C., Maldonado-Hódar, F. J. Carbon aerogels for catalysis applications: An overview. - *Carbon*, 2005, 43(3), 455-465.
- ¹⁹ Tamon, H., Ishizaka, M., Mikami, M., Okazaki, M. Porous structure of organic and carbon aerogels synthesized by sol-gel polycondensation of resorcinol with formaldehyde. - *Carbon*, 1997, 35(6), 791-796.
- ²⁰ Kim, S. J., Hwang, S. W., Hyun, S. H. Preparation of carbon aerogel electrodes for supercapacitor and their electrochemical characteristics. - *Journal of Materials Science*, 2005, 40(3), 725-731.
- ²¹ Lin, C., Ritter, A., Popov, B. N. Correlation of double-layer capacitance with the pore structure of sol-gel derived carbon aerogels. - *Journal of Electrochemical Society*, 1999, 146(10), 3639-3649.
- ²² Kuhn, J., Brandt, R., Mehling, H., Petricevic, R., Fricke, J. In situ infrared observation of the pyrolysis process of carbon aerogels. - *Journal of Non-Crystalline Solids*, 1998, 225, 58-63.
- ²³ <http://www.vkg.ee/eng/products-and-services/vkg-oil-as/phenols-and-phenol-products/total-oil-shale-phenols> (17.10.16)
- ²⁴ Perez-Caballero, F., Peikolainen, A. L., Uibu, M., Kuusik, R., Volobujeva, O., Koel, M. Preparation of carbon aerogels from 5-methylresorcinol-formaldehyde gels. - *Microporous and Mesoporous Materials*, 2008, 108, 230-236.
- ²⁵ Perez-Caballero, F., Peikolainen, A. L., Koel, M., Herbert, M., Galindo, A., Montilla, F. Preparation of the catalyst support from the oil-shale processing by-product. - *The Open Petroleum Engineering Journal*, 2008, 1, 42-46.
- ²⁶ Merzbacher, C. I., Meier S. R., Pierce, J. R., Korwin M. L. Carbon aerogels as broadband non-reflective materials. - *Journal of Non-Crystalline Solids*, 2001, 285, 210-215.
- ²⁷ Peikolainen, A. L., Volobujeva, O., Aav, R., Uibu, M., Koel, M. Organic acid catalyzed synthesis of 5-methylresorcinol based organic aerogels in acetonitrile. - *Journal of Porous Materials*, 2012, 19(2), 189-194.
- ²⁸ Pekala, R. W. Melamine-formaldehyde aerogels. - US Patent 5086085 A, 1992.
- ²⁹ Long, D. H., Liu, X. J., Qiao, W. M., Zhang, R., Zhan, L., Ling, L. C. Molecular design of polymer precursors for controlling microstructure of organic and carbon aerogels. - *Journal of Non-Crystalline Solids*, 2009, 355, 1252-1258.
- ³⁰ Zhang, R., Lu, Y. G., Zhan, L., Liang, X. Y., Wu, G. P., Ling L. C. Monolithic carbon aerogels from sol-gel polymerization of phenolic resoles and methylolated melamine. - *Carbon*, 2003, 41(8), 1660-1663.
- ³¹ Vesela, P., Slovak, V. Pyrolysis of N-doped organic aerogels with relation to sorption properties. - *Journal of Thermal Analysis and Calorimetry*, 2012, 108, 475-480.
- ³² Chen, S., Li, L., Lin, W. Non-noble metal-carbonized nitrogen-doped aerogel composites as electrocatalysts for the oxygen reduction reaction. - *International Conference on Materials for Renewable Energy and Environment (ICMREE)*, 2013, 1-3, 424-428.
- ³³ Jeon, D. H., Min, B. G., Oh, J. G., Nah, C., Park, S. J. Influence of nitrogen moieties on CO₂ capture of Carbon Aerogel. - *Carbon Letters*, 2015, 16(1), 57-61.
- ³⁴ Rasines, G., Lavela, P., Macias, C., Zafra, M. C., Tirado, J. L., Parra, J. B., Ania, C. O. N-doped monolithic carbon aerogel electrodes with optimized features for the electrosorption of ions. - *Carbon*, 2015, 83, 262-274.
- ³⁵ Rasines, G., Lavela, P., Macias, C., Zafra, M. C., Tirado, J. L., Ania, C. O. On the use of carbon black loaded nitrogen-doped carbon aerogel for the electrosorption of sodium chloride from saline water. - *Electrochimica Acta*, 2015, 170, 154-163.

- ³⁶ Bekyarova, E., Kaneko, K. Structure and physical properties of tailor-made Ce,Zr-doped carbon aerogels. - *Advanced Materials*, 2000, 12(21), 1625-1628.
- ³⁷ Yoshizawa, N., Hatori, H., Soneda, Y., Hanzawa, Y., Kaneko, K., Dresselhaus, M. S. Structure and electrochemical properties of carbon aerogels polymerized in the presence of Cu²⁺. - *Journal of Non-crystalline Solids*, 2003, 330, 99-105.
- ³⁸ Moerno-Castilla, C., Maldonado-Hódar, F. J., Rivera-Utrilla, J., Rodriguez-Castellón, E. Group 6 metal oxide-carbon aerogels. Their synthesis, characterization and catalytic activity in the skeletal isomerization of 1-butene – *Applied Catalysis A: General*, 1999, 183, 345-356.
- ³⁹ Maldonado-Hódar, F. J., Ferro-Garcia, M. A., Rivera-Utrilla, J., Moerno-Castilla, C. Synthesis and textural characteristics of organic aerogels, transition-metal-containing organic aerogels and their carbonized derivatives. - *Carbon*, 1999, 37(8), 1199-1205.
- ⁴⁰ Maldonado-Hódar, F. J., Moreno-Castilla, C., Perez-Cadenas, A. F. Surface morphology, metal dispersion, and pore texture of transition metal-doped monolithic carbon aerogels and steam-activated derivatives. - *Microporous and Mesoporous Materials*, 2004, 69, 119-125.
- ⁴¹ Czakkel, O., Geissler, E., Szilagy, I. M., Szekely, E., Laszlo, K. Cu-doped resorcinol-formaldehyde (RF) polymer and carbon aerogels. - *Journal of Colloid and Interface Science*, 2009, 337(2), 513-522.
- ⁴² Czakkel, O., Geissler, E., Moussaid, A., Koczka, B., László, K. Copper-containing resorcinol-formaldehyde networks. - *Microporous and Mesoporous Materials*, 2009, 126(3), 213-221.
- ⁴³ Maldonado-Hódar, F. J., Moreno-Castilla, C., Pérez-Cadenas, A. F. Catalytic combustion of toluene on platinum-containing monolithic carbon aerogels. - *Applied Catalysis B: Environmental*, 2004, 54(4), 217-224.
- ⁴⁴ Baumann, T. F., Fox, G. A., Satcher J. H., Yoshizawa, N., Fu, R. W., Dresselhaus, M.S. Synthesis and characterization of copper-doped carbon aerogels. - *Langmuir*, 2002, 18, 7073-7076.
- ⁴⁵ Fu, R. W., Baumann, T. F., Cronin, S., Dresselhaus, G., Dresselhaus, M. S., Satcher, J. H. Formation of graphitic structures in cobalt-and nickel-doped carbon aerogels. - *Langmuir*, 2005, 21(7), 2647-2651.
- ⁴⁶ Steiner, S. A., Baumann, T. F., Kong, J., Satcher, J. H., Dresselhaus, M. S. Iron-doped carbon aerogels: novel porous substrates for direct growth of carbon nanotubes. - *Langmuir*, 2007, 23(9), 5161-5166.
- ⁴⁷ Carrott, P. J. M., Marques, L. M., Ribeiro Carrott, M. M. L. Characterisation of the porosity of polymer and carbon aerogels containing Fe, Ni or Cu prepared from 2,4-dihydroxybenzoic acid by n-nonane pre-adsorption and density functional theory. – *Microporous and Mesoporous Materials*, 2010, 131, 75-81.
- ⁴⁸ Carrott, P. J. M., Marques, L. M., Ribeiro Carrott, M. M. L. Core-shell polymer aerogels prepared by co-polymerisation of 2,4-dihydroxybenzoic acid, resorcinol and formaldehyde. - *Microporous and Mesoporous Materials*, 2012, 158, 170-174.
- ⁴⁹ Lin, C., Ritter, J. A., Popov, B. N. Development of carbon-metal oxide supercapacitors from sol-gel derived carbon-ruthenium xerogels. - *Journal of Electrochemical Society*, 1999, 146(9), 3155-3160.
- ⁵⁰ Pajonk, G. M., Rao, A. V., Pinto, N., Ehrburger-Dolle, F., Gil, M.B. Monolithic carbon aerogels for fuel cell electrodes - *Preparation of Catalysts VII*, 1998, 118, 167-174.
- ⁵¹ Miller, J. M., Dunn, B. Morphology and electrochemistry of ruthenium/carbon aerogel nanostructures - *Langmuir*, 1998, 15, 799-806.

-
- ⁵² Saquing, C. D., Cheng, T. T., Aindow, M., Erkey, C. Preparation of Platinum/Carbon aerogel nanocomposites using a supercritical deposition method. – *Journal of Physical Chemistry B*, 2004, 108(23), 7716-7722.
- ⁵³ Li, J., Wang, X., Huang, Q., Dai, C., Gamboa, S., Sebastian, P. J. Preparation and characterization of RuO₂ center dot xH₂O/carbon aerogel composites for supercapacitors. – *Journal of Applied Electrochemistry*, 2007, 37(10), 1129-1135.
- ⁵⁴ Mukai S. R., Sugiyama T., Tamon H. Immobilization of heteropoly acids in the network structure of carbon gels. – *Applied Catalysis A-General*, 2003, 256, 99-105.
- ⁵⁵ Sánchez-Polo, M., Rivera-Utrilla, J. Photooxidation of naphthalene sulphonic acids in presence of transition metal-doped carbon aerogels. – *Applied Catalysis B-Environmental*, 2006, 69, 93-100.
- ⁵⁶ Sánchez-Polo, M., Rivera-Utrilla, J., Mendez-Díaz, J., López-Peñalver, J. Metal-doped carbon aerogels. New materials for water treatments. – *Industrial & Engineering Chemistry Research*, 2008, 47, 6001-6005.
- ⁵⁷ Martínez, S., Vallribera, A., Cotet, C. L., Popovici, M., Martín, L., Roig, A., Moreno-Mañas, M., Molins, E. Nanosized metallic particles embedded in silica and carbon aerogels as catalysts in the Mizoroki-Heck coupling reaction. – *New Journal of Chemistry*, 2005, 29, 1342-1345.
- ⁵⁸ Marie, J., Berthon-Fabry, S., Achard, P., Chatenet, M., Pradourat, A., Chainet, E. Highly dispersed platinum on carbon aerogels as supported catalysts for PEM fuel cell-electrodes: comparison of two different synthesis paths. – *Journal of Non-Crystalline Solids*, 2004, 350, 88-96.
- ⁵⁹ For reviews on lanthanides as catalysts see: a) Kobayashi, S., Yamashita, Y. Alkaline earth metal catalysts for asymmetric reactions. – *Accounts of Chemical Research*, 2011, 44, 58-71; b) Shibasaki, M., Kanai, M., Matsunaga, S., Kumagai, N. Recent Progress in Asymmetric Bifunctional Catalysis Using Multimetallic Systems. – *Accounts of Chemical Research*, 2009, 42(8), 1117-1127; c) Yao, Y., Nie, K. Homogeneous Catalysis. In D. A. Atwood (Ed), *The Rare Earth Elements; Fundamentals and Applications*, 2012, 459-474, John Wiley&Sons Ltd; d) Walrod, J. H., Atwood, D. A. Heterogeneous Catalysis. In D.A. Atwood (Ed), *The Rare Earth Elements; Fundamentals and Applications*, 2012, 475-479, John Wiley&Sons Ltd.
- ⁶⁰ For applications of lanthanides in organic synthesis, see: a) Molander, G. A. Application of lanthanide reagents in organic-synthesis. – *Chemical Reviews*, 1992, 92, 29-68; b) Marshman, R. Rare-earth triflates in organic-synthesis. – *Aldrichimica Acta*, 1995, 28(3), 77-84; c) Mori, Y., Kobayashi, S. Organic Synthesis. In D. A. Atwood (Ed), *The Rare Earth Elements; Fundamentals and Applications*, 2012, 437-458, John Wiley&Sons Ltd.
- ⁶¹ Yu, L., Chen, D., Li, J., Wang, P.G. Preparation, characterization, and synthetic uses of lanthanide(III) catalysts supported on ion exchange resins. – *Journal of Organic Chemistry*, 1997, 62(11), 3575-3581.
- ⁶² For references on lanthanide doped silica xerogels see: a) Klonkowski, A. M., Lis, S., Pietraszkiewicz, M., Hnatejko, Z., Czarnobaj, K., Elbanowski, M. Luminescence properties of materials with Eu(III) complexes: Role of ligand, coligand, anion, and matrix. – *Chemistry of Materials*, 2003, 15(3), 656-663; b) Zaitoun, M. A., Goken, D. M., Bailey, L. S., Kim, T., Lin, C. T. Thermoanalysis and emission properties of Eu³⁺/Eu²⁺ in Eu³⁺-doped xerogels. – *Journal of Physical Chemistry B*, 2000, 104(4), 189-196; c) Embert, F., Mehdi, A., Reye, C., Corriu, R. J. P. Synthesis and luminescence properties of monophasic organic-inorganic hybrid materials incorporating europium(III). – *Chemistry of Materials*, 2001, 13(12), 4542-4549.

-
- ⁶³ Martínez, S., Martín, L., Molins, E., Moreno-Manas, M., Roig, A., Vallribera, A. Europium-containing organic gels and organic and carbon aerogels. Preparation and initial applications in catalysis. *Monatshefte für Chemie*, 2006, 137, 627-633.
- ⁶⁴ Frackowiak, E., Beguin, F. Carbon materials for the electrochemical storage of energy in capacitors. – *Carbon*, 2001, 39, 937-950.
- ⁶⁵ Lee, Y. J., Jung, J. C., Park, S., Seo, J. G., Baeck, S. H., Yoon, J. R., Yi, J., Song, I. K. Preparation and characterization of metal-doped carbon aerogel for supercapacitor. - *Current Applied Physics*, 2010, 10(3), 947-951.
- ⁶⁶ Higgins, D. C., Chen, Z. Recent progress in non-precious metal catalysts for pem fuel cell applications. - *Canadian Journal of Chemical Engineering*, 2013, 91, 1881–1895.
- ⁶⁷ Gupta, S., Tryk, D., Bae, I., Aldred, W., Yeager, E. Heat-treated polyacrylonitrile-based catalysts for oxygen electroreduction. – *Journal of Applied Electrochemistry*, 1989, 19, 19–27.
- ⁶⁸ a) Chung, H. T., Won, J. H., Zelenay, P. Active and stable carbon nanotube/nanoparticle composite electrocatalyst for oxygen reduction. - *Nature Communications*, 2013, 4, 1922; b) Fu, X. G., Liu, Y. R., Cao, X. P., Jin, J. T., Liu, Q., Zhang, J. Y. FeCo-N-x embedded graphene as high performance catalysts for oxygen reduction reaction. - *Applied Catalysis B – Environmental*, 2013, 130, 143–151; c) Kong, A. G., Zhu, X. F., Han, Z., Yu, Y. Y., Zhang, Y. B., Dong, B., Shan, Y. K. Ordered hierarchically micro- and mesoporous Fe-N-x-embedded graphitic architectures as efficient electrocatalysts for oxygen reduction reaction. - *ACS Catalysis*, 2014, 4, 1793–1800; d) Yin, H., Zhang, C., Liu, F., Hou, Y. Hybrid of iron nitride and nitrogen-doped graphene aerogel as synergistic catalyst for oxygen reduction reaction. - *Advanced Functional Materials*, 2014, 24, 2930–2937.
- ⁶⁹ a) Niu, K. X., Yang, B. P., Cui, J. F., Jin, J. T., Fu, X. G., Zhao, Q. P., Zhang, J. Y. Graphene-based non-noble-metal Co/N/C catalyst for oxygen reduction reaction in alkaline solution. - *Journal of Power Sources*, 2013, 243, 65–71; b) Kong, A. G., Kong, Y. Y., Zhu, X. F., Han, Z., Shan, Y. K. Ordered mesoporous Fe (or Co)-N-graphitic carbons as excellent non-precious-metal electrocatalysts for oxygen reduction. - *Carbon*, 2014, 78, 49–59.
- ⁷⁰ Sarapuu, A., Samolberg, L., Kreek, K., Koel, M., Matisen, L., Tammeveski, K. Cobalt- and iron-containing nitrogen-doped carbon aerogels as non-precious metal catalysts for electrochemical reduction of oxygen. - *Journal of Electroanalytical Chemistry*, 2015, 746, 9–17.
- ⁷¹ Baker, W. S., Long, J. W., Stroud, R. M., Rolison, D. R. Sulfur-functionalized carbon aerogels: a new approach for loading high-surface-area electrode nanoarchitectures with precious metal catalysts. – *Journal of Non-Crystalline Solids*, 2004, 350, 80–87.
- ⁷² Marie, J., Berthon-Fabry, S., Chatenet, M., Chainet, E., Pirard, R., Cornet, N., Achard, P. Platinum supported on resorcinol-formaldehyde based carbon aerogels for PEMFC electrodes: influence of the carbon support on electrocatalytic properties. – *Journal of Applied Electrochemistry*, 2007, 37, 147–153.
- ⁷³ Kim, G. P., Lee, M., Lee, Y. J., Bae, S., Song, H. D., Song, I. K., Yi, J. Polymer-mediated synthesis of a nitrogen-doped carbon aerogel with highly dispersed Pt nanoparticles for enhanced electrocatalytic activity. - *Electrochimica Acta*, 2016, 193, 137-144.
- ⁷⁴ Jin, H., Zhang, H. M., Zhong, H. X., Zhang, J. L. Nitrogen-doped carbon xerogel: A novel carbon-based electrocatalyst for oxygen reduction reaction in proton exchange membrane (PEM) fuel cells. - *Energy and Environmental Science*, 2011, 4, 3389–3394.

- ⁷⁵ Liu, S. S., Zhang, H. M., Xu, Z., Zhong, H. X., Jin, H. Nitrogen-doped carbon xerogel as high active oxygen reduction catalyst for direct methanol alkaline fuel cell. - *International Journal of Hydrogen Energy*, 2012, 37(24), 19065–19072.
- ⁷⁶ Yang, W., Chen, S. Z., Lin, W. M. Oxygen reduction on non-noble metal electrocatalysts supported on N-doped carbon aerogel composites. - *International Journal of Hydrogen Energy*, 2012, 37, 942–945.
- ⁷⁷ Zhong, H. X., Zhang, H. M., Liu, S. S., Deng, C. W., Wang, M. R. Nitrogen-enriched carbon from melamine resins with superior oxygen reduction reaction activity. - *ChemSusChem*, 2013, 6, 807–812.
- ⁷⁸ Chen, S. Z., Yang, Y., Chen, W. P., Li, L. W., Zou, H. B. Synthesis of Co-loaded carbon aerogels for oxygen electro-reduction. - *New Carbon Materials*, 2013, 28, 454–460.
- ⁷⁹ Ye, S. Y., Vijh, A. K. Cobalt-carbonized aerogel nanocomposites electrocatalysts for the oxygen reduction reaction. - *International Journal of Hydrogen Energy*, 2005, 30(9), 1011–1115.
- ⁸⁰ Guilminot, E., Fischer, F., Chatenet, M., Rigacci, A., Berthon-Fabry, S., Achard, P., Chainet, E. Use of cellulose-based carbon aerogels as catalyst support for PEM fuel cell electrodes: electrochemical characterization. - *Journal of Power Sources*, 2007, 166(1), 104–111.
- ⁸¹ Wohlgemuth, S. A., Fellingner, T. P., Jaker, P., Antonietti, M. Tunable nitrogen doped carbon aerogels as sustainable electrocatalysts in the oxygen reduction reaction. - *Journal of Materials Chemistry A*, 2013, 1, 4002–4009.
- ⁸² Brun, N., Wohlgemuth, S. A., Osiceanu, P., Titirici, M. M. Original design of nitrogen-doped carbon aerogels from sustainable precursors: application as metal-free oxygen reduction catalysts. - *Green Chemistry*, 2013, 15, 2514–2524.
- ⁸³ Job, N., Maillard, F., Marie, J., Berthon-Fabry, S., Pirard, J. P., Chatenet, M. Electrochemical characterization of Pt/carbon xerogel and Pt/carbon aerogel catalysts: first insights into the influence of the carbon texture on the Pt nanoparticle morphology and catalytic activity. - *Journal of Materials Science*, 2009, 44, 6591–6600.
- ⁸⁴ Ye, S. Y., Vijh, A. K., Dao, L.H. A new fuel cell electrocatalyst based on carbonized polyacrylonitrile foam – the nature of platinum-support interactions. - *Journal of Electrochemical Society*, 1997, 144, 90–95.
- ⁸⁵ Ouattara-Brigaudet, M., Berthon-Fabry, S., Beauger, C., Chatenet, M., Job, N., Sennour, M., Achard, P. Influence of the carbon texture of platinum/carbon aerogel electrocatalysts on their behavior in a proton exchange membrane fuel cell cathode. - *International Journal of Hydrogen Energy*, 2012, 37(12), 9742–9757.
- ⁸⁶ Wohlgemuth, S.A., White, R. J., Willinger, M. G., Titirici, M. M., Antonietti, M. A one-pot hydrothermal synthesis of sulfur and nitrogen doped carbon aerogels with enhanced electrocatalytic activity in the oxygen reduction reaction. - *Green Chemistry*, 2012, 14, 1515–1523.
- ⁸⁷ Long, D. H., Zhang, J., Yang, J. H., Hu, Z. J., Cheng, G., Liu, X. M., Zhang, R., Zhan, L., Qiao, W. M., Ling, L. C. Chemical state of nitrogen in carbon aerogels issued from phenol-melamine-formaldehyde gels. - *Carbon*, 2008, 46(9), 1259–1262.
- ⁸⁸ Ruben, G.C., Pekala, R.W. High-resolution transmission electron-microscopy of the nanostructure of melamine-formaldehyde aerogels. - *Journal of Non-Crystalline Solids*, 1995, 186, 219–231.
- ⁸⁹ Smirnova, A., Wender, T., Goberman, D., Hu, Y. L., Aindow, M., Rhine, W., Sammes, N. M. Modification of carbon aerogel supports for PEMFC catalysts. - *International Journal of Hydrogen Energy*, 2009, 34, 8992–8997.

-
- ⁹⁰ Qu, L. T., Liu, Y., Baek, J. B., Dai, L. M. Nitrogen-doped graphene as efficient metal-free electrocatalyst for oxygen reduction in fuel cells. - *ACS Nano*, 2010, 4, 1321-1326.
- ⁹¹ Byon, H. R., Suntivich, J., Shao-Horn, Y. Graphene-based non-noble-metal catalysts for oxygen reduction reaction in acid. - *Chemistry of Materials*, 2011, 23, 3421-3428.
- ⁹² Cotet, L. C., Gich, M., Roig, A., Popescu, I. C., Cosoveanu, V., Molins, E., Danciu, V. Synthesis and structural characteristics of carbon aerogels with a high content of Fe, Co, Ni, Cu, and Pd. - *Journal of Non-Crystalline Solids*, 2006, 352, 2772-2777.
- ⁹³ Kreek, K., Kulp, M., Uibu, M., Mere, A., Koel, M. Preparation of metal-doped carbon aerogels from oil shale processing by-products. - *Oil Shale*, 2014, 31, 185-194.
- ⁹⁴ Ferrari, A. C., Robertson, J. Interpretation of Raman spectra of disordered and amorphous carbon. - *Physical Review B*, 2000, 6, 14095-14107.
- ⁹⁵ Kreek, K., Kriis, K., Maaten, B., Uibu, M., Mere, A., Kanger, T., Koel, M. Organic and carbon aerogels containing rare-earth metals: Their properties and application as catalysts. - *Journal of Non-Crystalline Solids*, 2014, 404, 43-48.
- ⁹⁶ Merline, D. J., Vukusic, S., Abdala, A. A. Melamine formaldehyde: curing studies and reaction mechanism. - *Polymer Journal*, 2013, 45, 413-419.
- ⁹⁷ Prasek, J., Drbohlavova, J., Chomoucka, J., Hubalek, J., Jasek, O., Adam, V., Kizek, R. Methods for carbon nanotubes synthesis-review. - *Journal of Materials Chemistry*, 2011, 21, 15872-15884.
- ⁹⁸ Liu, H., Zhang, Y., Li, R. Y., Sun, X. L., Desilets, S., Abou-Rachid, H., Jaidann, M., Lussier, L. S. Structural and morphological control of aligned nitrogen-doped carbon nanotubes. - *Carbon*, 2010, 48, 1498-1507.
- ⁹⁹ Yao, Y., Zhang, Q., Shi, J. Y., Zhang, Q. H. Preparation of nitrogen-doped carbon nanotubes with different morphologies from melamine-formaldehyde resin. - *ACS Applied Materials & Interfaces*, 2015, 7, 7413-7420.
- ¹⁰⁰ Kreek, K., Sarapuu, A., Samolberg, L., Joost, U., Mikli, V., Koel, M., Tammeveski, K. Cobalt-containing nitrogen-doped carbon aerogels as efficient electrocatalysts for the oxygen reduction reaction. - *Chemelectrochem*, 2015, 2, 2079-2088.
- ¹⁰¹ Liang, Y. Y., Li, Y. G., Wang, H. L., Zhou, J. G., Wang, J., Regier, T., Dai, H. J. Co₃O₄ nanocrystals on graphene as a synergistic catalyst for oxygen reduction reaction. - *Nature Materials*, 2011, 10, 780-786.
- ¹⁰² Su, Y. H., Zhu, Y. H., Jiang, H. L., Shen, J. H., Yang, X. L., Zou, W. J., Chen, J. D., Li, C. Z. Cobalt nanoparticles embedded in N-doped carbon as an efficient bifunctional electrocatalyst for oxygen reduction and evolution reactions. - *Nanoscale*, 2014, 6, 15080-15089.
- ¹⁰³ Kong, A. G., Mao, C. Y., Lin, Q. P., Wei, H., Bu, X. H., Feng, P. Y. From cage-in-cage MOF to N-doped and Co-nanoparticle-embedded carbon for oxygen reduction reaction. - *Dalton Transactions*, 2015, 44, 6748-6754.
- ¹⁰⁴ Lv, L. B., Ye, T. N., Gong, L. H., Wang, K. X., Su, J., Li, X. H., Chen, J. S. Anchoring cobalt nanocrystals through the plane of graphene: highly integrated electrocatalyst for oxygen reduction reaction. - *Chemistry of Materials*, 2015, 27, 544-549.
- ¹⁰⁵ Kottakkat, T., Bron, M. One-pot synthesis of cobalt-incorporated nitrogen-doped reduced graphene oxide as an oxygen reduction reaction catalyst in alkaline medium. - *ChemElectroChem*, 2014, 1, 2163-2171.
- ¹⁰⁶ Wang, Z. L., Xiao, S., Zhu, Z. L., Long, X., Zheng, X. L., Lu, X. H., Yang, S. H. Cobalt-embedded nitrogen doped carbon nanotubes: a bifunctional catalyst for oxygen

electrode reactions in a wide pH range. - *ACS Applied Materials & Interfaces*, 2015, 7, 4048–4055.

¹⁰⁷ a) Vikkisk, M., Kruusenberg, I., Joost, U., Shulga, E., Tammeveski, K. Electrocatalysis of oxygen reduction on nitrogen-containing multi-walled carbon nanotube modified glassy carbon electrodes. – *Electrochimica Acta*, 2013, 87, 709–716;
b) Vikkisk, M., Kruusenberg, I., Ratsos, S., Joost, U., Shulga, E., Kink, I., Rauwel, P., Tammeveski, K. Enhanced electrocatalytic activity of nitrogen-doped multi-walled carbon nanotubes towards the oxygen reduction reaction in alkaline media. - *RSC Advances*, 2015, 5, 59495–59505.

¹⁰⁸ Ma, Z. L., Guo, C. Z., Yin, Y. J., Zhang, Y. Q., Wu, H. J., Chen, C. G. The use of cheap polyaniline and melamine co-modified carbon nanotubes as active and stable catalysts for oxygen reduction reaction in alkaline medium. – *Electrochimica Acta*, 2015, 160, 357–362.

¹⁰⁹ Odedairo, T., Ma, J., Gu, Y., Zhou, W., Jin, J., Zhao, X. S., Zhu, Z. H. A new approach to nanoporous graphene sheets via rapid microwave-induced plasma for energy applications. - *Nanotechnology*, 2014, 25, 495604.

ACKNOWLEDGEMENTS

This research was carried out at the Chair of Analytical Chemistry in the Department of Chemistry at Tallinn University of Technology (TUT).

First of all, I would like to thank my supervisor, lead research scientist Mihkel Koel, for supporting me with advice and ideas. He has encouraged me throughout the years and helped to initiate various interesting collaborations.

Secondly, AS VKG and AS Carboshale are acknowledged for donating chemicals.

I would like to thank all of the people who have helped me carry out the research presented in this work. The following people are acknowledged for their involvement in this research: Mai Uibu and Tiit Kaljuvee from the Laboratory of Inorganic Materials at TUT; Maria Kulp, Anu Viitak and Tiina Aid from the Chair of Analytical Chemistry at TUT; Birgit Maaten, Kadri Kriis and Tõnis Kanger from the Chair of Organic Chemistry at TUT; Valdek Mikli from the Chair of Semiconductor Materials Technology at TUT, Arvo Mere from the Laboratory of Thin Film Chemical Technologies at TUT; Kriztian Kordas from the Microelectronics Research Unit at University of Oulu; Ave Sarapuu, Lars Samolberg and Kaido Tammeveski from Chair of Colloid and Environmental Chemistry at University of Tartu.

For financial support Estonian Ministry of Education and Research (PUT391) is acknowledged and EU Structural Funds project “Electroactive nanoporous carbon composite films technology” No 3.2.1101.12-0007. This work has partially been supported by the graduate school “Functional materials and technologies”. SA Archimedes is acknowledged for DoRa activity T6, T8 and Pluss 1.1.

ABSTRACT

In this thesis a method for preparing metal-doped organic and carbon aerogels was developed, the materials were characterised and tested as heterogeneous catalysts. The aerogels were prepared from 5-methylresorcinol (MR), which is a by-product of the local oil shale processing industry, and 2,6-dihydroxy-4-methylbenzoic acid (dHMBA), which can easily be synthesized from MR. dHMBA has an ion-exchange moiety (carboxylic group) that allowed the ion-exchange method to be used for metal-doping. The materials were doped with metals such as Co, Cu, Ni, La, Ce, Pr and Nd.

The properties of the materials and their dependence on the preparation conditions were discussed. The structure and morphology of metal-doped carbon aerogels were characterised using methods like nitrogen adsorption analysis, scanning electron microscopy, transmission electron microscopy, X-ray diffraction analysis, different elemental analysis techniques, etc.

It was shown that the developed method allowed us to easily control the metal content in aerogels. Varying the MR to dHMBA molar ratio in Co-, Cu- and Ni-doped aerogels during preparation enabled to change the metal content in organic aerogels from around 1 to 8 wt% and in carbon aerogels from around 1 to 15 wt%. Ln-doped aerogels had metal contents of approximately 12 and 22 wt% for OAs and CAs, respectively. All the metal-doped organic and carbon aerogels had high specific surface areas (about 250-520 m²/g) and pore volumes (about 300-900 mm³/g). The materials were micro- and mesoporous. During pyrolysis the Co-, Cu- and Ni-ions present in organic aerogels were reduced and metal nanoparticles formed in carbon aerogels. The size of nanoparticles ranged from 3 to 150 nm, depending on the type and amount of metal used for doping. However, the Ln-doped CAs remained amorphous and metal nanoparticles were not observed in their structure.

Ce-, La-, Nd- and Pr-doped OAs and CAs were tested as catalysts for the Michael addition reaction. The initial results showed that organic aerogels containing different lanthanides catalysed the Michael addition reaction efficiently, with conversions ranging from 82 to 97 %. For carbon aerogels the conversion was modest, 32 % (Pr-doped) to high, 92 % (Nd-doped).

The method developed for making metal-doped carbon aerogels was further modified to prepare active electrocatalysts for the oxygen reduction reaction. The cobalt-doped aerogels were also doped-with nitrogen by adding melamine during carbon aerogel preparation. The results showed that by varying the dHMBA or melamine content, the cobalt and nitrogen content in materials could easily be changed. Cobalt- and nitrogen doped carbon aerogels (Co-NCAs) showed high surface area and had both meso- and microporosity, although the increasing amount of melamine in the composition of aerogels decreased their surface area and pore volume. The morphology of the materials also changed drastically with increasing melamine amount. All the CAs had crystalline structures of cobalt and cobalt oxide present in them. Cobalt nanoparticles were present in all Co-NCAs and also carbon nanotube structures

had formed in those Co-NCAs that were prepared using higher melamine and cobalt concentrations.

The Co- and N-doped carbon aerogels were tested as electrocatalysts for the oxygen reduction reaction. The electrocatalytic activity of the materials for the reaction was rather high and depended on their composition. The materials with the highest Co content showed the highest activity for the oxygen reduction reaction, which can be associated with the coexistence of cobalt nanoparticles and N-doped carbon structures in them.

KOKKUVÕTE

Antud töös töötati välja meetod valmistamiseks metalle sisaldavaid orgaanilisi- ja süsinikaerogeele põlevkivitööstuse jääkproduktidest ning uuriti võimalusi nende materjalide kasutamiseks katalüsaatoritena. Aerogeelid valmistati 5-metüülresortsinoolist (MR), mis on fenoolne ühend mida eraldatakse põlevikivi töötlemisel tekkinud utteveest, ning 2,6-dihüdroksü-4-metüülbensoehappest (dHMBA), mida on võimalik lihtsalt sünteesida 5-metüülresortsinoolist. Kuna dHMBA molekul sisaldab karboksüülrühma, siis oli võimalik kasutada metallide viimiseks materjali ionivahetus meetodit, mis tagab metalli ionide ühtlase jaotumise. Selles töös valmistati koobaltit, vaske, niklit ja erinevaid lantanoide (La, Ce, Nd, Pr) sisaldavaid aerogeele.

Valmistatud aerogeelide struktuuri ja omadusi karakteriseeriti kasutades erinevaid meetodeid nagu lämmastik adsorptsioon analüüs, röntgendifraktsioon analüüs, skaneeriv ja transmissioon elektronmikroskoopia, mitmed erinevad elementsisalduse määramise meetodid jne. Tähelepanu pöörati seostele aerogeele valmistamise tingimuste ja omaduste vahel.

Tulemuste osas on näidatud, et välja töötatud meetodi puhul on võimalik lihtsalt kontrollida metallide sisaldust materjalis. Co-, Cu- ja Ni-sisaldavate aerogeelides oli võimalik MR ja dHMBA moolsuhet valmistamisel muutes varieerida metalli sisaldust orgaanilistes aerogeelides ühest kuni kaheksa protsendini ja süsinikaerogeelides ühest kuni viieteistkümne protsendini. Lantanoide sisaldavates orgaanilistes aerogeelides oli metalli sisaldus umbes 12% ning süsinikaerogeelides umbes 22%. Nii orgaanilised kui ka süsinikaerogeelid omasid kõrget eripinda (umbes 250-520 m²/g) ja poorsust (umbes 300-900 mm³/g). Co-, Cu- ja Ni-sisaldavate süsinikaerogeelide puhul olid tekkinud metalli nanoosakesed pürolüüsi käigus. Nende nanoosakeste suurused, jäädes vahemikku 3-150 nm, sõltusid kasutatud metallist ning selle sisaldusest materjalis. Lantanoide sisaldavate aerogeelide puhul metalli nanoosakeste teket ei täheldatud.

La-, Ce-, Nd- ja Pr-sisaldavaid orgaanilisi- ja süsinikaerogeele testiti katalüsaatoritena Michaeli reaktsioonis. Tulemused näitasid, et lantanoide sisaldavad orgaanilised aerogeelid omasid kõrget katalüütilist aktiivsust Michaeli reaktsioonis (konversioon oli 82-97 %). Kõik süsinikaerogeelid aga ei osutunud nii aktiivseks (konversioon 32-92%).

Selleks, et valmistada aktiivseid katalüsaatoreid hapniku redutseerumis reaktsiooni tarbeks kütuseelementides, modifitseeriti metalle sisaldavate süsinikaerogeelide valmistamise protseduuri nii, et koobaltit sisaldavad materjalid sisaldaksid ka lämmastikku. Selle tarbeks lisati melamiini valmistamisel. Tulemused näitasid, et muutes melamiini või dHMBA sisaldust materjalis, oli võimalik muuta koobalti ja lämmastiku sisaldust ning ka teisi materjali omadusi. Enamikel juhtudel oli tegu kõrge eripinna ja poorsusega materjalidega, mis sisaldasid nii mikro- kui ka mesopore. Täheldada võis, et melamiini osakaalu suurendamine materjalis vähendas nende eripinda ja pooride ruumala. Samuti mõjutas melamiini osakaalu suurenemine tugevalt

materjalide morfoloogiat. Koobaltit ja lämmastikku sisaldavad materjalid sisaldasid nii koobalti kui ka koobaltoksiidi kristallseid struktuure ning tekkinud olid metalli nanoosakesed. Süsinikaerogeelides, mis olid valmistatud kõrgema koobalti ja lämmastiku koguse juures, olid tekkinud ka süsiniknanotorud.

Koobaltit ja lämmastikku sisaldavate süsinikaerogeelide katalüütilist aktiivsust testiti hapniku redutseerumise reaktsioonis ning need materjalid omasid kõrget katalüütilist aktiivsust. Parimad olid kõige kõrgemat koobalti sisaldust omavad materjalid.

ORIGINAL PUBLICATIONS

Publication I

Kreek, K., Kulp, M., Uibu, M., Mere, A., Koel, M. Preparation of metal-doped carbon aerogels from oil shale processing by-products. - *Oil Shale*, 2014, 31, 185-194.

PREPARATION OF METAL-DOPED CARBON AEROGELS FROM OIL SHALE PROCESSING BY-PRODUCTS

KRISTIINA KREEK^{(a)*}, MARIA KULP^(a), MAI UIBU^(b),
ARVO MERE^(c), MIHKEL KOEL^(a)

- ^(a) Institute of Chemistry, Tallinn University of Technology, Akadeemia tee 15, 12618 Tallinn, Estonia
^(b) Laboratory of Inorganic Materials, Tallinn University of Technology, Ehitajate tee 5, 19086 Tallinn, Estonia
^(c) Institute of Physics, Tallinn University of Technology, Ehitajate tee 5, 19086 Tallinn, Estonia

Abstract. Carbon aerogels are nanostructured porous carbon materials, which can be produced from locally available phenolic compounds. A method for the preparation of metal-doped carbon aerogels from oil shale processing by-products 5-methylresorcinol and 2,6-dihydroxy-4-methylbenzoic acid was developed. Aerogels doped with Ni, Co and Cu were characterized by atomic absorption spectroscopy, nitrogen adsorption, transmission electron microscopy and X-ray diffraction.

The resulting materials exhibited pore diameters in microporous and mesoporous regions, high surface areas and pore volumes. The metal content in aerogels was found to be dependent on the amount of ion-exchange moiety and metal content as high as 14.5 wt% was achieved in carbon aerogels, where also metal nanoparticles had formed.

Keywords: aerogel, organic aerogel, carbon aerogel, 5-methylresorcinol, 2,6-dihydroxy-4-methyl benzoic acid, supercritical drying, oil shale, ion-exchange, metal-doped, nanoparticles.

1. Introduction

Nanoporous materials, due to their unique surface, structural and bulk properties, have attracted a lot of interest and acquired many important applications in several areas. Aerogel, as an example of a nanoporous material, is a low density material with high surface area and porosity. There are various types of aerogels which are prepared from different precursors.

* Corresponding author: e-mail kristiina.kreek@ttu.ee

Carbon aerogels are made by pyrolysing organic aerogels. For example, Pekala was the first to obtain organic aerogels by supercritically drying gels, which were made through sol-gel polymerization by using resorcinol (R) and formaldehyde (FA) as precursors [1, 2].

Previously, the preparation of aerogels from 5-methylresorcinol (MR) and 2,6-dihydroxy-4-methylbenzoic acid (dHMBA), has been studied in our laboratory. MR is a good alternative to resorcinol. Besides MR being a by-product of oil shale industry and therefore a locally available precursor, gels prepared from MR have also shown faster gelation times compared to gels prepared from resorcinol [3–5]. The preparation of aerogels from MR and dHMBA together showed that the structure and properties of aerogels are dependent on the molar ratio of MR to dHMBA. dHMBA differs from MR by being a bifunctional monomer and, in addition to being a monomer, also acts as a catalyst due to its acidic properties [6]. dHMBA can be synthesized from MR.

Doping of carbon aerogels prepared from MR and FA with palladium by using impregnation in supercritical CO₂ has been previously carried out, but to the authors' knowledge no attempt to dope aerogels prepared from dHMBA has been made before [5].

There is on-going activity to expand potential aerogel applications with the modification of carbon aerogels (CA) through the incorporation of metal species into carbon frameworks. Doping of carbon aerogels with metals modifies their structure, conductivity and catalytic activity [7–12]. There are different methods for preparing metal-doped carbon aerogels, which can roughly be divided into three categories, as was done by Moreno-Castilla and Maldonado-Hódar [13]. First, the metal precursor can be added to the initial mixture before gel formation, secondly, the metal precursor can be deposited onto the already existing organic or carbon aerogel and lastly, the ion-exchange method can be used [13].

The ion-exchange method for preparing metal-doped aerogels was first studied by Baumann et al. [12]. Carbon aerogels were prepared in which instead of resorcinol the researchers used the potassium salt of 2,4-dihydroxybenzoic acid (dHBA) in the sol-gel process, producing K⁺-doped hydrogels. This meant that each repeat unit of the gel contained a binding site for metal ions. The desired metal ion was deposited by exchanging the potassium ion in an ion-exchange process. A common carbon aerogel treatment process for gel drying and carbonization was used to generate metal-doped carbon aerogels.

Over the years, several studies on ion-exchange deposition have been reported [12, 14–20]. In these researches, the effect of different metals, pyrolysis temperature and different applications have been described. Recently, a paper was published in which the ion-exchange capacity of gels was altered by using together dHBA (ion-exchange moiety containing monomer) and resorcinol [21].

The goal of this work is to modify the preparation of aerogels from precursors MR and dHMBA, so that metal-doped carbon aerogels could be

obtained. The doping of materials with metals will be carried out similarly to the ion-exchange method developed by Baumann et al. [12], though in the current case two resorcinol derivatives (MR and dHMBA) will be used for aerogel preparation. Since only dHMBA has an ion-exchange moiety (carboxylic group), then the possibility of preparing aerogels with different metal contents, by changing the MR to dHMBA molar ratio, will be discussed. The process for preparation of metal-doped carbon aerogels from MR and dHMBA will be developed and properties of the obtained materials determined.

2. Experimental

2.1. Materials

5-methylresorcinol with a reported purity of > 99% was provided by AS VKG, Estonia and 2,6-dihydroxy-4-methylbenzoic acid, with a purity of > 99%, was provided by Carboshale OÜ, Estonia. Sodium acetate ($\text{CH}_3\text{COONa}\cdot 3\text{H}_2\text{O}$), with a purity of 99.7%, was obtained from Fisher Scientific, UK. The water used was purified using a Milli-Q water system. Acetonitrile, HPLC purity, was obtained from Rathburn Chemical Ltd., Germany. Formaldehyde (37 w/w solution in water) was purchased from Sigma-Aldrich. CO_2 (99.8%) was obtained from Eesti AGA AS.

The supercritical extraction system with a double clamp autoclave, 100 ml in volume, was constructed by NWA analytische Meßgeräte GmbH, Germany.

The MTF 12/38/400 pyrolysis oven with a maximum temperature of 1200 °C was from Carbolite, England.

2.2. Sample preparation

The gels were prepared by adding dHMBA and MR (MR:dHMBA molar ratio 1:1, 3:1 or 9:1) to the solvent (70 wt% acetonitrile and 30 wt% distilled water). The molar ratio of solvent (SOLV) to aromatic monomers (AM) was 35:1. The moles of aromatic monomers (AM) were calculated by adding up the moles of MR and dHMBA and the moles for the solvent were calculated by adding up the moles of acetonitrile and water. To the solution of aromatic monomers and solvent a stoichiometric amount of sodium acetate (NaOAc) to dHMBA was added (NaOAc:dHMBA molar ratio 1:1) to obtain the sodium salt of dHMBA. After that formaldehyde (FA) was added (AM:FA molar ratio 1:2) and, finally, another amount of NaOAc was added as a catalyst (AM:NaOAc molar ratio 50:1).

Glass molds containing the solutions were sealed and the mixture was allowed to gel and cure at 40 °C for 7 days. The obtained Na^+ -doped gels were orange and transparent. The gels were then soaked for 3 days in 0.1 M aqueous solutions of CuCl_2 , $\text{Co}(\text{NO}_3)_2\cdot 6\text{H}_2\text{O}$ and $\text{Ni}(\text{NO}_3)_2\cdot 6\text{H}_2\text{O}$, respectively. Each time the solution was renewed after 24 hours. After that the

gels were washed by soaking them in water for 24 hours, followed by acetone exchange which lasted 4 to 5 days. Acetone was changed every 24 hours. The gels were dried with supercritical CO₂. A more detailed description of the drying method has been published elsewhere [6]. Carbonization was performed in N₂ atmosphere by raising the temperature to 700 °C (2.5 °C/min), then to 900 °C (5 °C/min) and was kept at 900 °C for 1 hour.

2.3. Characterization

The bulk densities of carbon aerogels were calculated by measuring the dimensions and mass of each monolithic sample. Elemental analyses were performed by a Spectra AA 220F flame atomic absorption spectrometer (Australia). Nitrogen adsorption analyses were performed using a KELVIN 1042 Sorptometer (Costech International, Italy). Helium was used as a carrier gas, nitrogen as the adsorptive gas. Nitrogen adsorption data was taken at relative pressures from 0 to 1 and at liquid nitrogen temperature. The specific surface area (S_{BET}) was calculated according to the Brunauer-Emmett-Teller theory. The specific micropore volume (V_{mic}) was determined via the t-plot and the pore size distributions were determined using the Barrett-Johnner-Halendar (BJH) method from the desorption branch. The X-ray diffraction (XRD) pattern was recorded with a Rigaku Ultima IV diffractometer using the D/teX Ultra line detector (USA). Cu-K α radiation was used with a Ni filter for removing K β radiation. The recorded diffractograms were analysed by Rigaku PDXL software. Energy-filtered transmission electron microscopy (TEM) was carried out with the Leo 912 Omega microscope (Zeiss, Germany) at 120 kV, using a LaB₆ gun.

3. Results and discussion

In the previously developed method for the preparation of aerogels from MR and dHMBA, it was suggested that dHMBA, in addition to being a monomer, also acted as an acidic catalyst [6]. The method developed in this work involved, during gel preparation, the addition of NaOAc, which can also act as a catalyst. Therefore the role of dHMBA as a catalyst is not clear in the present case.

The method developed by Baumann et al. employed potassium carbonate to neutralize the solution and as a catalyst, but in the current work a stronger gel was obtained by using sodium acetate instead. This resulted in a slightly acidic solution (pH 5.5) due to the formation of acetic acid and, hence, incomplete neutralization of the solution.

After immersing the gels containing Na⁺ ions in the copper ions containing solution, the Na content in organic aerogels was measured and found to be about 0.005%. In comparison, the Na content in the aerogel, which had not been immersed in the solution containing copper ions, was 6.40%. It confirms that the exchange of sodium ions for copper ions takes place.

The authors studied which effect dHMBA has on the metal content in aerogels. Gels at MR to dHMBA molar ratios of 1:1, 3:1 and 9:1 were prepared and dried. The results are shown in Figure 1. It can be seen that with increasing dHMBA content in aerogels their metal content also increases. Therefore changing the MR to dHMBA molar ratio is an easy way to control the metal content in aerogels. Previously a study was performed where the ratio between the two phenolic compounds used (R and dHBA) was changed, to evaluate the ion-exchange capacity. Though it was also noted that at lower relative mole fractions of the ion-exchange monomer the ion-exchange capacity decreased, a change in metal content to the same extent as in the current case was not shown [21].

Subsequently, carbon aerogels at an MR:dHMBA molar ratio of 1:1 were prepared (Table). The metal content in carbon aerogels was about twice as high as in the organic aerogel. It can be explained by the decomposition of organic matter during pyrolysis.

The Table also presents data on the density, specific surface area and pore volume of metal-doped carbon aerogels. The density of organic aerogels ranged from 0.45 to 0.62 g/cm³ and that of carbon aerogels from 0.83 to 1.26 g/cm³, which is higher than for metal-doped carbon aerogels prepared from dHBA [16]. This may be explained by that in the present case the authors used higher solids content to prepare aerogels, which is known to cause higher densities [22]. Also, the diameter of gels decreased about 20% during the immersion of gels in metal ion solutions and during solvent exchange.

Nitrogen adsorption/desorption isotherms for metal-doped carbon aerogels are shown in Figure 2. The Table presents the specific surface areas and pore volumes of carbon aerogels doped with different metals. While comparing carbon aerogels that were doped with transition metals (Co, Cu, Ni) to the blank sample (Na containing), it was found that both specific surface areas and pore volumes were larger for the transition metal containing samples. The same effect has been observed before for aerogels prepared from dHBA (the blank sample contained potassium) [12, 16].

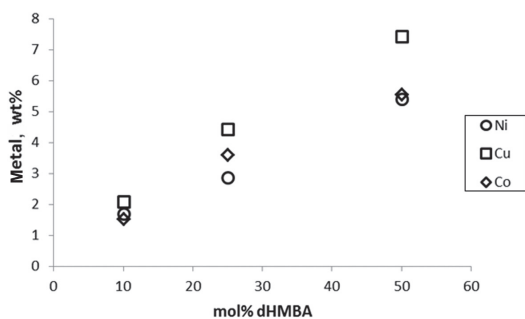


Fig. 1. Metal content in organic aerogels.

Table. Properties of metal-doped carbon aerogels

Sample	$\rho(\text{OA})_3$, g/cm ³	$\rho(\text{CA})_3$, g/cm ³	S_{BET} , m ² /g	$S_{\text{non-mic}}$, m ² /g	S_{mic} , m ² /g	% S_{mic} , %	V_{TOT} , mm ³ /g	V_{mic} , mm ³ /g	% V_{mic} , %	Metal, % OA	Metal, % CA
Na	0.58	0.83	286	153	133	46.5	429	47	11.0	6.40	-
Cu	0.45	1.01	464	173	291	62.7	607	103	17.0	7.43	14.5
Co	0.62	1.03	519	166	353	68.0	610	124	20.3	5.50	10.7
Ni	0.59	1.26	379	106	273	72.0	446	96	21.5	5.50	11.0

All the samples were prepared at an MR:dHMBA molar ratio of 1:1. OA is organic aerogel and CA is carbon aerogel. All the parameter values obtained apply to carbon aerogels, unless otherwise noted. ρ is the calculated density, S_{BET} is the BET surface area, S_{mic} is the microporous surface area, % S_{mic} is the percent of microporous surface area, V_{TOT} is the total pore volume, V_{mic} is the volume of micropores, % V_{mic} is the percent of microporous volume, metal % is the weight percent of metal in aerogels.

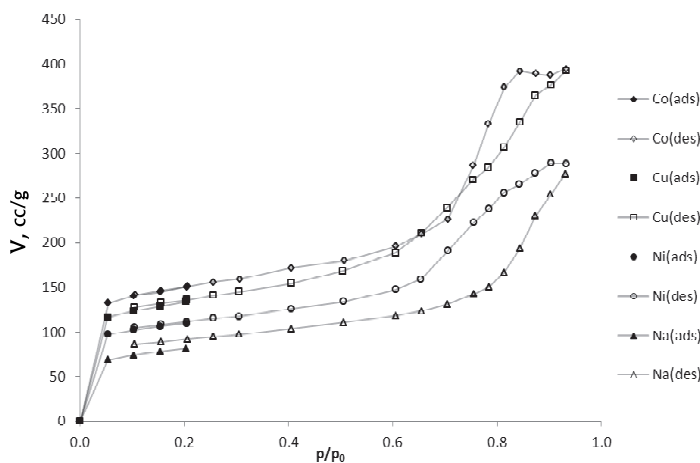


Fig. 2. Results of adsorption/desorption analysis of nitrogen; (ads) – adsorption isotherm, (des) – desorption isotherm.

Transition metal containing aerogels showed higher values of microporous surface area and microporous pore volume compared to the Na containing sample, the respective percentages being almost twice as high for the aerogels. The increase in micropore volume could be attributed to the transition metals favouring the formation of new microporosity or causing a stronger shrinkage of mesopores, which become micropores during carbon aerogel preparation as a result. The increase in pore volume of transition metal containing aerogels was due not only to the increase in microporosity, but also to the fact that the non-microporous volume of Cu and Co containing carbon aerogels was larger.

From Figure 3 it can be seen that the peak of pore size distribution (PSD) of the Na containing aerogel is at a pore diameter of 10–15 nm, whereas the peak for all the other doped aerogels is at 5–10 nm. This indicates that for carbon aerogels the addition of transition metals resulted in the reduction of pore diameter. This result is different from those obtained in a previous study, which showed that in case of carbon aerogels made from dHBA, incorporation of transition metals had no significant effect on pore size distribution [16].

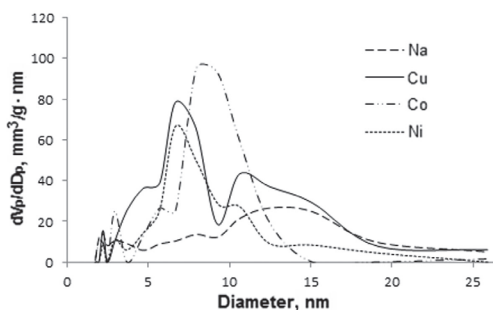


Fig. 3. Pore size distribution of metal-doped carbon aerogels (MR:dHMBA molar ratio 1:1).

The results of X-ray diffraction analysis of carbon aerogels are shown in Figure 4, revealing the presence of peaks corresponding to metals (oxidation state 0). This suggests that metal ions must have been reduced during carbon aerogel preparation. For the copper-doped carbon aerogel there is also a peak corresponding to copper(I)oxide, whose presence could have been caused by either incomplete reduction during pyrolysis or oxidization of copper afterwards. The diffractogram for nickel-doped carbon aerogel has also peaks corresponding to graphite (marked C in the figure). However, no graphitic structures were observed in TEM pictures, possibly due to low resolution.

TEM pictures of aerogels were taken to visualize metal nanoparticles in samples. Figure 5a shows an organic aerogel, which before drying was soaked in the solution of cobalt nitrate. No metal nanoparticles can be observed in this case, which is in agreement with the conclusion of a previous study that metal ions are uniformly distributed throughout the organic aerogel [12]. When the aerogel depicted in Figure 5a is pyrolysed (Fig. 5b), then nanoparticles emerge. These are uniformly distributed in the carbon matrix and their size is in the range of 10–60 nm. Figure 5c and d depict nickel- and copper-doped carbon aerogels prepared in the same conditions as the above-mentioned Co-doped carbon aerogel. The size of metal nanoparticles in these samples is in the range of 20–150 nm for nickel containing

carbon aerogels and 3–100 nm for copper containing carbon aerogels, showing that the metal nanoparticle diameters of different metals varied. For copper containing carbon aerogels the nanoparticles had also clustered together.

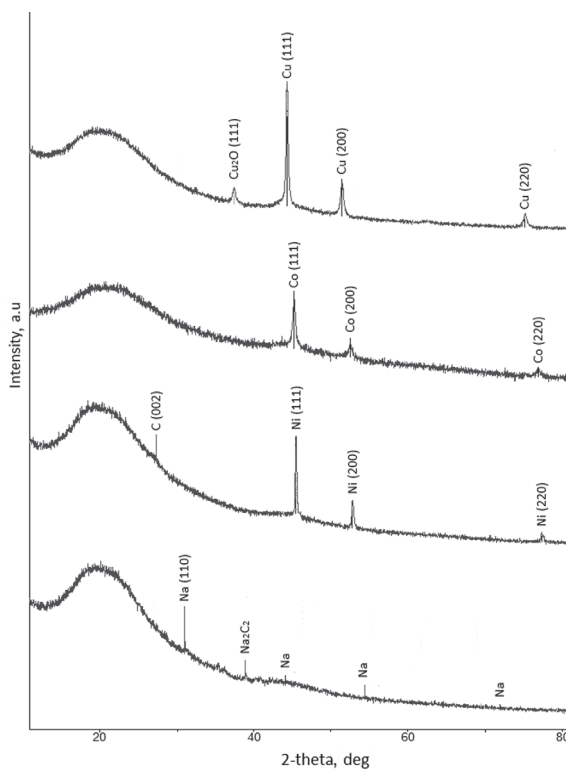


Fig. 4. Results of X-ray diffraction analysis of metal-doped carbon aerogels.

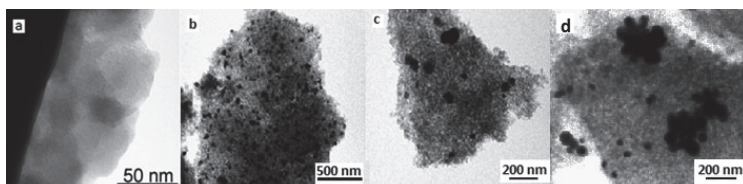


Fig. 5. TEM pictures of metal-doped aerogels. a: Co-doped organic aerogel; b: Co-doped carbon aerogel; c: Ni-doped carbon aerogel; d: Cu-doped carbon aerogel.

4. Conclusions

A method for preparing metal-doped carbon aerogels from oil shale processing by-products 5-methylresorcinol and 2,6-dihydroxy-4-methylbenzoic acid was developed. The ion-exchange process was used to introduce Ni, Co and Cu into carbon aerogels.

The specific surface area of metal-doped carbon aerogels was in the range of 380–520 m²/g and pore volume 446–610 mm³/g. It was shown that the metal content in carbon aerogels can be varied by changing the molar ratio of MR to dHMBA. In carbon aerogels the metal ions had reduced to metals during pyrolysis and formed metal nanoparticles. The size of metal nanoparticles ranged from 3 to 150 nm.

The method developed is suitable for preparing metal-doped carbon aerogels from oil shale processing by-products. The resulting materials have high surface area and porosity and it is possible to control their metal content.

Acknowledgements

The authors would like to thank Anna-Liisa Peikolainen for kind help and fruitful discussions, and Krisztian Kordas for providing TEM images. AS VKG and Carboshale OÜ are acknowledged for donating the chemicals. The financial support under the EU Structural Funds project “Electroactive nanoporous carbon composite films technology” No 3.2.1101.12-0007, and the European Regional Development Fund, Centre of Excellence TK114 “Mesosystems: Theory and Applications” is gratefully acknowledged.

REFERENCES

1. Pekala, R. W. Low density, resorcinol-formaldehyde aerogels. US Patent 4873218, 1989.
2. Pekala, R. W., Alviso, C. T., Kong, F. M., Hulse, S. S. Aerogels derived from multifunctional organic monomers. *J. Non-Cryst. Solids*, 1992, **145**, 90–98.
3. Pérez-Caballero, F., Peikolainen, A.-L., Uibu, M., Kuusik, R., Volobujeva, O., Koel, M. Preparation of carbon aerogels from 5-methylresorcinol-formaldehyde gels. *Micropor. Mesopor. Mat.*, 2008, **108**(1–3), 230–236.
4. Peikolainen, A.-L., Pérez-Caballero, F., Koel, M. Low-density organic aerogels from oil shale by-product 5-methylresorcinol. *Oil Shale*, 2008, **25**(3), 348–358.
5. Pérez-Caballero, F., Peikolainen, A.-L., Koel, M., Herbert, M., Galindo, A., Montilla, F. Preparation of the catalyst support from the oil-shale processing by-product. *Open Petrol. Eng. J.*, 2008, **1**(1), 42–46.
6. Peikolainen, A.-L., Volobujeva, O., Aav, R., Uibu, M., Koel, M. Organic acid catalyzed synthesis of 5-methylresorcinol based organic aerogels in acetonitrile. *J. Porous Mat.*, 2012, **19**(2), 189–194.
7. Moreno-Castilla, C., Maldonado-Hódar, F. J., Rivera-Utrilla, J., Rodríguez-Castellón, E. Group 6 metal oxide-carbon aerogels. Their synthesis, charac-

- terization and catalytic activity in the skeletal isomerization of 1-butene. *Appl. Catal. A-Gen.*, 1999, **183**(2), 345–356.
8. Maldonado-Hódar, F. J., Ferro-García, M. A., Rivera-Utrilla, J., Moreno-Castilla, C. Synthesis and textural characteristics of organic aerogels, transition metal-containing organic aerogels and their carbonized derivatives. *Carbon*, 1999, **37**(8), 1199–1205.
 9. Bekyarova, E., Kaneko, K. Structure and physical properties of tailor-made Ce,Zr-doped carbon aerogels. *Adv. Mater.*, 2000, **12**(21), 1625–1628.
 10. Bekyarova, E., Kaneko, K. Microporous nature of Ce, Zr-doped carbon aerogels. *Langmuir*, 1999, **15**(21), 7119–7121.
 11. Miller, J. M., Dunn, B. Morphology and electrochemistry of ruthenium/carbon aerogel nanostructures. *Langmuir*, 1999, **15**(3), 799–806.
 12. Baumann, T. F., Fox, G. A., Satcher, J. H., Yoshizawa, N., Fu, R., Dresselhaus, M. S. Synthesis and characterization of copper-doped carbon aerogels. *Langmuir*, 2002, **18**(18), 7073–7076.
 13. Moreno-Castilla, C., Maldonado-Hódar, F. J. Carbon aerogels for catalysis applications: An overview. *Carbon*, 2005, **43**(3), 455–465.
 14. Fu, R., Baumann, T. F., Cronin, S., Dresselhaus, G., Dresselhaus, M. S., Satcher, J. H. Formation of graphitic structures in cobalt- and nickel-doped carbon aerogels. *Langmuir*, 2005, **21**(7), 2647–2651.
 15. Steiner, S. A., Baumann, T. F., Kong, J., Satcher, J. H., Dresselhaus, M. S. Iron-doped carbon aerogels: novel porous substrates for direct growth of carbon nanotubes. *Langmuir*, 2007, **23**(9), 5161–5166.
 16. Cotet, L. C., Gich, M., Roig, A., Popescu, I. C., Cosoveanu, V., Molins, E., Danciu, V. Synthesis and structural characteristics of carbon aerogels with a high content of Fe, Co, Ni, Cu, and Pd. *J. Non-Cryst. Solids*, 2006, **352**(26–27), 2772–2777.
 17. Marie, J., Berthon-Fabry, S., Achard, P., Chatenet, M., Pradourat, A., Chainet, E. Highly dispersed platinum on carbon aerogels as supported catalysts for PEM fuel cell-electrodes: comparison of two different synthesis paths. *J. Non-Cryst. Solids*, 2004, **350**, 88–96.
 18. Martínez, S., Vallribera, A., Cotet, C. L., Popovici, M., Martín, L., Roig, A., Moreno-Mañas, M., Molins, E. Nanosized metallic particles embedded in silica and carbon aerogels as catalysts in Mizoroki-Heck coupling reaction. *New J. Chem.*, 2005, **29**, 1342–1345.
 19. Carrott, P. J. M., Marques, L. M., Ribeiro Carrott, M. M. L. Characterisation of the porosity of polymer and carbon aerogels containing Fe, Ni or Cu prepared from 2,4-dihydroxybenzoic acid by *n*-nonane pre-adsorption and density functional theory. *Micropor. Mesopor. Mat.*, 2010, **131**(1–3), 75–81.
 20. Marques, L. M., Conceição, F. L., Ribeiro Carrott, M. M. L., Carrott, P. J. M. Diffusion of gases in metal containing carbon aerogels. *Fuel Process. Technol.*, 2011, **92**(2), 229–233.
 21. Carrott, P. J. M., Marques, L. M., Ribeiro Carrott, M. M. L. Core-shell polymer aerogels prepared by co-polymerisation of 2,4-dihydroxybenzoic acid, resorcinol and formaldehyde. *Micropor. Mesopor. Mat.*, 2012, **158**, 170–174.
 22. Al-Muhtaseb, S. A., Ritter, J. A. Preparation and properties of resorcinol-formaldehyde organic and carbon aerogels. *Adv. Mater.*, 2003, **15**(2), 101–114.

Presented by A. Kogerman

Received July 2, 2013

Copyright of Oil Shale is the property of Teaduste Akadeemia Kirjastus and its content may not be copied or emailed to multiple sites or posted to a listserv without the copyright holder's express written permission. However, users may print, download, or email articles for individual use.

Publication II

Kreek, K., Kriis, K., Maaten, B., Uibu, M., Mere, A., Kanger, T., Koel, M. Organic and carbon aerogels containing rare-earth metals: Their properties and application as catalysts. – *Journal of Non-Crystalline Solids*, 2014, 404, 43-48.



Contents lists available at ScienceDirect

Journal of Non-Crystalline Solids

journal homepage: www.elsevier.com/locate/jnoncrysol

Organic and carbon aerogels containing rare-earth metals: Their properties and application as catalysts

Kristiina Kreek^{a,*}, Kadri Kriis^a, Birgit Maaten^a, Mai Uibu^b, Arvo Mere^c, Tõnis Kanger^a, Mihkel Koel^a^a Institute of Chemistry, Tallinn University of Technology, Akadeemia tee 15, 12618 Tallinn, Estonia^b Laboratory of Inorganic Materials, Tallinn University of Technology, Ehitajate tee 5, 19086 Tallinn, Estonia^c Institute of Physics, Tallinn University of Technology, Ehitajate tee 5, 19086 Tallinn, Estonia

ARTICLE INFO

Article history:

Received 6 May 2014

Received in revised form 11 July 2014

Available online 13 August 2014

Keywords:

Lanthanide;

Catalyst;

Michael reaction;

Organic aerogel;

Carbon aerogel;

Metal-doped

ABSTRACT

Lanthanide-doped organic and carbon aerogels were obtained based on the modified resorcinol-formaldehyde aerogel preparation procedure. The prepared materials were tested as catalysts for the Michael reaction.

Organic aerogels were prepared by sol-gel polymerization of 2,6-dihydroxy-4-methylbenzoic acid (dHMBA) mixed with 5-methylresorcinol (MR) and formaldehyde. The resulting gels were doped with $\text{Ln}(\text{NO}_3)_3$ ($\text{Ln} = \text{Ce, La, Nd, Pr}$) by ion-exchange and further dried with supercritical CO_2 . Pyrolysis of organic aerogels at 900 °C in N_2 atmosphere resulted in metal-doped carbon aerogels.

The mostly mesoporous materials contained up to 12 wt.% of metal in organic aerogels and 22 wt.% in carbon aerogels. The materials were amorphous and crystal structures were not formed during pyrolysis.

Ln -doped aerogels were tested as catalysts for Michael addition reaction. Organic aerogels doped with different lanthanides catalyze the Michael reaction efficiently with conversions ranging between 82 and 97% in 24 h. For Ln -doped carbon aerogels the conversion was modest (32%) to high (92%).

© 2014 Elsevier B.V. All rights reserved.

1. Introduction

Aerogels as nanoporous materials have attracted a lot of interest and found many important applications in several areas due to their unique surface, structural and bulk properties. The most common method for making organic aerogels (OAs) involves the sol-gel polymerization of resorcinol and formaldehyde and subsequent supercritical drying of the gel [1,2]. Upon pyrolysis of OAs, carbon aerogels (CAs) are produced in which the initial morphology of the OAs remains, but surface areas can be higher and also the nonconductive OAs become electrically conductive.

The addition of metal species to carbon aerogels has been studied before and several methods have been used for the deposition of metal species [3]. The incorporation of metals modifies the structure, conductivity and catalytic activity of the materials obtained [4–7]. One of the methods used for doping is the ion-exchange method in which gels having an ion-exchange moiety are prepared [8].

Lanthanides are widely used as catalysts in organic synthesis, because lanthanide-mediated reactions display high chemo- and stereoselectivities [9]. Due to the high coordination numbers (f-block elements), lanthanides can promote organic reactions catalytically rather than stoichiometrically. Their association with substrates and

dissociation of products occurs fast, giving high catalyst efficiency. Lanthanide complexes have great advantages as Lewis acid catalysts for carbon-carbon bond forming reactions [10,11]; including the Michael reaction [12,13].

The use of a lanthanide salt as an efficient catalyst for the Michael reaction was first reported in 1993 by Scettri and co-workers [14]. This article broke the previous unwritten rule that the catalyst had to be a complex bearing diolato ligands [15], it was shown that these species would be readily generated in situ from the 1,3-dicarbonyl compound. Since then, other lanthanide species of La, Sc and Yb have been studied as catalysts in conjugate additions [16,17].

Due to the various advantages of supported catalysts, it is important to find the right support for lanthanides. Aerogels are good candidates for catalyst carriers, because of their high surface area and continuous porosity. The use of carbon aerogels as catalyst carriers has been reviewed before [3]. Support or entrapment of lanthanides or lanthanide species in aerogels has been rarely studied [6,18,19]. As far as we know, only one example about the use of lanthanide-aerogels as heterogeneous catalysts in Michael reaction has been described [19].

This paper presents the first known attempt to prepare of La-, Ce-, Pr- and Nd-doped organic and carbon aerogels. Their properties were studied and the materials tested as catalysts in a reaction which needs lanthanide ions for catalytic activity. The materials used for making the aerogel are by-products of the local oil-shale processing industry [20,21].

* Corresponding author. Tel./fax: +372 620 28 28.

E-mail address: kristiina.kreek@tu.ee (K. Kreek).

Table 1
Density, metal content and N₂-adsorption analysis results for organic aerogels (OA) and carbon aerogels (CA). ρ is calculated density, S_{BET} is the BET surface area, V_{TOT} is total pore volume, V_{mic} is the volume of micropores, $V_{\text{mic}\%}$ is the percent of microporous volume and Metal% is the weight percent of metal in aerogels. The uncertainty for N₂-analysis results is $\leq 3\%$.

	$\rho(\text{OA}),$ g/cm ³	$\rho(\text{CA}),$ g/cm ³	S_{BET} (OA), m ² /g	V_{TOT} (OA), mm ³ /g	V_{mic} (OA), mm ³ /g	S_{BET} (CA), m ² /g	V_{TOT} (CA), mm ³ /g	V_{mic} (CA), mm ³ /g	$V_{\text{mic}\%}$ (CA), %	Metal% (OA), %	Metal% (CA), %
La	0.54 ± 0.03	1.16 ± 0.08	429	889	2	321	477	58	12	11.0 ± 1.1	22 ± 2.2
Ce	0.52 ± 0.09	1.03 ± 0.1	393	734	2.5	368	533	78	14.6	10.7 ± 1.1	21 ± 2.1
Pr	0.53 ± 0.06	1.14 ± 0.06	371	721	3.1	255	302	55	18.2	11.5 ± 1.2	21 ± 2.1
Nd	0.53 ± 0.07	1.08 ± 0.08	378	659	2	257	301	52	17.3	11.3 ± 1.1	22 ± 2.2
Na	0.58 ± 0.06	0.83 ± 0.1	221	643	0	30	19	9	47.0	6.4 ± 0.6	–

2. Materials and methods

2.1. Materials

5-Methylresorcinol (5-MR) with a reported purity of >99% was provided by VKG AS, Estonia and 2,6-dihydroxy-4-methylbenzoic acid (dHMBA), with a purity of >99% was donated by CarboShale OÜ, Estonia. Sodium acetate trihydrate, with a purity of 99.7%, was obtained from Fisher Chemical, UK. The water used was purified using a Milli-Q water system. Acetonitrile, HPLC purity, was obtained from Rathburn Chemical Ltd., Germany. Formaldehyde (37 w/w solution in water) was purchased from Sigma-Aldrich. CO₂ (99.8%) was obtained from Eestri AGA AS. Lanthanide carbonates were obtained from Molycorp Silmet, Estonia and were turned into nitrates. The supercritical extraction system with a double clamp autoclave, 100 mL in volume, was constructed by NWA Analytische Meßgeräte GmbH, Germany. The pyrolysis oven type MTF 12/38/400 with a maximum temperature of 1200 °C was from Carbolite, England.

2.2. Sample preparation

The two aromatic monomers (AM) used, 5-MR and dHMBA (molar ratio of 5-MR/dHMBA = 1), were added to the solvent (70 wt.% acetonitrile and 30 wt.% distilled water). The molar ratio of solvent to aromatic monomers (5-MR and dHMBA) was 35. The moles of aromatic monomers were calculated by adding the moles of 5-MR and dHMBA and the moles for the solvent were calculated by addition of the moles of acetonitrile and water. A stoichiometric amount of sodium acetate (NaOAc) was added to dHMBA (molar ratio of NaOAc/dHMBA = 1) to obtain the sodium salt of dHMBA. After that formaldehyde (FA) was added to the solution (AM/FA molar ratio 0.5) and finally another amount of NaOAc as a catalyst was added (AM/NaOAc molar ratio 50).

Glass molds containing the solutions were sealed and the mixture was allowed to gel and cure at 40 °C for 7 days. The obtained Na⁺-doped gels were orange and transparent. The gels were then soaked for 3 days in 0.1 M aqueous solutions of lanthanide nitrates [La(NO₃)₃, Ce(NO₃)₃, Nd(NO₃)₃, Pr(NO₃)₃], respectively. Each time the solutions of lanthanide nitrates were renewed after 24 h. After that the gels were washed by soaking them in water for 24 h, followed by acetone exchange which lasted 4 to 5 days. Acetone was changed every 24 h. The gels were dried with supercritical CO₂. A more detailed description of the drying method is published elsewhere [22]. Carbonization was performed in N₂ atmosphere by raising the temperature to 700 °C (2.5 °C/min), from then on to 900 °C (5 °C/min) and was kept at 900 °C for 1 h.

2.3. Characterization

The bulk densities of organic and carbon aerogels were calculated by measuring the dimensions and mass of three monolithic samples and calculating the average. Standard deviations are added to Table 1. Lanthanide contents were measured using an OPTIMA 7300 DV ICP OES,

PerkinElmer. The uncertainty of the results is <10%. Nitrogen adsorption analyses were performed using a KELVIN 1042 Sorptometer built by Costech International. Helium was used as a carrier gas, nitrogen as the adsorptive gas. Nitrogen adsorption data was taken at relative pressures from 0 to 1 and at liquid nitrogen temperature. The specific surface area (S_{BET}) was calculated according to the Brunauer-Emmet-Teller (BET) theory. The specific micropore volume (V_{mic}) was determined via the t-plot and the pore size distributions were determined using the Barrett-Johner-Halendar (BJH) method from the desorption branch. The uncertainty of the method is $\leq 3\%$. The X-ray diffraction (XRD) pattern was recorded with a Rigaku Ultima IV diffractometer by using a DtexUltra line detector. Cu-K α radiation was used with a Ni filter for removing K β radiation. The recorded diffractograms were analyzed by Rigaku PDXL software. Energy-filtered transmission electron microscopy (TEM) was carried out with a Leo 912 Omega microscope at 120 kV, using a LaB₆ gun. Fourier transform infrared spectroscopy (FT-IR) was performed using a TENSOR 27 (Bruker) FT-IR spectrometer. Raman spectroscopy was carried out using a Raman spectrometer (Horiba Jobin Yvon LabRam HR800). Thermogravimetric analysis was carried out using TG-DTA Setaram Labsys Evo in Ar atmosphere with the same heating program as was used during pyrolysis.

2.4. Experimental data on Michael reaction

0.006 mmol of the catalyst (3 mol% Ln with respect to the limiting reagent) was carried into the reaction vessel. 0.4 ml of CH₂Cl₂, 0.6 mmol (excess of 3 times) of 3-buten-2-one **2** and 0.2 mmol of ethyl 2-oxocyclopentanecarboxylate **1** (limiting reagent) were added and the mixture was stirred at room temperature for 24 h. Conversion of the product **3** was determined by GC. For OAs a catalyst loading of 7.5 mg and for CA 4.0 mg was used.

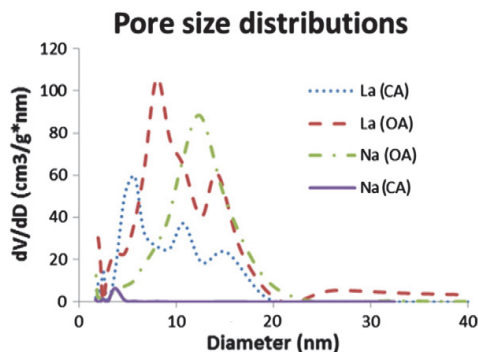


Fig. 1. Pore size distributions of OA-s and CA-s.

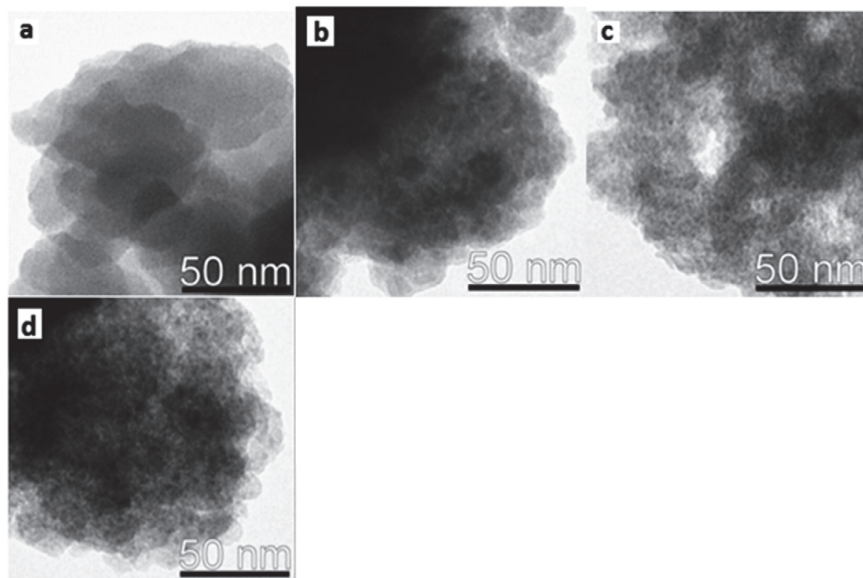


Fig. 2. TEM pictures of aerogels: (a, b) La-doped organic aerogel; (c, d) La-doped carbon aerogel.

3. Results and discussion

3.1. Materials characterization

The method for introducing lanthanides into aerogels involves the exchange of sodium ions for lanthanide ions in the ion-exchange moiety. The wt.% of lanthanides in aerogels (measured by ICP-MS) is shown in Table 1. The theoretical (about 11 wt.%, if all the ion-exchange moieties were available for binding) and measured wt.% of lanthanides in organic aerogels are similar, enabling one to conclude that the ion-exchange of sodium ions for lanthanides was successful. After pyrolysis the wt.% of lanthanides increased about twice. It can be attributed to the combustion of organic matter.

The results of nitrogen adsorption analysis for organic and carbon aerogels (Table 1) show that the materials are mostly mesoporous. The total pore volumes and specific surface area of organic aerogels were higher than those of carbon aerogels. This indicates that carbonization during pyrolysis decreased the pore volume of aerogels, also their pore size is smaller (Fig. 1). Organic aerogels have a very small microporous pore volume, while the V_{mic} of carbon aerogels can be up to 18.2%. A certain portion of the microporosity was probably formed additionally during pyrolysis, but some amount was likely generated due to the shrinking of mesopores.

As a reference, a blank sample, which was not immersed in an aqueous solution of lanthanide salt (contained sodium instead), was prepared. The surface areas and pore volumes of lanthanide-doped aerogels are higher for both OA-s and CA-s compared to the blank samples.

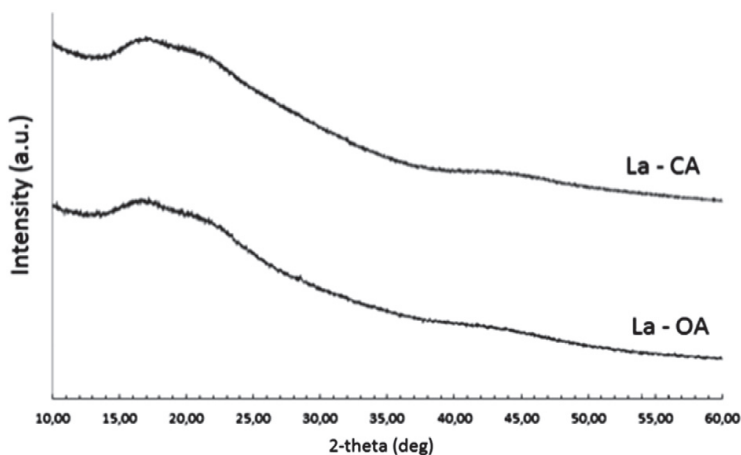


Fig. 3. XRD analysis results of La-doped organic and carbon aerogels.

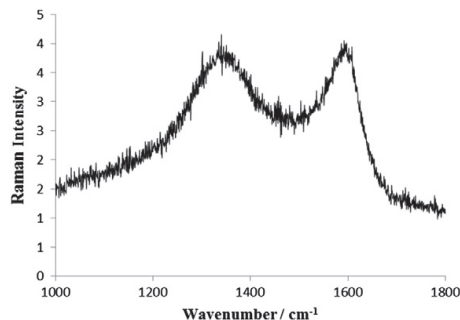


Fig. 4. Raman spectra of La-doped carbon aerogel.

For carbon aerogels the difference in surface area and pore volume between lanthanide-doped aerogels and the blank sample is vast. During pyrolysis most of the mesoporosity disappeared in the blank sample, whereas for aerogels with lanthanides the decrease was not this drastic.

The morphology of the prepared materials was determined from the TEM pictures of organic and carbon aerogels, which were taken from different locations and are shown in Fig. 2. Images a and b correspond to La-doped organic aerogel and c and d to La-doped carbon aerogels. Judging from the pictures, the materials seem to mostly consist of the amorphous aerogel matrix, without sharply distinguishable nanoparticles. In previous studies, no distinguishable nanoparticles in organic aerogels were observed [8,21]. During pyrolysis aerogels enriched with metal ions tend to reduce and form metal nanoparticles. In this work it was not observed, which confirms the fact that lanthanides require stronger reducing agents.

This is also confirmed by XRD analysis results illustrated in Fig. 3. Both La-OAs and -CAs are amorphous materials with no peaks referring to crystal structures in aerogels. For metal-doped carbon aerogels it is common that crystal structures are formed during pyrolysis [8,23], but in this case the material remained amorphous.

Raman spectroscopy on CAs was performed to evaluate the nature of carbon [24]. In Fig. 4 the peak at 1590 cm^{-1} (G-band) can be attributed to the $2E_{2g}$ mode, which is present in both ordered and amorphous carbon materials. The peak at 1330 cm^{-1} (D-band) can be attributed to the A_{1g} mode, which is associated with defects in the G layers of graphenic carbon.

The IR spectra of La-OA and La-CA are shown in Fig. 5. For La-OA there are absorptions present at several wavenumbers. Absorption at wavenumber 1590 cm^{-1} can be attributed to an asymmetric stretching

from carboxylic salt. The stretching at 1240 cm^{-1} can be attributed to the C–O bond from phenolic compounds and at 1100 cm^{-1} to the C–O bond from methylene ether bridges. However, for the same aerogel after pyrolysis only a small absorption band at 3420 cm^{-1} , which can be attributed to the O–H bond from adsorbed water, can be observed. This shows that the initial organic material underwent transformation during pyrolysis.

To describe the changes in mass that take place during pyrolysis of the organic aerogel, thermogravimetric analysis was conducted in Ar atmosphere for La-OA and the results are shown in Fig. 6. The overall mass loss during pyrolysis was 39%. It can be seen from the first derivative curve that the biggest rate of change takes place before $100\text{ }^{\circ}\text{C}$ when water is being eliminated. After that the changes taking place are smaller.

3.2. Ln-doped aerogels as catalyst for Michael reaction

The Michael addition reaction is one of the most versatile methods for the formation of carbon–carbon bonds, and has been widely used to generate valuable building blocks in organic synthesis.

Herein, we report our preliminary results by testing Ln-doped aerogels as catalysts in the Michael addition of ethyl 2-oxocyclopentanecarboxylate **1** to 3-buten-2-one **2** (Scheme 1).

The conversions of the Michael donor **1** catalyzed by organic and carbon aerogels are shown in Table 2. Ln-doped OAs were active catalysts in the Michael reaction with conversions of the starting keto ester ranging from 82 to 97% in 24 h.

La-, Pr- and Nd-doped carbon aerogels also exhibited activity in the Michael reaction. In case of the Ce-doped CAs the formation of several by-products was observed. The activity of CAs was not as high as that of OAs. This is due to the structural and chemical changes that take place during carbonization. After pyrolysis all lanthanide species might not be available for the catalytic reaction anymore and the lanthanide ions previously bound to the ion-exchange center might have formed new bonds.

In a previous study the formation of Eu mixed oxides during pyrolysis, which proved to not catalyze the reaction, was confirmed [19]. However, in our case the presence of oxides could not be confirmed by XRD analysis. This could be the reason for our CAs being catalytically active, since it is known that metal oxides are mostly inert as catalysts in Michael additions [19].

The results obtained with OA-s and CA-s as catalysts in the Michael addition are preliminary. Clearly, the experimental procedure used for determining the conversions needs further development, particularly the method for obtaining a small homogeneous amount of catalyst.

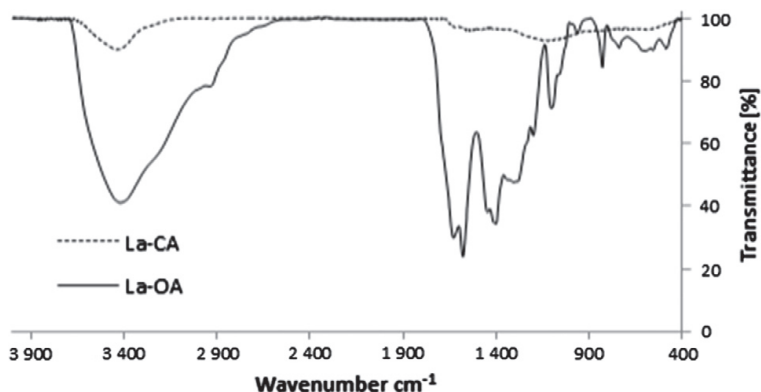


Fig. 5. FT-IR spectra of La-doped organic and carbon aerogel.

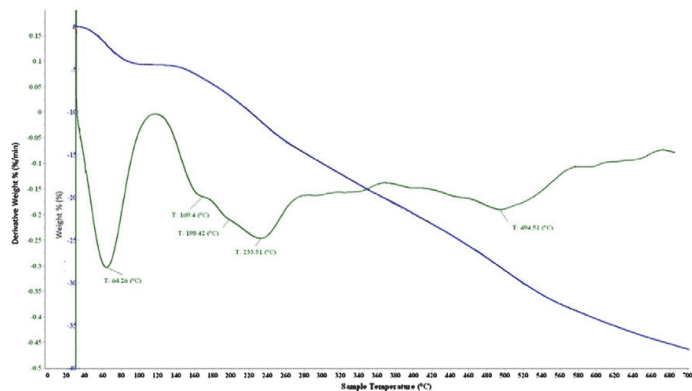
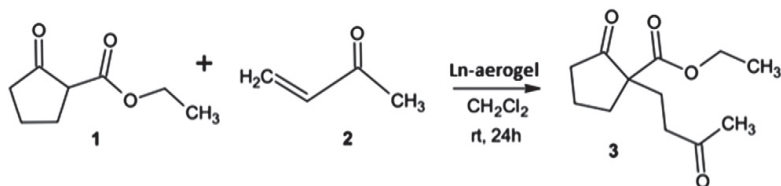


Fig. 6. Thermogravimetry analysis results. Blue line – weight loss (%); green line – derivative weight loss (%/min).



Scheme 1. Michael reaction of ethyl 2-oxocyclopentanecarboxylate **1** with 3-buten-2-one **2** in the presence of Ln-aerogels as catalysts.

4. Conclusions

A method for preparing Ln-doped (Ln = La, Ce, Nd, Pr) organic and carbon aerogels with catalytic activity in the Michael reaction was developed.

Using 5-methylresorcinol, 2,6-dihydroxy-4-methylbenzoic acid and formaldehyde to produce gels allows doping of aerogels with Ln species (Ln = Ce, La, Nd, Pr) through the ion-exchange method.

The mostly mesoporous materials with pore size diameters around 5–15 nm contained up to 12wt% of metal in organic aerogels and 22wt% in carbon aerogels. The specific surface area and pore volume of organic aerogels were higher than those of carbon aerogels. The materials were amorphous and no crystal structures were formed during pyrolysis.

In the Michael addition Ln-doped aerogels acted as catalysts. Organic aerogels with different lanthanides catalyze the Michael reaction efficiently. For carbon aerogels the conversion was modest (Pr) to high (Nd).

Table 2

Michael reaction of ethyl 2-oxocyclopentanecarboxylate **1** with 3-buten-2-one **2** in the presence of Ln-aerogels as catalysts.^a

Element	Conversion, %	
	OA	CA
La	84 ± 11 ^a	49 ± 23 ^a
Ce	82	–
Nd	97	92
Pr	91	32

^a For La-OA and -CA the percentages shown in Table 2 are the average of three separate experiments with added standard deviation. The conversion for La-OA was 93%, 72% and 87% respectively, and for La-CA respectively 73%, 46% and 27%.

Acknowledgments

The authors would like to thank Krisztian Kordas and Anne-Riika Leino for providing TEM images, Tiina Aid for performing FT-IR spectroscopy, Tiit Kaljuvee for thermogravimetric analyses and Jüri Krustok for carrying out Raman spectroscopy. VKG AS and CarboShale OÜ are acknowledged for donating the phenolic compounds and Molycorp Silmet for donating lanthanide salts. The authors thank the Estonian Ministry of Education and Research (Grant No. IUT 19–32) for financial support. This study was also financially supported by the European Union through the European Regional Development Fund project: TK114 “Mesosystems: Theory and Applications” (3.2.0101.11-0029) and by EU Structural Funds project “Electroactive nanoporous carbon composite films technology” No 3.2.1101.12-0007.

References

- [1] Pekala, R. W. Low density, resorcinol-formaldehyde aerogels. US patent 4873218, 1989.
- [2] R.W. Pekala, C.T. Alviso, F.M. Kong, S.S. Hulsey, Aerogels derived from multifunctional organic monomers, *J. Non-Cryst. Solids* 145 (1992) 90–98.
- [3] C. Moreno-Castilla, F.J. Maldonado-Hódar, Carbon aerogels for catalysis applications, *Carbon* 43 (2005) 455–465.
- [4] C. Moreno-Castilla, F.J. Maldonado-Hódar, J. Rivera-Utrilla, E. Rodríguez-Castellón, Group 6 metal oxide-carbon aerogels. Their synthesis, characterization and catalytic activity in skeletal isomerization of 1-butene, *Appl. Catal. A* 183 (1999) 345–356.
- [5] F.J. Maldonado-Hódar, M.A. Ferro-García, J. Rivera-Utrilla, C. Moreno-Castilla, Synthesis and textural characteristics of organic aerogels, transition metal-containing organic aerogels and their carbonized derivatives, *Carbon* 37 (1999) 1199–1205.
- [6] E. Bekyarova, K. Kaneko, Structure and physical properties of tailor-made Ce, Zr-doped carbon aerogels, *Adv. Mater.* 12 (2000) 1625–1628.
- [7] J.M. Miller, B. Dunn, Morphology and electrochemistry of ruthenium/carbon aerogel nanostructures, *Langmuir* 15 (1999) 799–806.

- [8] T.F. Baumann, G.A. Fox, J.H. Satcher, N. Yoshizawa, R. Fu, M.S. Dresselhaus, Synthesis and characterization of copper-doped carbon aerogels, *Langmuir* 18 (2002) 7073–7076.
- [9] For reviews on lanthanides as catalysts see:
- a) Yingming Yao, Kun Nie, Homogeneous catalysis, in: David A. Atwood (Ed.), *The Rare Earth Elements: Fundamentals and Applications*, John Wiley&Sons Ltd, 2012, pp. 459–474;
- b) John Hamilton Walrod II, David A. Atwood, Heterogeneous catalysis, in: David A. Atwood (Ed.), *The Rare Earth Elements: Fundamentals and Applications*, John Wiley&Sons Ltd, 2012, pp. 475–479.
- [10] M. Shibasaki, H. Sasai, Catalytic asymmetric carbon-carbon bond-forming reaction utilizing rare earth metal complexes, *Pure Appl. Chem.* 68 (3) (1996) 523–530.
- [11] K. Mikami, M. Terada, H. Matsuzawa, "Asymmetric" catalysis by lanthanide complexes, *Angew. Chem. Int. Ed.* 41 (2002) 3554–3571.
- [12] J. Christoffers, Transition-metal catalysis of the michael reaction of 1,3-dicarbonyl compounds and acceptor-activated alkenes, *Eur. J. Org. Chem.* 7 (1998) 1259–1266.
- [13] Comelles, J., Moreno-Mañas, M., Vallribera, A. Michael additions catalyzed by transition metals and lanthanide species. A review. *ARKIVOC*, 2005, ix, 207–238.
- [14] F. Bonadies, A. Lattanzi, L.R. Orelli, S. Pesci, A. Scettri, Lanthanides in organic synthesis: Eu³⁺-catalyzed Michael addition of 1,3-dicarbonyl compounds, *Tetrahedron Lett.* 34 (1993) 7649–7650.
- [15] J.H. Nelson, P.N. Howells, G.C. DeLullo, G.L. Landen, Nickel-catalyzed michael additions of β -dicarbonyls, *J. Org. Chem.* 45 (1980) 1246–1249.
- [16] X. Yang, X. Zhou, L. Lin, L. Chang, X. Liu, X. Feng, Highly enantioselective direct Michael addition of nitroalkanes to nitroolefins catalyzed by La(OTf)₃/N, N'-dioxide complexes, *Angew. Chem. Int. Ed.* 47 (2008) 7079–7081.
- [17] J. Comelles, À. Pericas, M. Moreno-Mañas, A. Vallribera, G. Drudis-Solé, A. Lledos, T. Parella, A. Roglans, S. García-Granda, L. Rocas-Fernández, Highly enantioselective electrophilic amination and michael addition of cyclic β -ketoesters induced by lanthanides and (S, S)-ip-pybox: the mechanism, *J. Org. Chem.* 72 (2007) 2077–2087.
- [18] For references on lanthanide grafting on silica xerogels see:
- a) A.M. Klonkowski, S. Lis, M. Pietraszkiewicz, Z. Hnatejko, K. Czarnobaj, M. Elbanowski, Luminescence properties of materials with Eu(III) complexes: role of ligand, coligand, anion, and matrix, *Chem. Mater.* 15 (2003) 656–663;
- b) M.A. Zaitoun, D.M. Goken, L.S. Bailey, T. Kim, C.T. Lin, Thermoanalysis and emission properties of Eu³⁺/Eu²⁺ in Eu³⁺-doped xerogels, *J. Phys. Chem.* 104 (2000) 189–196;
- c) F. Embert, A. Mehdi, C. Reye, R.J.P. Corriu, Synthesis and luminescence properties of monophasic organic-inorganic hybrid materials incorporating europium(III), *Chem. Mater.* 13 (2001) 4542–4549.
- [19] S. Martínez, L. Martín, E. Molins, M. Moreno-Mañas, A. Roig, A. Vallribera, Europium-containing organic gels and organic and carbon aerogels. Preparation and initial applications in catalysis, *Monatsh. Chem.* 137 (2006) 627–633.
- [20] F. Pérez-Caballero, A.-L. Peikolaimein, M. Uibu, R. Kuusik, O. Volobujeva, M. Koel, Preparation of carbon aerogels from 5-methylresorcinol-formaldehyde gels, *Micro-porous Mesoporous Mater.* 108 (2008) 230–236.
- [21] K. Kreek, M. Kulp, M. Uibu, A. Mere, K. Koel, Preparation of Metal-doped Carbon Aerogels from Local Oil Shale Processing By-products, *Oil Shale* 31 (2) (2014) 185–194.
- [22] A.-L. Peikolaimein, O. Volobujeva, R. Aav, M. Uibu, M. Koel, Organic acid catalysed synthesis of 5-methylresorcinol based organic aerogels in acetonitrile, *J. Porous. Mater.* 19 (2012) 189–194.
- [23] L.C. Cotet, M. Gich, A. Roig, I.C. Popescu, V. Cosoveanu, E. Molins, et al., Synthesis and structural characteristics of carbon aerogels with a high content of Fe, Co, Ni, Cu, and Pd, *J. Non-Cryst. Solids* 352 (2006) 2772–2777.
- [24] A.C. Ferrari, J. Robertson, *Phys. Rev. B* 61 (2000) 14095–14107.

Publication III

Kreek, K., Sarapuu, A., Samolberg, L., Joost, U., Mikli, V., Koel, M., Tammeveski, K. Cobalt-containing nitrogen-doped carbon aerogels as efficient electrocatalysts for the oxygen reduction reaction. – *Chemelectrochem*, 2015, 2, 2079-2088.

Cobalt-Containing Nitrogen-Doped Carbon Aerogels as Efficient Electrocatalysts for the Oxygen Reduction Reaction

Kristiina Kreek,^[b] Ave Sarapuu,^{*[a]} Lars Samolberg,^[a] Urmas Joost,^[c] Valdek Mikli,^[d] Mihkel Koel,^[b] and Kaido Tammeveski^[a]

The electrocatalysis of the oxygen reduction reaction (ORR) on cobalt-containing nitrogen-doped carbon aerogels (CAs) was studied in alkaline solution. CA-based catalyst materials with varied compositions were prepared through the sol-gel polymerisation of organic precursors (resorcinol derivatives and melamine), followed by insertion of Co by using an ion-exchange process and pyrolysis. The concentrations of the precursors had a large effect on the structure and physicochemical properties of the materials, as characterised by using SEM,

XRD, XPS, atomic adsorption spectroscopy, and N₂-adsorption analysis. The electrocatalytic activity of Co-containing N-doped CAs for the ORR was higher than that of nitrogen-free CA, and this activity increased with increasing Co content. The most active catalyst materials supported the four-electron reduction of O₂ and short-term stability tests indicated their high durability. Co-containing N-doped CAs can be regarded as a promising class of material for the cathode catalysts of alkaline membrane fuel cells.

1. Introduction

Currently, the development of efficient and stable, non-precious-metal catalysts for the oxygen reduction reaction (ORR) is one of the most important issues in optimising the cost and performance of low-temperature fuel cells.^[1–3] A promising class of catalysts is transition-metal-containing nitrogen-doped carbon materials (M/N/C catalysts) that can be prepared through the pyrolysis of a carbon support in the presence of a nitrogen precursor and a transition-metal (usually Co or Fe) salt.^[1,2] Since early studies for the ORR on this type of pyrolysed material by Yeager and co-workers in 1989,^[4] the electrocatalytic activity of M/N/C catalysts has been significantly improved and it currently approaches that of commercial Pt/C catalysts in acidic solution.^[2] In alkaline solutions, their activity is even higher and, in some cases, can surpass that of the Pt-based catalysts.^[5–7] Still, further enhancement of the volumetric activity of M/N/C catalysts remains a great challenge that can be approached by optimising the catalyst structure, increasing the density of the active sites and average active-site turnover frequency (TOF).^[1] However, rational design of M/N/C catalysts is impeded by uncertainties in the exact structures of the

active sites for the ORR, the complexity of the reaction mechanism and the uncontrollability of the synthesis processes.^[11]

M/N/C catalysts can be synthesised from various carbon nanomaterials, such as carbon black, carbon nanotubes, graphene, and so forth.^[3] Alternatively, porous N-doped carbon structures can be obtained through the carbonisation of nitrogen-containing organic polymers. For instance, carbon aerogels (CAs) are often prepared through pyrolysis of organic aerogels^[8] that can be synthesised by using various methods; the most studied process involves the synthesis of resorcinol–formaldehyde gel by using the sol-gel method and subsequent supercritical drying.^[9] To prepare nitrogen-doped CAs or xerogels, pyrolysis in a NH₃ atmosphere^[10,11] or nitrogen-containing precursors for gel preparation^[12–15] can be used. High surface area, low mass density as well as high electrical conductivity and chemical stability make CAs good electrode materials for low-temperature fuel cells, among other applications.^[8,16]

Oxygen reduction has been studied on various catalysts based on N-doped CAs or xerogels. For instance, nitrogen doping has been shown to increase the electrocatalytic activity for the ORR with CAs prepared from sustainable precursors through hydrothermal carbonisation,^[17–19] however, the ORR activity of these materials in alkaline solution is still considerably lower than that of the Pt/C catalyst.^[17–19] Recently, activities similar to that of Pt/C have been reached on metal-free N-doped CAs prepared from ionic liquids.^[20] CAs synthesised in the presence of transition metals have shown moderate activities for the ORR in acidic solution,^[10,13,14,21,22] but, in alkaline solution, activities comparable to that of commercial Pt/C have been reached.^[11,22] High ORR activities were also observed on N-doped CAs containing cobalt-oxide nanoparticles that were prepared from commercial melamine sponge.^[23] Similarly, high

[a] Dr. A. Sarapuu, L. Samolberg, Dr. K. Tammeveski
Institute of Chemistry, University of Tartu
Ravila 14 A, 50411 Tartu (Estonia)
E-mail: ave.sarapuu@ut.ee

[b] K. Kreek, Dr. M. Koel
Institute of Chemistry, Tallinn University of Technology
Akadeemia tee 15, 12618 Tallinn (Estonia)

[c] Dr. U. Joost
Institute of Physics, University of Tartu
Ravila 14C, 50411 Tartu (Estonia)

[d] Dr. V. Mikli
Center for Materials Research, Tallinn University of Technology
Ehitajate tee 5, 19086, Tallinn (Estonia)

Table 1. Elemental composition, N₂-adsorption analysis results and ORR mass activity for CAs.

Sample	Monomer [mol %]			Elemental composition [wt %]				S_{BET} [m ² g ⁻¹]	V_{TOT} [mm ³ g ⁻¹]	V_{MIC} [mm ³ g ⁻¹]	MA ^[a] [A g ⁻¹]
	Mel	MR	dHMBA	Co	N	C	H				
Co-NCA1	30	60	10	2.0	1.6	87.0	1.3	370	330	85	2.8
Co-NCA2	30	45	25	4.3	2.5	82.2	1.0	314	230	70	3.2
Co-NCA3	40	40	20	4.1	2.9	80.2	1.4	461	399	95	3.4
Co-NCA4	60	15	25	5.3	2.6	81.0	0.7	316	228	54	14.4
Co-NCA5	75	0	25	5.6	8.4	68.9	1.2	118	93	1.5	12.5
Co-CA ^[b]	0	75	25	2.6	0.03	n.d.	n.d.	n.d.	n.d.	n.d.	2.3
NCA ^[b]	60	15	25	0	14.3	65.2	1.3	n.d.	n.d.	n.d.	0.23

[a] At -0.2 V. [b] n.d. = not determined.

activities for different N-doped carbon materials containing nanoparticles of cobalt oxides^[24–30] or metallic cobalt^[31–34] have been observed in several other studies, and a synergistic effect of N-doped carbon and cobalt or cobalt-oxide nanoparticles on the electrocatalytic activity for ORR has been proposed.^[24–27, 29, 31]

In this study, N-doped CAs were prepared through the pyrolysis of organic aerogels synthesised from 5-methylresorcinol (MR), which is a locally available by-product from the oil-shale industry, and its derivative, 2,6-dihydroxy-4-methylbenzoic acid (dHMBA).^[35] Melamine (Mel) was used as a nitrogen-containing precursor and the ion-exchange method was employed for metal doping.^[36, 37] Considering that Co- and Fe-containing N-doped CAs previously prepared by our group showed high activity for the ORR,^[15] we were interested in exploring how the concentrations of the organic precursors affected the physical properties and the ORR activities of the resulting CAs.

2. Results and Discussion

2.1. Physicochemical Characterisation of CA-based Catalysts

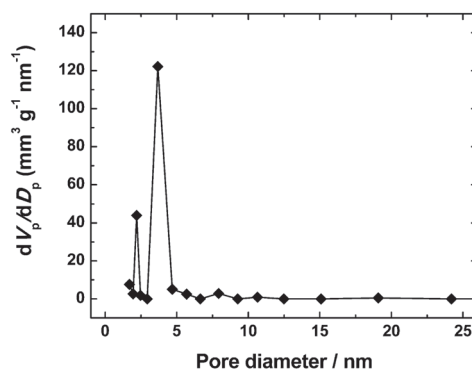
The composition of CAs was varied during the preparation process, using different amounts of melamine, MR and dHMBA to study the effects on the properties of CAs. Table 1 shows the molar percentages of monomers that were used during the preparation of different samples and the measured elemental compositions. Co-containing N-doped CAs prepared by using different amounts of monomers are denoted Co-NCA1, Co-NCA2, and so forth (Table 1). For comparison, nitrogen-free Co-containing CA (Co-CA) and a cobalt-free material (NCA) were also prepared; in the latter case, the ion-exchange procedure was not performed.

The molar percentage (mol%) of dHMBA was varied from 10 to 25. It can be noted that, with the increase in the amount of dHMBA in the composition of the aerogel, the Co content also increased (Table 1). This is attributed to dHMBA having the ion-exchange moiety (the carboxylic group) that binds Co²⁺ during immersion in cobalt-nitrate solution. As previously concluded, the higher amount of dHMBA in the sample increased the weight percent of metal in the aerogels.^[37]

The melamine content was also varied during gel preparation. The nitrogen content in cobalt-containing samples was changed from 1.6 to 8.4 wt% by increasing the amount of mel-

amine (Table 1). The carbon content in the samples was also affected by the increasing amount of melamine, decreasing from 87 to 69 wt% by increasing the amount of melamine.

Brunauer–Emmett–Teller (BET) analysis was used to determine the specific surface areas and pore volumes for the CAs (Table 1). Samples Co-NCA1 to Co-NCA4 had high BET surface areas ($S_{\text{BET}} = 314\text{--}461\text{ m}^2\text{ g}^{-1}$) and total pore volumes (V_{TOT}) from 228 to 399 mm³ g⁻¹. Figure 1 shows the pore-size distribution

**Figure 1.** Pore-size distribution analysis results for Co-NCA2.

of sample Co-NCA2, indicating that this material has mostly pores with the diameters (D_p) of 2 and 4 nm.

Co-NCA5 had significantly lower S_{BET} and V_{TOT} values. During preparation, Co-NCA5 had the highest melamine content and no MR was added. The S_{BET} and V_{TOT} values for the organic aerogel precursor of Co-NCA5 were also measured and the respective results were 868 m² g⁻¹ and 1490 mm³ g⁻¹. This shows that a drastic reduction in specific surface area and pore volume occurred during pyrolysis.

Thermogravimetric analysis (TGA) results in Figure 2 show the mass-loss curves of organic aerogels (precursors of Co-NCA1–Co-NCA5) during pyrolysis in an Ar atmosphere. The mass loss was between 56 and 80%, with the highest being for Co-NCA1. Samples that were prepared by using higher melamine contents (Co-NCA3 to Co-NCA5) had similar mass losses (60–65 wt%). The mass-loss curve is smooth in shape, without abrupt changes for Co-NCA1 and Co-NCA2. However, for Co-

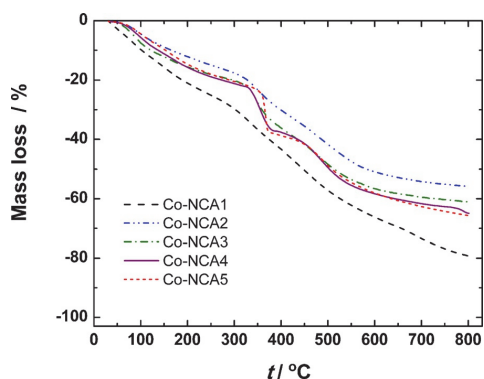


Figure 2. TGA results for organic aerogel precursors of the CA materials.

NCA4 and Co-NCA5, there is a steep change at 340–370 °C. Melamine resins have also shown large mass loss, owing to the decomposition and evaporation of the products generated in that temperature range.^[36] The decomposition of melamine and, therefore, the structure of the material could explain the smaller surface area and porosity of CAs prepared with higher melamine contents.

The surface morphologies of the CAs were evaluated by using scanning electron microscopy (SEM; Figure 3). The morphology of the CA prepared with the highest MR content (Co-NCA1) is similar to that of resorcinol/formaldehyde CAs^[39] with a grainy structure composed of linked spheres (Figure 3a and 3b). The Co-NCA2 aerogel was prepared by using more melamine and less MR than for Co-NCA1. In the structure of the Co-NCA2 (Figure 3d), separate particles forming the aerogel network are not visible and the morphology is different from that of the resorcinol/formaldehyde CAs. This is also the case in samples prepared with higher melamine contents (Co-NCA4 and Co-NCA5), where the surfaces of the aerogels appear to be composed of particles merged together. This shows that the addition of resorcinol derivatives is necessary to keep the bead-like structure that is associated with resorcinol/formaldehyde CAs. The structure of melamine-rich aerogels will be affected by the sudden mass loss and decomposition of melamine during pyrolysis.

Figure 3c shows an SEM image of Co-NCA1 taken by using backscattered electron (BSE) imaging, where brighter spots can be assigned to Co particles. These are evenly distributed in the sample and have sizes ranging from 5 to 40 nm (Figures 3a–c). The cobalt nanoparticles in Co-NCA3 are also evenly distributed (cf. Figure 3g) and the sizes are larger (10–100 nm) than in Co-NCA1 (Figures 3e and 3f). This is probably caused by the increased amount of metal in the aerogel.^[36,37] Samples Co-NCA4 and Co-NCA5 have smaller nanoparticles (10–40 nm) than Co-NCA3, and SEM images show the formation of long cylindrical structures with a diameter of about 20 nm, which appear to be carbon nanotubes (CNTs) or nanoribbons (Figures 3h, 3j and 3k). The BSE image (Figure 3j) shows brighter spots (Co nanoparticles) at the end of the long structures. For-

mation of CNTs during pyrolysis in the presence of cobalt is a well-known process, and cobalt nanoparticles are used as a catalyst in the synthesis of CNTs when using chemical vapour deposition.^[40] Cobalt has also been shown to induce the formation of nanoribbons in CAs.^[41] From the nitrogen-containing precursors, N-doped CNTs can be synthesised. For instance, CNTs have been prepared by using chemical vapour deposition with melamine and iron precursors.^[42] In addition, the formation of nitrogen-doped CNTs through the pyrolysis of melamine–formaldehyde resin in the presence of iron has recently been demonstrated.^[43] Therefore, it can be assumed that long carbon nanostructures in Co-NCA4 and Co-NCA5 are also nitrogen-doped CNTs.

Figure 4 shows X-ray diffraction (XRD) peaks for crystalline Co in all samples, which is an expected result under these pyrolysis conditions.^[37] A small peak attributed to Co_3O_4 indicates oxidation of the surface of Co nanoparticles. Formation of graphitic structures is clearly visible in samples Co-NCA1 and Co-NCA2. In Co-NCA5, a peak at the same location cannot be identified. This shows that the increasing melamine content inhibits the formation of graphitic structures in this case. In the diffraction patterns shown in Figure 4, there are a few other small peaks visible at various degrees. The identification of these peaks is problematic, owing to the limited amount of data. It is likely that various cobalt–carbon, cobalt–nitrogen or nitrogen–carbon structures have also formed in the CAs.

X-ray photoelectron spectroscopy (XPS) was used to analyse the surface composition of the catalysts. High-resolution XPS spectra for Co-NCA4 and NCA are presented in Figure 5. The N 1s peaks were deconvoluted into four symmetrical peaks, corresponding to different nitrogen species: pyridinic (398.1 eV), pyrrolic (399.9 eV), graphitic (401.0 eV) and pyridine-N-oxide (403.3 eV).^[19] Similar nitrogen species are typically found in M/N/C catalysts.^[2] It can be seen that, in both catalyst materials, the largest peak belongs to pyridinic nitrogen. Pyridinic and graphitic nitrogen are considered to be the most active centres for oxygen electroreduction.^[44] It is also evident that the relative amount of pyrrolic and graphitic N is larger for Co-NCA4. It has been shown earlier that the presence of Co increases the percentage of graphitic N centres^[34] that play an important role in ORR electrocatalysis.^[45] Analysis of the Co 2p peaks suggested that Co may be present as $\text{Co}(\text{OH})_2$ on the surface. However, the interpretation of XPS spectra of transition metals is complicated, because of the complexity of their 2p spectra (peak asymmetries, complex multiplet splitting, uncertain and overlapping binding energies, etc.).^[46] Therefore, it is also possible that combinations of other oxides, hydroxides and N-coordinated metal ions might result in similar spectra.

2.2. Oxygen Reduction on CA-based Catalysts

The electrocatalytic behaviours of various CAs for the ORR were studied by using the rotating disc electrode (RDE) method in 0.1 M KOH solution. A set of RDE polarisation curves for Co-NCA4 in Figure 6 shows that this material is a rather active catalyst for the ORR, as, from the onset potential at

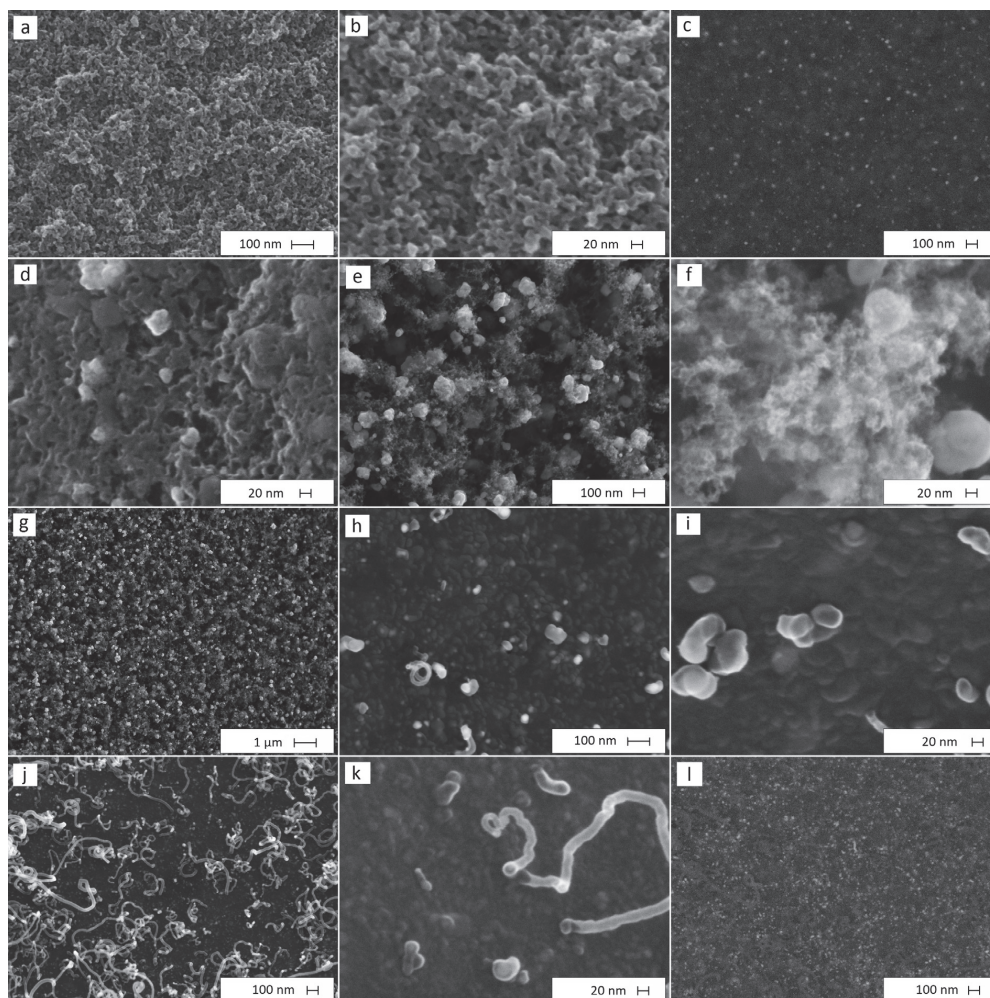


Figure 3. SEM images for a,b) Co-NCA1, c) Co-NCA1 (backscattered electron imaging), d) Co-NCA2, e–g) Co-NCA3, h, i) Co-NCA4, j, k) Co-NCA5 and l) Co-NCA5 (backscattered electron imaging taken at the same spot as in Figure 5j).

about -0.17 V, the current increases sharply and reaches its diffusion-limited value at approximately -0.3 V.

A comparison of RDE voltammetry curves of O_2 reduction for Co-containing N-doped CAs of different compositions is presented in Figure 7a. It appears that two materials, Co-NCA4 and Co-NCA5, are most active; the half-wave potentials ($E_{1/2}$) for these are -0.210 and -0.219 V, respectively, which are only about 20–30 mV more negative than that of the commercial Pt/C catalyst. The other three materials are slightly less active, the $E_{1/2}$ values being in the range between -0.258 and -0.270 V. The activities of Co-NCA4 and Co-NCA5 are rather similar to that of Co-containing N-doped CAs prepared from commercial melamine sponge^[23] and slightly lower than that of Fe-containing N-doped CAs synthesised from ionic liquids,^[22]

but considerably higher compared to some metal-free CAs.^[18, 19]

To analyse the RDE data, the Koutecky–Levich equation [Eq. (1)] was used:^[47]

$$\frac{1}{j} = \frac{1}{j_k} + \frac{1}{j_d} = -\frac{1}{nFkC_{O_2}^b} - \frac{1}{0.62nFD_{O_2}^{2/3}v^{-1/6}C_{O_2}^b\omega^{1/2}} \quad (1)$$

where j is the measured current density, j_k and j_d are kinetic and diffusion-limited current densities, respectively, n is the number of electrons transferred per O_2 molecule, k is the rate constant for O_2 reduction, F is the Faraday constant (96485 C mol $^{-1}$), ω is the electrode rotation rate (rad s $^{-1}$), $C_{O_2}^b$ is

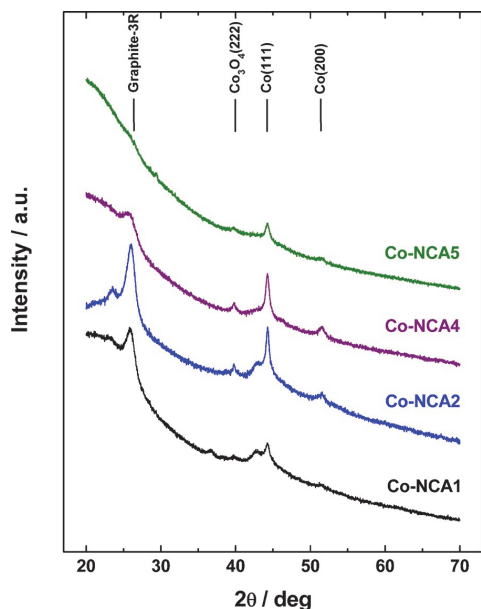


Figure 4. XRD analysis results for the CA materials.

the concentration of oxygen in the bulk ($1.2 \times 10^{-6} \text{ mol cm}^{-3}$),^[48] D_{O_2} is the diffusion coefficient of oxygen ($1.9 \times 10^{-5} \text{ cm}^2 \text{ s}^{-1}$)^[48] and ν is the kinematic viscosity of the solution ($0.01 \text{ cm}^2 \text{ s}^{-1}$).^[49] From the slopes of the Koutecky–Levich plots, the number of electrons transferred per O_2 molecule (n) can be calculated by using Equation (1). Figure 7b shows the Koutecky–Levich plots and the values of n for Co-containing N-doped CAs. It is evident that the ORR yields water as the main product at negative potentials for these materials, as $3.9 < n <$

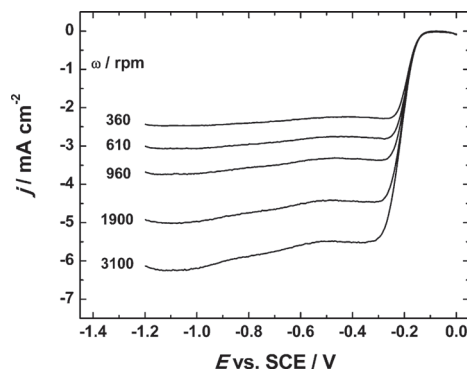


Figure 6. RDE voltammetry curves of oxygen reduction on a Co-NCA4 catalyst in O_2 -saturated 0.1 M KOH; $\nu = 10 \text{ mV s}^{-1}$.

4.0, and only Co-NCA2 shows slightly lower n values. At more positive potentials, the value of n gradually decreases until $3.3 < n < 3.7$ at -0.5 V , as a result of increasing production of peroxide. Peroxide production is lower on the most active catalysts, for instance, the peroxide yield on Co-NCA4 is about 15% at low overpotentials and it decreases to zero at -1 V . Low levels of peroxide production on metal-containing N-doped CAs have been observed in earlier studies^[14,22,23] and it is an important pre-requisite for the application of these materials as cathode catalysts on low-temperature fuel cells.^[50]

For a more direct comparison of the electrocatalytic activities, the ORR mass activities (MAs) of the CAs were calculated by using Equation (2):

$$\text{MA} = I_k / m \quad (2)$$

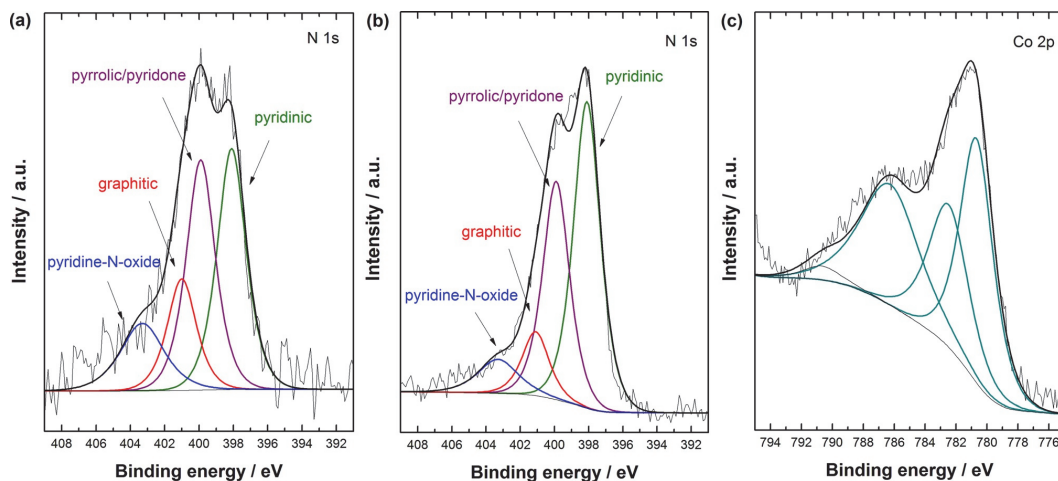


Figure 5. XPS spectra in the N 1s (a, b) and Co 2p (c) regions for Co-NCA4 (a, c) and NCA (b) catalysts.

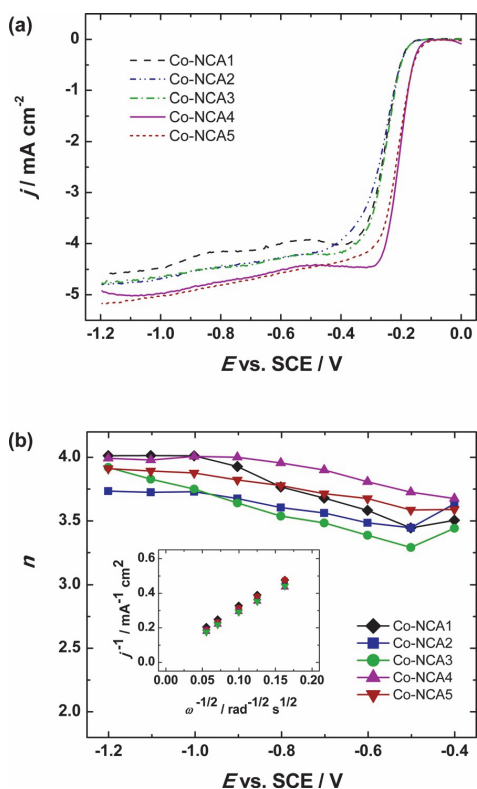


Figure 7. RDE voltammograms of oxygen reduction (a) and dependence of the number of electrons transferred per O_2 molecule on potential (b) for Co-containing N-doped CAs in O_2 -saturated 0.1 M KOH; $\nu = 10 \text{ mVs}^{-1}$, $\omega = 1900 \text{ rpm}$. Inset shows the Koutecky–Levich plots at -0.6 V .

where i_k is the kinetic current at a certain potential and m is the mass of the catalyst on the electrode surface (Table 1). The values of MA at -0.2 V are highest for Co-NCA4 and Co-NCA5 and about four times lower for the other three materials. According to the results of elemental analysis, these two most active materials also have higher cobalt contents. Increasing ORR activity with increasing Co content has been observed for Co_3O_4 -containing N-doped graphene, and it has been suggested that one of the active reaction sites in these hybrid materials could be Co-oxide nanoparticles.^[24] The total nitrogen content is highest for Co-NCA5, but much lower for Co-NCA4, although the activities are similar. This suggests that only a small fraction of nitrogen is composing the active centres for the ORR and the remaining part is either in a passive form or inaccessible to O_2 molecules. According to the literature, only certain types of nitrogen centres are considered to be involved in ORR electrocatalysis,^[2] and the activity of the catalysts does not directly depend on the total nitrogen content.^[27,50,51] The surface area and pore volume do not seem to have a large effect on the ORR activity of the materials, because Co-NCA5, which has a low surface area and porosity, has a similar activity to Co-NCA4, which has much higher S_{BET} and V_{TOT} values. How-

ever, the nanotubes or nanoribbons observed for Co-NCA4 and Co-NCA5 may contribute to the higher activity of these materials. Both the metal-free^[52] and transition-metal-containing^[32,53] N-doped CNTs have been shown to be very active catalysts for the ORR in alkaline solutions. This may arise from improved electrical conductivity of metal/CNT hybrid materials.^[28] In addition, embedded transition-metal nanoparticles in N-doped CNTs can lower the local work function of the carbon surface and, thereby, enhance the ORR activity.^[54] Subsurface iron or iron carbide have been suggested to increase the ORR activity of nitride-modified carbon fibres through the stabilisation of the peroxide intermediate.^[7]

For comparison, O_2 reduction was also studied on cobalt- and nitrogen-free CAs (Figure 8a). In accordance with the earli-

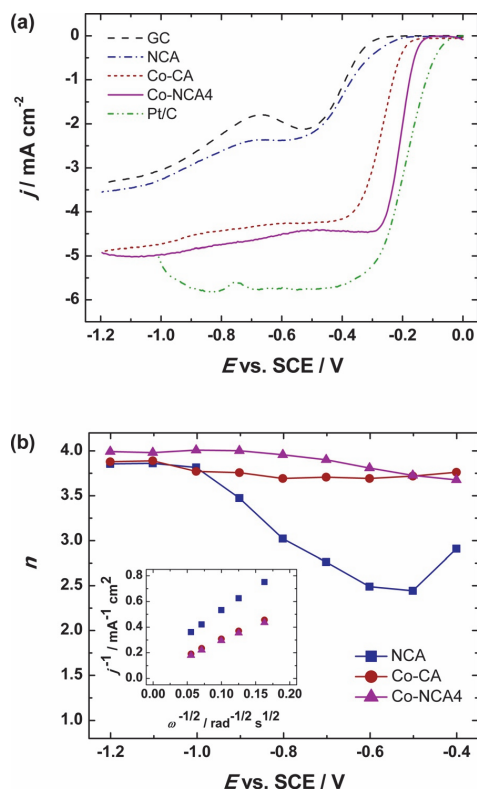


Figure 8. RDE voltammograms of oxygen reduction (a) and dependence of the number of electrons transferred per O_2 molecule on potential (b) for CA-based catalysts, glassy carbon and Pt/C catalyst in O_2 -saturated 0.1 M KOH; $\nu = 10 \text{ mVs}^{-1}$, $\omega = 1900 \text{ rpm}$. Inset shows the Koutecky–Levich plots at -0.6 V .

er results,^[15] the ORR activity of the cobalt-free material (NCA) was much lower than that of the Co-containing catalysts; the $E_{1/2}$ value of O_2 reduction on this material was -0.434 V and MA = 0.23 Ag^{-1} . In addition, the value of n was considerably lower for NCA compared to metal-containing CAs (Figure 8b).

Higher activities and lower peroxide yields of metal-containing N-doped carbon catalysts, as compared to the metal-free materials, have been observed in several studies,^[6,55] and it has been proposed that the peroxide intermediate is further reduced to OH^- on metal-nitrogen coordinated centres in alkaline solution.^[56] Interestingly, the Co-containing CA prepared from precursors not containing nitrogen (Co-CA) showed much higher activity for the ORR compared to NCA, but it was lower than that of Co-NCA4 (see Figure 8a and Table 1). Cobalt and cobalt-oxide nanoparticles have been suggested to play an important role in ORR electrocatalysis in alkaline solution. For instance, the N-doped graphene and Co_3O_4 nanoparticles supported on undoped graphene showed rather high activities towards the ORR, but the activity was further increased for Co_3O_4 /N-doped graphene, suggesting a synergetic effect between cobalt-oxide nanoparticles and N-containing centres.^[24,25] Similar results have been obtained on CoO-containing N-doped reduced graphene oxide (rGO).^[26,27] In addition, the activity of Co_3O_4 /N-doped mesoporous graphene decreased with decreasing Co_3O_4 loading in the catalyst.^[29] Therefore, the highest activities observed for Co-NCA4 and Co-NCA5 can also be attributed to the higher Co content in the catalysts.

There are several explanations in the literature for the synergetic effect of cobalt or cobalt-oxide nanoparticles and N-doped carbon on the ORR kinetics. For instance, it has been attributed to the increase in bonding strength between carbon and the catalyst, owing to nitrogen doping.^[24,29] A dual-site mechanism of the ORR in alkaline solution has been proposed for N-doped carbon catalysts derived from cobalt precursors and polypyrrole, according to which the O_2 molecule is first adsorbed on Co- N_x -type site and converted to HO_2^- , which is further reduced on oxide-coated Co nanoparticles.^[57] Alternatively, based on the results obtained on a graphene-based catalyst, it has been suggested that the N-doped graphene domains adjacent to the Co nanoparticles are the main active sites for the ORR, whereas the Co-N-C structures at the interface of Co nanoparticles and N-doped graphene help to activate O_2 molecules for better ORR activity.^[34] Density functional theory (DFT) calculations have indicated that, in N-doped rGO-based catalysts, a stable $\text{rGO}(\text{N})-\text{Co}^{\text{II}}-\text{O}-\text{Co}^{\text{II}}-\text{rGO}(\text{N})$ structure is most likely the active species for the ORR.^[26]

The results obtained in this study also indicate that the most active electrocatalysts contain both cobalt and nitrogen precursors; however, a rather facile $4e^-$ reduction of O_2 on nitrogen-free material implies that the main active sites may be cobalt and/or cobalt-oxide nanoparticles. It is also evident that the Co content is higher for the nitrogen-containing CAs compared to Co-CA (Table 1). It has been demonstrated that, in the synthesis of Co-containing N-doped rGO, the presence of nitrogen helped to increase the amount of cobalt.^[27] Although the metal-free nitrogen-containing materials have, in some cases, shown very high activity for the ORR in alkaline solution,^[51,52,58] the activity of Co-free N-doped CA was rather low and there was no obvious dependence of the ORR activity on the nitrogen content for the other CA-based catalysts.

The mass-transfer-corrected Tafel plots of O_2 reduction on various catalysts were constructed on the basis of the RDE

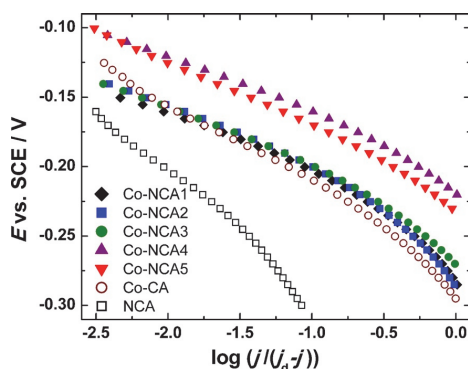


Figure 9. Mass-transfer-corrected Tafel plots for O_2 reduction on CA-based catalysts in 0.1 M KOH; $\omega = 1900$ rpm.

data (Figure 9). The Tafel slope values were in the range between -39 and -47 mV for all Co-containing N-doped materials at low overpotentials, which is consistent with the results obtained for N-doped graphene-containing Co_3O_4 nanoparticles^[24,25] and suggests that protonation of adsorbed O_2^- may be the rate-limiting step.^[24] For Co-CA, the slope was -53 mV, which also coincides well with the slope value for Co_3O_4 nanoparticles supported on non-doped graphene.^[24] For the Pt/C catalyst, a slope value of -61 mV was found, as usually observed for Pt catalysts at low overpotentials in alkaline media.^[59] Cobalt-free material showed the highest Tafel slope value (-76 mV).

To evaluate the durability of the most active CA-based catalyst in electrochemical conditions, it was subjected to a short-term stability test (1000 potential cycles between 0 and -0.6 V at 100 mV s^{-1} in O_2 -saturated 0.1 M KOH). A comparison of RDE results before and after potential cycling showed that this material is very stable, as the $E_{1/2}$ value shifted by only about 2 mV in the negative direction, and the kinetic current at

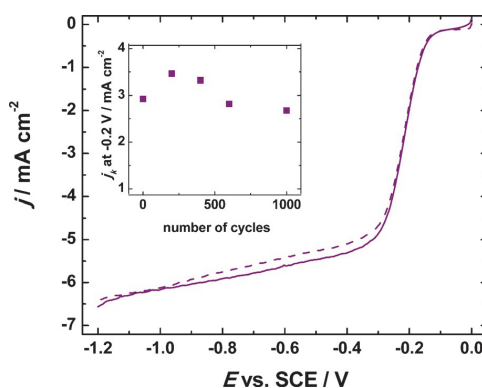


Figure 10. RDE voltammetry curves of oxygen reduction on Co-NCA4 catalyst in O_2 -saturated 0.1 M KOH before and after stability testing; $\nu = 10 \text{ mV s}^{-1}$, $\omega = 1900$ rpm. Inset shows the change in j_k values, calculated at -0.2 V during potential cycling.

–0.2 V decreased by about 8% (Figure 10). M/N/C catalysts generally show much higher durability than noble-metal-based catalysts in alkaline and acidic solutions, which can be explained by the incorporation of the active centres into the carbon framework. If degradation of the active centres occurs on the surface, some new centres are exposed to the solution and the ORR activity of the catalyst remains high.^[60] It has also been suggested that nitrogen doping of the carbon support increases the strength of the interaction between the cobalt-oxide nanoparticles and carbon, thereby preventing catalyst agglomeration and increasing the stability of the catalyst.^[29] Higher durability of N-doped CAs, as compared to Pt/C catalysts, has been observed in both acidic^[10,14] and alkaline^[11] solutions. In addition, similarly to the other M/N/C catalysts, these materials show high methanol tolerance and are, thus, promising catalysts for direct methanol fuel cells.^[11,18]

By changing the relative amount of precursors in the synthesis of organic aerogels, the chemical composition of resulting CAs can easily be varied. However, the morphological features of the CAs, most importantly the pore structure and size distribution, also depend on the composition of organic gels and influence the performance of the catalysts. It is important to further optimise the synthesis procedure, to prepare CA-based materials with high density of active sites for ORR and favourable pore structure, which would likely result in even more active electrocatalysts.

3. Conclusions

Cobalt-containing nitrogen-doped CAs were prepared from resorcinol derivatives and melamine, and an ion-exchange process was used to introduce metal into the aerogels. The results showed that, by varying the dHMBA or melamine content, the compositions of the CAs can be altered. CAs showed high surface area and had both meso- and microporosity. The increasing amount of melamine in the compositions of the aerogels decreased the surface areas and pore volumes, owing to the rapid change in mass taking place during pyrolysis, which was demonstrated by using TGA. The SEM images showed the structures of the CAs to be similar to those of resorcinol/formaldehyde aerogels for CAs prepared with low melamine contents, but the structure changed with increasing melamine content. XRD analysis revealed the presence of crystalline structures of cobalt and cobalt oxide and SEM images confirmed the presence of cobalt nanoparticles. In CAs prepared with higher melamine and cobalt contents, CNT structures had also formed.

The electrocatalytic activity of Co-containing N-doped CAs for the ORR was rather high and depended on the composition. The materials with the highest Co content showed the highest ORR activities, which can be associated with the coexistence of cobalt nanoparticles and N-doped carbon structures. The durability of these materials is high in alkaline solution and they mostly support the 4e⁻ pathway of O₂ reduction, thus showing great promise for applications as cathode catalysts in alkaline fuel cells.

Experimental Section

Materials and Preparation of CAs

5-Methylresorcinol (MR), with a reported purity of >99% was provided by VKG AS (Estonia) and 2,6-dihydroxy-4-methylbenzoic acid (dHMBA), with a purity of >99%, was donated by CarboShale OÜ (Estonia). Melamine (Mel), with a purity of >99%, was purchased from Aldrich (USA). Anhydrous sodium carbonate, with a purity of 99.8%, was purchased from Riedel-de Haen (Germany). Formaldehyde (FA) (37 wt% solution in water) was purchased from Sigma-Aldrich. CO₂ (99.8%) was obtained from Eesti AGA AS (Estonia). Cobalt(II) nitrate hexahydrate (>98%) was purchased from Sigma-Aldrich (USA). The Milli-Q water system was used to obtain ultrapure (18.2 MΩ cm) water.

A supercritical extraction system with a double-clamp autoclave (100 mL in volume) was constructed by NWA Analytische Meßgeräte GmbH (Germany). The pyrolysis oven, type MTF 12/38/400, with a maximum temperature of 1200 °C was from Carbolite (United Kingdom).

The preparation of metal-doped CAs was based on the ion-exchange method.^[36,37] The amounts of substances (in grams) to be used for gel preparation were calculated by using Equation (3):

$$\frac{\text{substances}}{\text{water}} = \frac{\text{monomers} + \text{FA} + \text{Na}_2\text{CO}_3}{\text{water added} + \text{water from FA solution}} = 0.25 \quad (3)$$

The ratio of substances to water was always kept at 0.25. The amounts of the monomers (Mel, MR and dHMBA) used were varied during preparation from 0 to 75 mol% [Eq. (4)]:

$$x \% (\text{Mel}) + y \% (\text{MR}) + z \% (\text{dHMBA}) = 100 \% (\text{monomers}) \quad (4)$$

The amount of sodium carbonate used was calculated by adding the amount needed for converting dHMBA into the sodium salt of dHMBA (molar ratio of dHMBA to Na₂CO₃=2) and an additional amount as catalyst (molar ratio of monomers to Na₂CO₃=100). The molar ratio of FA to melamine was 3.7 and that of FA to resorcinol derivatives (MR and dHMBA) was 2. At first, two separate solutions were prepared in two vials. In one vial, a mixture of Mel, FA solution and half of the water was prepared. The mixture was kept at 70 °C for about 25 min to allow the Mel to dissolve. In the second vial, a mixture of MR, dHMBA, sodium carbonate and half of the water was prepared. Both homogeneous solutions were poured into one vial, mixed, and then poured into a glass test tubes and allowed to gel and cure for 4 days at 85 °C.

To obtain Co²⁺-doped gels, the hydrogels were soaked in a 0.1 M solution of cobalt nitrate for 3 days (the solution was changed every 24 h), after which the sodium ions bound to the ion-exchange moiety (the carboxylic group) were exchanged for cobalt ions.

In order to use supercritical CO₂ drying for aerogel preparation, solvent exchange was carried out for acetone by changing the solution every 24 h, starting with a 25:75 mixture of acetone and water and proceeding with 50:50 and 75:25 mixtures and finally with 100% acetone for 2 days. A more detailed description of the method used for supercritical drying has been published elsewhere.^[61]

The CAs were prepared through pyrolysis in a N₂ atmosphere by heating at 10 °C min⁻¹ to 800 °C and maintaining at this temperature for 1 h. Co-containing N-doped aerogels prepared with different amounts of the monomers are denoted as Co-NCA1, Co-NCA2, and so forth (Table 1). For comparison, nitrogen-free Co-containing CA (Co-CA) and cobalt-free (NCA) materials were also prepared; in the latter case, the ion-exchange procedure was not performed.

Physicochemical Characterisation of Catalyst Materials

Elemental analyses were performed by the vario MICRO cube (Elementar, Germany) and the cobalt content was measured by using a Spectra AA 220F flame atomic absorption spectrometer (Varian, USA). SEM images were taken using a ZEISS ULTRA 55 (Germany) microscope. Nitrogen-adsorption analyses were performed by using a KELVIN 1042 Sorptometer built by Costech International (USA). Helium was used as a carrier gas and N₂ as the adsorptive gas. Nitrogen-adsorption data were taken at relative pressures (p/p_0) from 0 to 1 and at liquid-nitrogen temperature. The specific surface area (S_{BET}) was calculated according to the BET theory. The specific micropore volume (V_{MC}) was determined by using the t -plot, whereas the pore-size distributions were determined by using the Barrett-Joyner-Halenda (BJH) method from the desorption branch. The XRD pattern was recorded with a Rigaku Ultima IV diffractometer by using a DtexUltra line detector. CuK α radiation was used, with a Ni filter to remove K β radiation. The recorded diffraction patterns were analysed by using Rigaku PDXL software. TGA tests were conducted by using Labsys Evo TG-DTA 1600 °C (Setaram, France) and heating the samples in an Ar atmosphere at 10 °C min⁻¹ to 800 °C. The XPS measurements were carried out with a SCIENTA SES-100 spectrometer by using a non-monochromated MgK α X-ray source (incident energy = 1253.6 eV), a take-off angle of 90° and a source power of 300 W. The pressure in the analysis chamber was below 10⁻⁹ Torr. Raw data were processed by using CasaXPS software,^[62] data processing involved removal of k - α and k - β satellites, removal of the background and fitting of the components. Background removal was performed by using a Tougaard background; for fitting components, the Gauss-Lorentz hybrid function was used (GL 30, Gauss 70%, Lorentz 30%) for the best fit.

Determination of Electrocatalytic Activity Towards the ORR

Glassy carbon (GC) discs (GC20-5S, Tokai Carbon) with a geometric area (A) of 0.2 cm² were used as electrode substrates. The GC electrodes were polished to a mirror finish with 1 and 0.3 μm alumina slurries (Buehler) and sonicated in Milli-Q water for 5 min. The CAs were ball-milled to fine powders and the catalyst ink was prepared by mixing the catalyst (4 mg), Nafion solution (40 μL ; 5 wt% solution in lower alcohols, Aldrich) and 2-propanol (960 μL). The ink was subjected to ultrasonication for at least 40 min and the GC electrode was drop-coated twice with 5 μL aliquots of the catalyst, resulting in a loading of 200 $\mu\text{g cm}^{-2}$, which has been determined as the optimal loading for this type of material.^[15] For the 20 wt% Pt catalyst supported on Vulcan carbon XC-72 (E-TEK), the same ink formulation and coating procedure were used, resulting in a loading of 40 $\mu\text{g cm}^{-2}$ of Pt on the electrode. The catalyst-coated electrodes were dried in an oven at 65 °C for at least 30 min before measurements.

The electrocatalytic activities of the CAs were evaluated by the RDE method, using an EDI101 rotator and a CTV101 speed control unit (Radiometer). The potential was applied by using an Autolab

potentiostat/galvanostat PGSTAT30 (Eco Chemie B.V., The Netherlands). Experiments were conducted in a three-electrode glass cell at room temperature (23 \pm 1 °C). A Pt wire served as the counter electrode and a saturated calomel electrode (SCE) was used as the reference; all potentials were referred to this electrode. Electrochemical experiments were carried out in 0.1 M KOH solution, prepared from KOH pellets (p.a. quality, Sigma-Aldrich) and saturated with Ar (99.999%, AGA) or O₂ (99.999%, AGA). A continuous flow of gas over the solution was maintained during the electrochemical measurements. The RDE polarisation curves at various electrode rotation rates (ω) between 360 and 3100 rpm were obtained by scanning the potential from 0 to -1.2 V at a scan rate (v) of 10 mV s⁻¹. For data presentation and analysis, the background current registered in O₂-free solution was subtracted from the experimental current and current densities were calculated per geometric area of the electrode (A).

Acknowledgements

The authors would like to thank Maria Kulp, Tiina Aid and Anu Viitak for carrying out and helping with elemental analysis. Tiit Kaljuvee is kindly acknowledged for doing the TGA, Mai Uibu for N₂-adsorption analysis and Arvo Mere for XRD analysis. VKG AS and Carboshale OÜ are acknowledged for donating the phenolic compounds. The authors thank the Estonian Ministry of Education and Research (IUT20-16 and PUT391) and the Estonian Research Council (Grant No. 9323) for financial support.

Keywords: carbon aerogels · electrocatalysis · nitrogen doping · non-precious metal catalysts · oxygen reduction

- [1] a) F. Jaouen, E. Proietti, M. Lefevre, R. Chenitz, J.-P. Dodelet, G. Wu, H. T. Chung, C. M. Johnston, P. Zelenay, *Energy Environ. Sci.* **2011**, *4*, 114–130; b) Z. W. Chen, D. Higgins, A. P. Yu, L. Zhang, J. J. Zhang, *Energy Environ. Sci.* **2011**, *4*, 3167–3192; c) D. C. Higgins, Z. Chen, *Can. J. Chem. Eng.* **2013**, *91*, 1881–1895.
- [2] G. Wu, P. Zelenay, *Acc. Chem. Res.* **2013**, *46*, 1878–1889.
- [3] K. N. Wood, R. O'Hayre, S. Pylypenko, *Energy Environ. Sci.* **2014**, *7*, 1212–1249.
- [4] S. Gupta, D. Tryk, I. Bae, W. Aldred, E. Yeager, *J. Appl. Electrochem.* **1989**, *19*, 19–27.
- [5] a) H. T. Chung, J. H. Won, P. Zelenay, *Nat. Commun.* **2013**, *4*, 1922; b) X. G. Fu, Y. R. Liu, X. P. Cao, J. T. Jin, Q. Liu, J. Y. Zhang, *Appl. Catal. B* **2013**, *130*, 143–151; c) A. G. Kong, X. F. Zhu, Z. Han, Y. Y. Yu, Y. B. Zhang, B. Dong, Y. K. Shan, *ACS Catal.* **2014**, *4*, 1793–1800; d) H. Yin, C. Zhang, F. Liu, Y. Hou, *Adv. Funct. Mater.* **2014**, *24*, 2930–2937.
- [6] a) K. X. Niu, B. P. Yang, J. F. Cui, J. T. Jin, X. G. Fu, Q. P. Zhao, J. Y. Zhang, *J. Power Sources* **2013**, *243*, 65–71; b) A. G. Kong, Y. Y. Kong, X. F. Zhu, Z. Han, Y. K. Shan, *Carbon* **2014**, *78*, 49–59.
- [7] K. Strickland, E. Miner, Q. Jia, U. Tyllus, N. Ramaswamy, W. Liang, M.-T. Sougrati, F. Jaouen, S. Mukerjee, *Nat. Commun.* **2015**, *6*, 7343.
- [8] J. Shen, D. Y. Guan, in *Aerogels Handbook* (Eds.: M. A. Aegerter, N. Leventis, M. M. Koebel), Springer, New York **2011**, pp. 813–827.
- [9] a) R. W. Pekala, US patent 4873218, **1989**; b) R. W. Pekala, C. T. Alviso, F. M. Kong, S. S. Hulse, *J. Non-Cryst. Solids* **1992**, *145*, 90–98.
- [10] H. Jin, H. M. Zhang, H. X. Zhong, J. L. Zhang, *Energy Environ. Sci.* **2011**, *4*, 3389–3394.
- [11] S. S. Liu, H. M. Zhang, Z. Xu, H. X. Zhong, H. Jin, *Int. J. Hydrogen Energy* **2012**, *37*, 19065–19072.
- [12] a) D. H. Long, J. Zhang, J. H. Yang, Z. J. Hu, G. Cheng, X. M. Liu, R. Zhang, L. Zhan, W. M. Qiao, L. C. Ling, *Carbon* **2008**, *46*, 1259–1262; b) G. C. Ruben, R. W. Pekala, *J. Non-Cryst. Solids* **1995**, *186*, 219–231.
- [13] W. Yang, S. Z. Chen, W. M. Lin, *Int. J. Hydrogen Energy* **2012**, *37*, 942–945.

- [14] H. X. Zhong, H. M. Zhang, S. S. Liu, C. W. Deng, M. R. Wang, *ChemSusChem* **2013**, *6*, 807–812.
- [15] A. Sarapuu, L. Samolberg, K. Kreek, M. Koel, L. Matisen, K. Tammeveski, *J. Electroanal. Chem.* **2015**, *746*, 9–17.
- [16] a) J. Biener, M. Stadermann, M. Suss, M. A. Worsley, M. M. Biener, K. A. Rose, T. F. Baumann, *Energy Environ. Sci.* **2011**, *4*, 656–667; b) R. W. Pekala, J. C. Farmer, C. T. Alviso, T. D. Tran, S. T. Mayer, J. M. Miller, B. Dunn, *J. Non-Cryst. Solids* **1998**, *225*, 74–80.
- [17] S. A. Wohlgemuth, R. J. White, M. G. Willinger, M. M. Titirici, M. Antonietti, *Green Chem.* **2012**, *14*, 1515–1523.
- [18] S. A. Wohlgemuth, T. P. Fellinger, P. Jaker, M. Antonietti, *J. Mater. Chem. A* **2013**, *1*, 4002–4009.
- [19] N. Brun, S. A. Wohlgemuth, P. Osiceanu, M. M. Titirici, *Green Chem.* **2013**, *15*, 2514–2524.
- [20] K. Elumeeva, N. Fechler, T. P. Fellinger, M. Antonietti, *Mater. Horiz.* **2014**, *1*, 588–594.
- [21] a) A. Smirnova, T. Wender, D. Goberman, Y. L. Hu, M. Aindow, W. Rhine, N. M. Sammes, *Int. J. Hydrogen Energy* **2009**, *34*, 8992–8997; b) S. Y. Ye, A. K. Vijh, *Int. J. Hydrogen Energy* **2005**, *30*, 1011–1015.
- [22] K. Elumeeva, J. Ren, M. Antonietti, T.-P. Fellinger, *ChemElectroChem* **2015**, *2*, 584–591.
- [23] B. You, P. Q. Yin, L. N. An, *Small* **2014**, *10*, 4352–4361.
- [24] Y. Y. Liang, Y. G. Li, H. L. Wang, J. G. Zhou, J. Wang, T. Regier, H. J. Dai, *Nat. Mater.* **2011**, *10*, 780–786.
- [25] T. Odedairo, J. Ma, Y. Gu, W. Zhou, J. Jin, X. S. Zhao, Z. H. Zhu, *Nanotechnology* **2014**, *25*, 495604.
- [26] Q. G. He, Q. Li, S. Khene, X. M. Ren, F. E. Lopez-Suarez, D. Lozano-Castello, A. Bueno-Lopez, G. Wu, *J. Phys. Chem. C* **2013**, *117*, 8697–8707.
- [27] T. Kottakkat, M. Bron, *ChemElectroChem* **2014**, *1*, 2163–2171.
- [28] Y. Y. Liang, H. L. Wang, P. Diau, W. Chang, G. S. Hong, Y. G. Li, M. Gong, L. M. Xie, J. G. Zhou, J. Wang, T. Z. Regier, F. Wei, H. J. Dai, *J. Am. Chem. Soc.* **2012**, *134*, 15849–15857.
- [29] J. J. Xiao, X. J. Bian, L. Liao, S. Zhang, C. Ji, B. H. Liu, *ACS Appl. Mater. Interfaces* **2014**, *6*, 17654–17660.
- [30] a) D. K. Huang, Y. P. Luo, S. H. Li, B. Y. Zhang, Y. Shen, M. K. Wang, *Nano Res.* **2014**, *7*, 1054–1064; b) G. J. Zhang, C. X. Li, J. Liu, L. Zhou, R. H. Liu, X. Han, H. Huang, H. L. Hu, Y. Liu, Z. H. Kang, *J. Mater. Chem. A* **2014**, *2*, 8184–8189; c) W. Xia, R. Q. Zou, L. An, D. G. Xia, S. J. Guo, *Energy Environ. Sci.* **2015**, *8*, 568–576.
- [31] Y. H. Su, Y. H. Zhu, H. L. Jiang, J. H. Shen, X. H. L. Yang, W. J. Zou, J. D. Chen, C. Z. Li, *Nanoscale* **2014**, *6*, 15080–15089.
- [32] Z. L. Wang, S. Xiao, Z. L. Zhu, X. Long, X. L. Zheng, X. H. Lu, S. H. Yang, *ACS Appl. Mater. Interfaces* **2015**, *7*, 4048–4055.
- [33] a) A. G. Kong, C. Y. Mao, Q. P. Lin, X. Wei, X. H. Bu, P. Y. Feng, *Dalton Trans.* **2015**, *44*, 6748–6754; b) C. Han, X. J. Bo, Y. F. Zhang, M. Li, A. Nsabimana, L. P. Guo, *Nanoscale* **2015**, *7*, 5607–5611.
- [34] L. B. Lv, T. N. Ye, L. H. Gong, K. X. Wang, J. Su, X. H. Li, J. S. Chen, *Chem. Mater.* **2015**, *27*, 544–549.
- [35] F. Pérez-Caballero, A. L. Peikola, M. Uibu, R. Kuusik, O. Volobujeva, M. Koel, *Microporous Mesoporous Mater.* **2008**, *108*, 230–236.
- [36] T. F. Baumann, G. A. Fox, J. H. Satcher, N. Yoshizawa, R. W. Fu, M. S. Dresselhaus, *Langmuir* **2002**, *18*, 7073–7076.
- [37] K. Kreek, M. Kulp, M. Uibu, A. Mere, M. Koel, *Oil Shale* **2014**, *31*, 185–194.
- [38] D. J. Merline, S. Vukusic, A. A. Abdala, *Polym. J.* **2013**, *45*, 413–419.
- [39] S. A. Al-Muhtaseb, J. A. Ritter, *Adv. Mater.* **2003**, *15*, 101–114.
- [40] J. Prasek, J. Drbohlavova, J. Chomoucka, J. Hubalek, O. Jasek, V. Adam, R. Kizek, *J. Mater. Chem.* **2011**, *21*, 15872–15884.
- [41] R. W. Fu, T. F. Baumann, S. Cronin, G. Dresselhaus, M. S. Dresselhaus, J. H. Satcher, *Langmuir* **2005**, *21*, 2647–2651.
- [42] H. Liu, Y. Zhang, R. Y. Li, X. L. Sun, S. Desilets, H. Abou-Rachid, M. Jaidann, L. S. Lussier, *Carbon* **2010**, *48*, 1498–1507.
- [43] Y. Yao, B. Q. Zhang, J. Y. Shi, Q. H. Yang, *ACS Appl. Mater. Interfaces* **2015**, *7*, 7413–7420.
- [44] G. Liu, X. G. Li, J. W. Lee, B. N. Popov, *Catal. Sci. Technol.* **2011**, *1*, 207–217.
- [45] M. Ferrandon, A. J. Kropf, D. J. Myers, K. Artyushkova, U. Kramm, P. Bogdanoff, G. Wu, C. M. Johnston, P. Zelenay, *J. Phys. Chem. C* **2012**, *116*, 16001–16013.
- [46] M. C. Biesinger, B. P. Payne, A. P. Grosvenor, L. W. M. Lau, A. R. Gerson, R. S. Smart, *Appl. Surf. Sci.* **2011**, *257*, 2717–2730.
- [47] A. J. Bard, L. R. Faulkner, *Electrochemical Methods*, 2nd ed., Wiley, New York, **2001**.
- [48] R. E. Davis, G. L. Horvath, C. W. Tobias, *Electrochim. Acta* **1967**, *12*, 287–297.
- [49] *CRC Handbook of Chemistry and Physics*, 82nd ed. (Ed.: D. R. Lide), CRC Press, Boca Raton, **2001**.
- [50] I. Kruusenberg, S. Ratto, M. Vikkisk, P. Kanninen, T. Kallio, A. M. Kannan, K. Tammeveski, *J. Power Sources* **2015**, *281*, 94–102.
- [51] S. Ratto, I. Kruusenberg, M. Vikkisk, U. Joost, E. Shulga, I. Kink, T. Kallio, K. Tammeveski, *Carbon* **2014**, *73*, 361–370.
- [52] a) M. Vikkisk, I. Kruusenberg, U. Joost, E. Shulga, K. Tammeveski, *Electrochim. Acta* **2013**, *87*, 709–716; b) M. Vikkisk, I. Kruusenberg, S. Ratto, U. Joost, E. Shulga, I. Kink, P. Rauwel, K. Tammeveski, *RSC Adv.* **2015**, *5*, 59495–59505.
- [53] Z. L. Ma, C. Z. Guo, Y. J. Yin, Y. Q. Zhang, H. J. Wu, C. G. Chen, *Electrochim. Acta* **2015**, *160*, 357–362.
- [54] D. H. Deng, L. Yu, X. Q. Chen, G. X. Wang, L. Jin, X. L. Pan, J. Deng, G. Q. Sun, X. H. Bao, *Angew. Chem. Int. Ed.* **2013**, *52*, 371–375; *Angew. Chem.* **2013**, *125*, 389–393.
- [55] a) J. Masa, A. Q. Zhao, W. Xia, Z. Y. Sun, B. Mei, M. Muhler, W. Schuhmann, *Electrochem. Commun.* **2013**, *34*, 113–116; b) A. Serov, M. H. Robson, K. Artyushkova, P. Atanassov, *Appl. Catal. B* **2012**, *127*, 300–306; c) S. Jiang, C. Z. Zhu, S. J. Dong, *J. Mater. Chem. A* **2013**, *1*, 3593–3599.
- [56] a) N. Ramaswamy, U. Tylus, Q. Y. Jia, S. Mukerjee, *J. Am. Chem. Soc.* **2013**, *135*, 15443–15449; b) U. Tylus, Q. Y. Jia, K. Strickland, N. Ramaswamy, A. Serov, P. Atanassov, S. Mukerjee, *J. Phys. Chem. C* **2014**, *118*, 8999–9008.
- [57] T. S. Olson, S. Pylypenko, P. Atanassov, K. Asazawa, K. Yamada, H. Tanaka, *J. Phys. Chem. C* **2010**, *114*, 5049–5059.
- [58] M. Vikkisk, I. Kruusenberg, U. Joost, E. Shulga, I. Kink, K. Tammeveski, *Appl. Catal. B* **2014**, *147*, 369–376.
- [59] K. Tammeveski, M. Arulepp, T. Tenno, C. Ferrater, J. Claret, *Electrochim. Acta* **1997**, *42*, 2961–2967.
- [60] a) J. Zhang, S. Y. Wu, X. Chen, M. Pan, S. C. Mu, *J. Power Sources* **2014**, *271*, 522–529; b) G. Wu, C. M. Johnston, N. H. Mack, K. Artyushkova, M. Ferrandon, M. Nelson, J. S. Lezama-Pacheco, S. D. Conradson, K. L. More, D. J. Myers, P. Zelenay, *J. Mater. Chem.* **2011**, *21*, 11392–11405.
- [61] A. L. Peikola, O. Volobujeva, R. Aav, M. Uibu, M. Koel, *J. Porous Mater.* **2012**, *19*, 189–194.
- [62] N. Fairley, CasaXPS version 2.3.12, 2000.

Manuscript received: June 26, 2015
Final Article published: September 15, 2015

Curriculum vitae

1. Personal data

Name Kristiina Kreek
Date and place of birth 02.08.1988, Tallinn, Estonia
E-mail address kristiina.kreek@ttu.ee

2. Education

Educational Institution	Graduation year	Education (field of study/degree)
Tallinn Secondary Science School	2007	Secondary education
Tallinn University of Technology	2010	Applied Chemistry and Biotechnology/ B.Sc.
Tallinn University of Technology	2012	Applied Chemistry and Biotechnology/ M.Sc. (Cum Laude)

3. Language competence/skills

Language	Level
Estonian	Fluent
English	Fluent
Russian	Basic skills

4. Special courses

Period	Educational or other organisation
10.04.2011-23.04.2016	Erasmus European University Dedicated to „Green Chemistry“, Bethune IUT, France
2012-2014	Graduate School „Functional Materials and Processes“, Tallinn University of Technology, Estonia
2013-2015	POKE training school, Sustainable Chemistry and Process Technology in the Northern Baltic Sea Region
25.01.2016-29.01.2016	MICACT Training School 2: Modelling and Ionic Electroactive Polymers, University of Tartu, Estonia

5. Professional employment

Period	Organisation	Position
01.01.2013-31.12.2015	Tallinn University of Technology	engineer
01.09.2016-	Tallinn University of Technology	engineer
2012-2015	Tallinn University of Technology	teaching in the field of analytical chemistry

6. Research activity

01.03.2015-30.06.2015

University of Lisbon (Portugal), the group of Carlos Nieto de Castro. Working with ionanofluids and thermal conductivity measurements.

Elulookirjeldus

1. Isikuandmed

Nimi Kristiina Kreek
Sünniaeg ja -koht 02.08.1988, Tallinn, Eesti
E-posti aadress kristiina.kreek@ttu.ee

2. Hariduskäik

Õppeasutus	Lõpetamise aeg	Haridus (eriala/kraad)
Tallinna Reaalkool	2007	Keskharidus
Tallinna Tehnikaülikool	2010	Rakenduskeemia ja biotehnoloogia/bakalaureusekraad
Tallinna Tehnikaülikool	2012	Rakenduskeemia ja biotehnoloogia/magistrikraad (Cum Laude)

3. Keelteoskus

Keel	Tase
Eesti keel	kõrgtase
Inglise keel	kõrgtase
Vene keel	algtase

4. Täiendusõpe

Õppimise aeg	Täiendusõppe korraldaja
10.04.2011-23.04.2016	Rohelisele keemiale pühendatud Erasmuse Euroopa Ülikool, Bethune, Prantsusmaa
2012-2014	Doktorikool „Funktsionaalsed materjalid ja tehnoloogiad“, Tallinna Tehnikaülikool, Eesti
2013-2015	POKE training school, Sustainable Chemistry and Process Technology in the Northern Baltic Sea Region
25.01.2016-29.01.2016	MICACT doktorikool 2: modelleerimine ja ioonsed elektroaktiivsed polümeerid, Tartu Ülikool

5. Teenistuskäik

Töötamise aeg	Tööandja nimetus	Ametikoht
01.01.2013- 31.12.2015	Tallinna Tehnikaülikool	insener
01.09.2016-	Tallinna Tehnikaülikool	insener
2012-2015	Tallinna Tehnikaülikool	õppetöö läbiviimine analüütilise keemia alal

6. Teadustegevus

01.03.2015-30.06.2015

Lissaboni Ülikool (Portugal),
Carlos Nieto de Castro rühm.
Ionanofluidumite uurimine and
soojusjuhtivuse mõõtmised.

**DISSERTATIONS DEFENDED AT
TALLINN UNIVERSITY OF TECHNOLOGY ON
NATURAL AND EXACT SCIENCES**

1. **Olav Kongas**. Nonlinear Dynamics in Modeling Cardiac Arrhythmias. 1998.
2. **Kalju Vanatalu**. Optimization of Processes of Microbial Biosynthesis of Isotopically Labeled Biomolecules and Their Complexes. 1999.
3. **Ahto Buldas**. An Algebraic Approach to the Structure of Graphs. 1999.
4. **Monika Drews**. A Metabolic Study of Insect Cells in Batch and Continuous Culture: Application of Chemostat and Turbidostat to the Production of Recombinant Proteins. 1999.
5. **Eola Valdre**. Endothelial-Specific Regulation of Vessel Formation: Role of Receptor Tyrosine Kinases. 2000.
6. **Kalju Lott**. Doping and Defect Thermodynamic Equilibrium in ZnS. 2000.
7. **Reet Koljak**. Novel Fatty Acid Dioxygenases from the Corals *Plexaura homomalla* and *Gersemia fruticosa*. 2001.
8. **Anne Paju**. Asymmetric oxidation of Prochiral and Racemic Ketones by Using Sharpless Catalyst. 2001.
9. **Marko Vendelin**. Cardiac Mechanoenergetics *in silico*. 2001.
10. **Pearu Peterson**. Multi-Soliton Interactions and the Inverse Problem of Wave Crest. 2001.
11. **Anne Menert**. Microcalorimetry of Anaerobic Digestion. 2001.
12. **Toomas Tiivel**. The Role of the Mitochondrial Outer Membrane in *in vivo* Regulation of Respiration in Normal Heart and Skeletal Muscle Cell. 2002.
13. **Olle Hints**. Ordovician Scolecodonts of Estonia and Neighbouring Areas: Taxonomy, Distribution, Palaeoecology, and Application. 2002.
14. **Jaak Nõlvak**. Chitinozoan Biostratigraphy in the Ordovician of Baltoscandia. 2002.
15. **Liivi Kluge**. On Algebraic Structure of Pre-Operad. 2002.
16. **Jaanus Lass**. Biosignal Interpretation: Study of Cardiac Arrhythmias and Electromagnetic Field Effects on Human Nervous System. 2002.
17. **Janek Peterson**. Synthesis, Structural Characterization and Modification of PAMAM Dendrimers. 2002.
18. **Merike Vaher**. Room Temperature Ionic Liquids as Background Electrolyte Additives in Capillary Electrophoresis. 2002.
19. **Valdek Mikli**. Electron Microscopy and Image Analysis Study of Powdered Hardmetal Materials and Optoelectronic Thin Films. 2003.
20. **Mart Viljus**. The Microstructure and Properties of Fine-Grained Cermets. 2003.
21. **Signe Kask**. Identification and Characterization of Dairy-Related *Lactobacillus*. 2003.
22. **Tiiu-Mai Laht**. Influence of Microstructure of the Curd on Enzymatic and Microbiological Processes in Swiss-Type Cheese. 2003.
23. **Anne Kuusksalu**. 2–5A Synthetase in the Marine Sponge *Geodia cydonium*. 2003.
24. **Sergei Bereznev**. Solar Cells Based on Polycrystalline Copper-Indium Chalcogenides and Conductive Polymers. 2003.

25. **Kadri Kriis.** Asymmetric Synthesis of C₂-Symmetric Bimorpholines and Their Application as Chiral Ligands in the Transfer Hydrogenation of Aromatic Ketones. 2004.
26. **Jekaterina Reut.** Polypyrrole Coatings on Conducting and Insulating Substrates. 2004.
27. **Sven Nõmm.** Realization and Identification of Discrete-Time Nonlinear Systems. 2004.
28. **Olga Kijatkina.** Deposition of Copper Indium Disulphide Films by Chemical Spray Pyrolysis. 2004.
29. **Gert Tamberg.** On Sampling Operators Defined by Rogosinski, Hann and Blackman Windows. 2004.
30. **Monika Übner.** Interaction of Humic Substances with Metal Cations. 2004.
31. **Kaarel Adamberg.** Growth Characteristics of Non-Starter Lactic Acid Bacteria from Cheese. 2004.
32. **Imre Vallikivi.** Lipase-Catalysed Reactions of Prostaglandins. 2004.
33. **Merike Peld.** Substituted Apatites as Sorbents for Heavy Metals. 2005.
34. **Vitali Syritski.** Study of Synthesis and Redox Switching of Polypyrrole and Poly(3,4-ethylenedioxythiophene) by Using *in-situ* Techniques. 2004.
35. **Lee Põllumaa.** Evaluation of Ecotoxicological Effects Related to Oil Shale Industry. 2004.
36. **Riina Aav.** Synthesis of 9,11-Secosterols Intermediates. 2005.
37. **Andres Braunbrück.** Wave Interaction in Weakly Inhomogeneous Materials. 2005.
38. **Robert Kitt.** Generalised Scale-Invariance in Financial Time Series. 2005.
39. **Juss Pavelson.** Mesoscale Physical Processes and the Related Impact on the Summer Nutrient Fields and Phytoplankton Blooms in the Western Gulf of Finland. 2005.
40. **Olari Ilison.** Solitons and Solitary Waves in Media with Higher Order Dispersive and Nonlinear Effects. 2005.
41. **Maksim Säkki.** Intermittency and Long-Range Structurization of Heart Rate. 2005.
42. **Enli Kiipli.** Modelling Seawater Chemistry of the East Baltic Basin in the Late Ordovician–Early Silurian. 2005.
43. **Igor Golovtsov.** Modification of Conductive Properties and Processability of Polyparaphenylene, Polypyrrole and polyaniline. 2005.
44. **Katrin Laos.** Interaction Between Furcellaran and the Globular Proteins (Bovine Serum Albumin β -Lactoglobulin). 2005.
45. **Arvo Mere.** Structural and Electrical Properties of Spray Deposited Copper Indium Disulphide Films for Solar Cells. 2006.
46. **Sille Ehala.** Development and Application of Various On- and Off-Line Analytical Methods for the Analysis of Bioactive Compounds. 2006.
47. **Maria Kulp.** Capillary Electrophoretic Monitoring of Biochemical Reaction Kinetics. 2006.
48. **Anu Aaspõllu.** Proteinases from *Vipera lebetina* Snake Venom Affecting Hemostasis. 2006.
49. **Lyudmila Chekulayeva.** Photosensitized Inactivation of Tumor Cells by Porphyrins and Chlorins. 2006.

50. **Merle Uudsemaa.** Quantum-Chemical Modeling of Solvated First Row Transition Metal Ions. 2006.
51. **Tagli Pitsi.** Nutrition Situation of Pre-School Children in Estonia from 1995 to 2004. 2006.
52. **Angela Ivask.** Luminescent Recombinant Sensor Bacteria for the Analysis of Bioavailable Heavy Metals. 2006.
53. **Tiina Lõugas.** Study on Physico-Chemical Properties and Some Bioactive Compounds of Sea Buckthorn (*Hippophae rhamnoides* L.). 2006.
54. **Kaja Kasemets.** Effect of Changing Environmental Conditions on the Fermentative Growth of *Saccharomyces cerevisiae* S288C: Auxo-accelerostat Study. 2006.
55. **Ildar Nisamedtinov.** Application of ¹³C and Fluorescence Labeling in Metabolic Studies of *Saccharomyces* spp. 2006.
56. **Alar Leibak.** On Additive Generalisation of Voronoï's Theory of Perfect Forms over Algebraic Number Fields. 2006.
57. **Andri Jagomägi.** Photoluminescence of Chalcopyrite Tellurides. 2006.
58. **Tõnu Martma.** Application of Carbon Isotopes to the Study of the Ordovician and Silurian of the Baltic. 2006.
59. **Marit Kauk.** Chemical Composition of CuInSe₂ Monograin Powders for Solar Cell Application. 2006.
60. **Julia Kois.** Electrochemical Deposition of CuInSe₂ Thin Films for Photovoltaic Applications. 2006.
61. **Iiona Oja Açıık.** Sol-Gel Deposition of Titanium Dioxide Films. 2007.
62. **Tiia Anmann.** Integrated and Organized Cellular Bioenergetic Systems in Heart and Brain. 2007.
63. **Katrin Trummal.** Purification, Characterization and Specificity Studies of Metalloproteinases from *Vipera lebetina* Snake Venom. 2007.
64. **Gennadi Lessin.** Biochemical Definition of Coastal Zone Using Numerical Modeling and Measurement Data. 2007.
65. **Enno Pais.** Inverse problems to determine non-homogeneous degenerate memory kernels in heat flow. 2007.
66. **Maria Borissova.** Capillary Electrophoresis on Alkylimidazolium Salts. 2007.
67. **Karin Valmsen.** Prostaglandin Synthesis in the Coral *Plexaura homomalla*: Control of Prostaglandin Stereochemistry at Carbon 15 by Cyclooxygenases. 2007.
68. **Kristjan Piirimäe.** Long-Term Changes of Nutrient Fluxes in the Drainage Basin of the Gulf of Finland – Application of the PolFlow Model. 2007.
69. **Tatjana Dedova.** Chemical Spray Pyrolysis Deposition of Zinc Sulfide Thin Films and Zinc Oxide Nanostructured Layers. 2007.
70. **Katrin Tomson.** Production of Labelled Recombinant Proteins in Fed-Batch Systems in *Escherichia coli*. 2007.
71. **Cecilia Sarmiento.** Suppressors of RNA Silencing in Plants. 2008.
72. **Vilja Mardla.** Inhibition of Platelet Aggregation with Combination of Antiplatelet Agents. 2008.
73. **Maie Bachmann.** Effect of Modulated Microwave Radiation on Human Resting Electroencephalographic Signal. 2008.
74. **Dan Hüvonen.** Terahertz Spectroscopy of Low-Dimensional Spin Systems. 2008.
75. **Ly Villo.** Stereoselective Chemoenzymatic Synthesis of Deoxy Sugar Esters Involving *Candida antarctica* Lipase B. 2008.

76. **Johan Anton.** Technology of Integrated Photoelasticity for Residual Stress Measurement in Glass Articles of Axisymmetric Shape. 2008.
77. **Olga Volobujeva.** SEM Study of Selenization of Different Thin Metallic Films. 2008.
78. **Artur Jõgi.** Synthesis of 4'-Substituted 2,3'-dideoxynucleoside Analogues. 2008.
79. **Mario Kadastik.** Doubly Charged Higgs Boson Decays and Implications on Neutrino Physics. 2008.
80. **Fernando Pérez-Caballero.** Carbon Aerogels from 5-Methylresorcinol-Formaldehyde Gels. 2008.
81. **Sirje Vaask.** The Comparability, Reproducibility and Validity of Estonian Food Consumption Surveys. 2008.
82. **Anna Menaker.** Electrosynthesized Conducting Polymers, Polypyrrole and Poly(3,4-ethylenedioxythiophene), for Molecular Imprinting. 2009.
83. **Lauri Ilison.** Solitons and Solitary Waves in Hierarchical Korteweg-de Vries Type Systems. 2009.
84. **Kaia Ernits.** Study of In₂S₃ and ZnS Thin Films Deposited by Ultrasonic Spray Pyrolysis and Chemical Deposition. 2009.
85. **Veljo Sinivee.** Portable Spectrometer for Ionizing Radiation "Gammamapper". 2009.
86. **Jüri Virkepu.** On Lagrange Formalism for Lie Theory and Operadic Harmonic Oscillator in Low Dimensions. 2009.
87. **Marko Piirsoo.** Deciphering Molecular Basis of Schwann Cell Development. 2009.
88. **Kati Helmja.** Determination of Phenolic Compounds and Their Antioxidative Capability in Plant Extracts. 2010.
89. **Merike Sõmera.** Sobemoviruses: Genomic Organization, Potential for Recombination and Necessity of P1 in Systemic Infection. 2010.
90. **Kristjan Laes.** Preparation and Impedance Spectroscopy of Hybrid Structures Based on CuIn₃Se₅ Photoabsorber. 2010.
91. **Kristin Lippur.** Asymmetric Synthesis of 2,2'-Bimorpholine and its 5,5'-Substituted Derivatives. 2010.
92. **Merike Luman.** Dialysis Dose and Nutrition Assessment by an Optical Method. 2010.
93. **Mihhail Berezovski.** Numerical Simulation of Wave Propagation in Heterogeneous and Microstructured Materials. 2010.
94. **Tamara Aid-Pavlidis.** Structure and Regulation of BDNF Gene. 2010.
95. **Olga Bragina.** The Role of Sonic Hedgehog Pathway in Neuro- and Tumorigenesis. 2010.
96. **Merle Randrüüt.** Wave Propagation in Microstructured Solids: Solitary and Periodic Waves. 2010.
97. **Marju Laars.** Asymmetric Organocatalytic Michael and Aldol Reactions Mediated by Cyclic Amines. 2010.
98. **Maarja Grossberg.** Optical Properties of Multinary Semiconductor Compounds for Photovoltaic Applications. 2010.
99. **Alla Maloverjan.** Vertebrate Homologues of Drosophila Fused Kinase and Their Role in Sonic Hedgehog Signalling Pathway. 2010.

100. **Priit Pruunsild**. Neuronal Activity-Dependent Transcription Factors and Regulation of Human *BDNF* Gene. 2010.
101. **Tatjana Knjazeva**. New Approaches in Capillary Electrophoresis for Separation and Study of Proteins. 2011.
102. **Atanas Katerski**. Chemical Composition of Sprayed Copper Indium Disulfide Films for Nanostructured Solar Cells. 2011.
103. **Kristi Timmo**. Formation of Properties of CuInSe_2 and $\text{Cu}_2\text{ZnSn}(\text{S,Se})_4$ Monograin Powders Synthesized in Molten KI. 2011.
104. **Kert Tamm**. Wave Propagation and Interaction in Mindlin-Type Microstructured Solids: Numerical Simulation. 2011.
105. **Adrian Popp**. Ordovician Proetid Trilobites in Baltoscandia and Germany. 2011.
106. **Ove Pärn**. Sea Ice Deformation Events in the Gulf of Finland and This Impact on Shipping. 2011.
107. **Germo Väli**. Numerical Experiments on Matter Transport in the Baltic Sea. 2011.
108. **Andrus Seiman**. Point-of-Care Analyser Based on Capillary Electrophoresis. 2011.
109. **Olga Katargina**. Tick-Borne Pathogens Circulating in Estonia (Tick-Borne Encephalitis Virus, *Anaplasma phagocytophilum*, *Babesia* Species): Their Prevalence and Genetic Characterization. 2011.
110. **Ingrid Sumeri**. The Study of Probiotic Bacteria in Human Gastrointestinal Tract Simulator. 2011.
111. **Kairit Zovo**. Functional Characterization of Cellular Copper Proteome. 2011.
112. **Natalja Makarytsheva**. Analysis of Organic Species in Sediments and Soil by High Performance Separation Methods. 2011.
113. **Monika Mortimer**. Evaluation of the Biological Effects of Engineered Nanoparticles on Unicellular Pro- and Eukaryotic Organisms. 2011.
114. **Kersti Tepp**. Molecular System Bioenergetics of Cardiac Cells: Quantitative Analysis of Structure-Function Relationship. 2011.
115. **Anna-Liisa Peikolainen**. Organic Aerogels Based on 5-Methylresorcinol. 2011.
116. **Leeli Amon**. Palaeoecological Reconstruction of Late-Glacial Vegetation Dynamics in Eastern Baltic Area: A View Based on Plant Macrofossil Analysis. 2011.
117. **Tanel Peets**. Dispersion Analysis of Wave Motion in Microstructured Solids. 2011.
118. **Liina Kaupmees**. Selenization of Molybdenum as Contact Material in Solar Cells. 2011.
119. **Allan Olsper**. Properties of VPg and Coat Protein of Sobemoviruses. 2011.
120. **Kadri Koppel**. Food Category Appraisal Using Sensory Methods. 2011.
121. **Jelena Gorbatšova**. Development of Methods for CE Analysis of Plant Phenolics and Vitamins. 2011.
122. **Karin Viipsi**. Impact of EDTA and Humic Substances on the Removal of Cd and Zn from Aqueous Solutions by Apatite. 2012.
123. **David Schryer**. Metabolic Flux Analysis of Compartmentalized Systems Using Dynamic Isotopologue Modeling. 2012.
124. **Ardo Illaste**. Analysis of Molecular Movements in Cardiac Myocytes. 2012.

125. **Indrek Reile**. 3-Alkylcyclopentane-1,2-Diones in Asymmetric Oxidation and Alkylation Reactions. 2012.
126. **Tatjana Tamberg**. Some Classes of Finite 2-Groups and Their Endomorphism Semigroups. 2012.
127. **Taavi Liblik**. Variability of Thermohaline Structure in the Gulf of Finland in Summer. 2012.
128. **Priidik Lagemaa**. Operational Forecasting in Estonian Marine Waters. 2012.
129. **Andrei Errapart**. Photoelastic Tomography in Linear and Non-linear Approximation. 2012.
130. **Külliki Krabbi**. Biochemical Diagnosis of Classical Galactosemia and Mucopolysaccharidoses in Estonia. 2012.
131. **Kristel Kaseleht**. Identification of Aroma Compounds in Food using SPME-GC/MS and GC-Olfactometry. 2012.
132. **Kristel Kodar**. Immunoglobulin G Glycosylation Profiling in Patients with Gastric Cancer. 2012.
133. **Kai Rosin**. Solar Radiation and Wind as Agents of the Formation of the Radiation Regime in Water Bodies. 2012.
134. **Ann Tiiman**. Interactions of Alzheimer's Amyloid-Beta Peptides with Zn(II) and Cu(II) Ions. 2012.
135. **Olga Gavrilova**. Application and Elaboration of Accounting Approaches for Sustainable Development. 2012.
136. **Olesja Bondarenko**. Development of Bacterial Biosensors and Human Stem Cell-Based *In Vitro* Assays for the Toxicological Profiling of Synthetic Nanoparticles. 2012.
137. **Katri Muska**. Study of Composition and Thermal Treatments of Quaternary Compounds for Monograin Layer Solar Cells. 2012.
138. **Ranno Nahku**. Validation of Critical Factors for the Quantitative Characterization of Bacterial Physiology in Accelerostat Cultures. 2012.
139. **Petri-Jaan Lahtvee**. Quantitative Omics-level Analysis of Growth Rate Dependent Energy Metabolism in *Lactococcus lactis*. 2012.
140. **Kerti Orumets**. Molecular Mechanisms Controlling Intracellular Glutathione Levels in Baker's Yeast *Saccharomyces cerevisiae* and its Random Mutagenized Glutathione Over-Accumulating Isolate. 2012.
141. **Loreida Timberg**. Spice-Cured Sprats Ripening, Sensory Parameters Development, and Quality Indicators. 2012.
142. **Anna Mihhalevski**. Rye Sourdough Fermentation and Bread Stability. 2012.
143. **Liisa Arike**. Quantitative Proteomics of *Escherichia coli*: From Relative to Absolute Scale. 2012.
144. **Kairi Otto**. Deposition of In₂S₃ Thin Films by Chemical Spray Pyrolysis. 2012.
145. **Mari Sepp**. Functions of the Basic Helix-Loop-Helix Transcription Factor TCF4 in Health and Disease. 2012.
146. **Anna Suhhova**. Detection of the Effect of Weak Stressors on Human Resting Electroencephalographic Signal. 2012.
147. **Aram Kazarjan**. Development and Production of Extruded Food and Feed Products Containing Probiotic Microorganisms. 2012.

148. **Rivo Uiboupin**. Application of Remote Sensing Methods for the Investigation of Spatio-Temporal Variability of Sea Surface Temperature and Chlorophyll Fields in the Gulf of Finland. 2013.
149. **Tiina Kriščiunaite**. A Study of Milk Coagulability. 2013.
150. **Tuuli Levandi**. Comparative Study of Cereal Varieties by Analytical Separation Methods and Chemometrics. 2013.
151. **Natalja Kabanova**. Development of a Microcalorimetric Method for the Study of Fermentation Processes. 2013.
152. **Himani Khanduri**. Magnetic Properties of Functional Oxides. 2013.
153. **Julia Smirnova**. Investigation of Properties and Reaction Mechanisms of Redox-Active Proteins by ESI MS. 2013.
154. **Mervi Sepp**. Estimation of Diffusion Restrictions in Cardiomyocytes Using Kinetic Measurements. 2013.
155. **Kersti Jääger**. Differentiation and Heterogeneity of Mesenchymal Stem Cells. 2013.
156. **Victor Alari**. Multi-Scale Wind Wave Modeling in the Baltic Sea. 2013.
157. **Taavi Päll**. Studies of CD44 Hyaluronan Binding Domain as Novel Angiogenesis Inhibitor. 2013.
158. **Allan Niidu**. Synthesis of Cyclopentane and Tetrahydrofuran Derivatives. 2013.
159. **Julia Geller**. Detection and Genetic Characterization of *Borrelia* Species Circulating in Tick Population in Estonia. 2013.
160. **Irina Stulova**. The Effects of Milk Composition and Treatment on the Growth of Lactic Acid Bacteria. 2013.
161. **Jana Holmar**. Optical Method for Uric Acid Removal Assessment During Dialysis. 2013.
162. **Kerti Ausmees**. Synthesis of Heterobicyclo[3.2.0]heptane Derivatives *via* Multicomponent Cascade Reaction. 2013.
163. **Minna Varikmaa**. Structural and Functional Studies of Mitochondrial Respiration Regulation in Muscle Cells. 2013.
164. **Indrek Koppel**. Transcriptional Mechanisms of BDNF Gene Regulation. 2014.
165. **Kristjan Pilt**. Optical Pulse Wave Signal Analysis for Determination of Early Arterial Ageing in Diabetic Patients. 2014.
166. **Andres Anier**. Estimation of the Complexity of the Electroencephalogram for Brain Monitoring in Intensive Care. 2014.
167. **Toivo Kallaste**. Pyroclastic Sanidine in the Lower Palaeozoic Bentonites – A Tool for Regional Geological Correlations. 2014.
168. **Erki Kärber**. Properties of ZnO-nanorod/In₂S₃/CuInS₂ Solar Cell and the Constituent Layers Deposited by Chemical Spray Method. 2014.
169. **Julia Lehner**. Formation of Cu₂ZnSnS₄ and Cu₂ZnSnSe₄ by Chalcogenisation of Electrochemically Deposited Precursor Layers. 2014.
170. **Peep Pitk**. Protein- and Lipid-rich Solid Slaughterhouse Waste Anaerobic Co-digestion: Resource Analysis and Process Optimization. 2014.
171. **Kaspar Valgepea**. Absolute Quantitative Multi-omics Characterization of Specific Growth Rate-dependent Metabolism of *Escherichia coli*. 2014.
172. **Artur Noole**. Asymmetric Organocatalytic Synthesis of 3,3'-Disubstituted Oxindoles. 2014.

173. **Robert Tsanev**. Identification and Structure-Functional Characterisation of the Gene Transcriptional Repressor Domain of Human Gli Proteins. 2014.
174. **Dmitri Kartofelev**. Nonlinear Sound Generation Mechanisms in Musical Acoustic. 2014.
175. **Sigrid Hade**. GIS Applications in the Studies of the Palaeozoic Graptolite Argillite and Landscape Change. 2014.
176. **Agne Velthut-Meikas**. Ovarian Follicle as the Environment of Oocyte Maturation: The Role of Granulosa Cells and Follicular Fluid at Pre-Ovulatory Development. 2014.
177. **Kristel Hälvin**. Determination of B-group Vitamins in Food Using an LC-MS Stable Isotope Dilution Assay. 2014.
178. **Mailis Päre**. Characterization of the Oligoadenylate Synthetase Subgroup from Phylum Porifera. 2014.
179. **Jekaterina Kazantseva**. Alternative Splicing of *TAF4*: A Dynamic Switch between Distinct Cell Functions. 2014.
180. **Jaanus Suurväli**. Regulator of G Protein Signalling 16 (RGS16): Functions in Immunity and Genomic Location in an Ancient MHC-Related Evolutionarily Conserved Synteny Group. 2014.
181. **Ene Viiard**. Diversity and Stability of Lactic Acid Bacteria During Rye Sourdough Propagation. 2014.
182. **Kristella Hansen**. Prostaglandin Synthesis in Marine Arthropods and Red Algae. 2014.
183. **Helike Löhelaid**. Allene Oxide Synthase-lipoxygenase Pathway in Coral Stress Response. 2015.
184. **Normunds Stivrīns**. Postglacial Environmental Conditions, Vegetation Succession and Human Impact in Latvia. 2015.
185. **Mary-Liis Kütt**. Identification and Characterization of Bioactive Peptides with Antimicrobial and Immunoregulating Properties Derived from Bovine Colostrum and Milk. 2015.
186. **Kazbulat Šogenov**. Petrophysical Models of the CO₂ Plume at Prospective Storage Sites in the Baltic Basin. 2015.
187. **Taavi Raadik**. Application of Modulation Spectroscopy Methods in Photovoltaic Materials Research. 2015.
188. **Reio Pöder**. Study of Oxygen Vacancy Dynamics in Sc-doped Ceria with NMR Techniques. 2015.
189. **Sven Siir**. Internal Geochemical Stratification of Bentonites (Altered Volcanic Ash Beds) and its Interpretation. 2015.
190. **Kaur Jaanson**. Novel Transgenic Models Based on Bacterial Artificial Chromosomes for Studying BDNF Gene Regulation. 2015.
191. **Niina Karro**. Analysis of ADP Compartmentation in Cardiomyocytes and Its Role in Protection Against Mitochondrial Permeability Transition Pore Opening. 2015.
192. **Piret Laht**. B-plexins Regulate the Maturation of Neurons Through Microtubule Dynamics. 2015.
193. **Sergei Žari**. Organocatalytic Asymmetric Addition to Unsaturated 1,4-Dicarbonyl Compounds. 2015.
194. **Natalja Buhhalko**. Processes Influencing the Spatio-temporal Dynamics of Nutrients and Phytoplankton in Summer in the Gulf of Finland, Baltic Sea. 2015.

195. **Natalia Maticiu**. Mechanism of Changes in the Properties of Chemically Deposited CdS Thin Films Induced by Thermal Annealing. 2015.
196. **Mario Öeren**. Computational Study of Cyclohexylhemicucurbiturils. 2015.
197. **Mari Kalda**. Mechanoenergetics of a Single Cardiomyocyte. 2015.
198. **Ieva Grudzinska**. Diatom Stratigraphy and Relative Sea Level Changes of the Eastern Baltic Sea over the Holocene. 2015.
199. **Anna Kazantseva**. Alternative Splicing in Health and Disease. 2015.
200. **Jana Kazarjan**. Investigation of Endogenous Antioxidants and Their Synthetic Analogues by Capillary Electrophoresis. 2016.
201. **Maria Safonova**. SnS Thin Films Deposition by Chemical Solution Method and Characterization. 2016.
202. **Jekaterina Mazina**. Detection of Psycho- and Bioactive Drugs in Different Sample Matrices by Fluorescence Spectroscopy and Capillary Electrophoresis. 2016.
203. **Karin Rosenstein**. Genes Regulated by Estrogen and Progesterone in Human Endometrium. 2016.
204. **Aleksei Tretjakov**. A Macromolecular Imprinting Approach to Design Synthetic Receptors for Label-Free Biosensing Applications. 2016.
205. **Mati Danilson**. Temperature Dependent Electrical Properties of Kesterite Monograin Layer Solar Cells. 2016.
206. **Kaspar Kevvai**. Applications of ¹⁵N-labeled Yeast Hydrolysates in Metabolic Studies of *Lactococcus lactis* and *Saccharomyces Cerevisiae*. 2016.
207. **Kadri Aller**. Development and Applications of Chemically Defined Media for Lactic Acid Bacteria. 2016.
208. **Gert Preegel**. Cyclopentane-1,2-dione and Cyclopent-2-en-1-one in Asymmetric Organocatalytic Reactions. 2016.
209. **Jekaterina Služenikina**. Applications of Marine Scatterometer Winds and Quality Aspects of their Assimilation into Numerical Weather Prediction Model HIRLAM. 2016.
210. **Erkki Kask**. Study of Kesterite Solar Cell Absorbers by Capacitance Spectroscopy Methods. 2016.
211. **Jürgen Arund**. Major Chromophores and Fluorophores in the Spent Dialysate as Cornerstones for Optical Monitoring of Kidney Replacement Therapy. 2016.
212. **Andrei Šamarin**. Hybrid PET/MR Imaging of Bone Metabolism and Morphology. 2016.
213. **Kairi Kasemets**. Inverse Problems for Parabolic Integro-Differential Equations with Instant and Integral Conditions. 2016.
214. **Edith Soosaar**. An Evolution of Freshwater Bulge in Laboratory Scale Experiments and Natural Conditions. 2016.
215. **Peeter Laas**. Spatiotemporal Niche-Partitioning of Bacterioplankton Community across Environmental Gradients in the Baltic Sea. 2016.
216. **Margus Voolma**. Geochemistry of Organic-Rich Metalliferous Oil Shale/Black Shale of Jordan and Estonia. 2016.
217. **Karin Ojamäe**. The Ecology and Photobiology of Mixotrophic Alveolates in the Baltic Sea. 2016.
218. **Anne Pink**. The Role of CD44 in the Control of Endothelial Cell Proliferation and Angiogenesis. 2016.